Università
Ca'Foscari
Venezia

Corso di Dottorato di ricerca in

Scienza e Gestione dei Cambiamenti Climatici

Ciclo XXIX

Tesi di Ricerca

Advanced Modeling and Data Assimilation Methods for the Design of Sustained Marine Monitoring Networks

Settore scientifico disciplinare di afferenza: GEO/12

Coordinatore del dottorato:

Prof. Carlo Barbante

Supervisore:

Prof.ssa Nadia Pinardi

Co-supervisore:

Dr.ssa Simona Masina

Dottorando:

Ali Aydoğdu

Matricola 956108

ACKNOWLEDGMENTS

I would like to express my deepest gratitude to my supervisor Prof. Nadia Pinardi. It was a privilege to have such a great mentor. The external co-advisors for this thesis are Prof. Emin Özsoy and Prof. Tomislava Vukicevic. I owe Prof. Emin Özsoy a lot for supporting me since my early research career. I was very lucky to have the opportunity to work with Prof. Tomislava Vukicevic during my research period in Lecce. I learned a lot from her outlook on research.

While oscillating between the joy and pain of doing research, there was a day in Boulder in which I was convinced that, most probably, I'll be able to finish my PhD. I would like to thank Dr. Gökhan Danabaşoğlu, Dr. Jeffrey Anderson and Dr. Alicia Karspeck for leading me during my abroad research period in NCAR. Many thanks also to Tim Hoar, Jonathan Hendricks, Nancy Collins and Kevin Raeder in DaReS as well as all the people in the oceanography section. for their support, hospitality and friendship.

I appreciate Prof. Sarantis Sofianos and Prof. Marilaure Grégorie for reviewing this thesis and sharing their helpful comments with me.

The main funding for my research is provided by Ca' Foscari University of Venice. I thank everybody on the background in the name of Federica Varosio who never hesitated to help when I needed. There was a partial support for the first part of my research from EU JERICO project of CMCC/Bologna in which I had a chance to work with Dr. Srdjan Dobricic. Another partial funding was provided by OceanLab CMCC/Lecce. I thank all friends there for their warm welcome, in particular Francesca Macchia for supporting my research.

I want to thank Dr. Özgür Gürses for taking the grand challenge of working on the Turkish Straits System. Significant part of this study is built on his priceless efforts. Prof. Emin Özsoy, Ersin Tutsak, Dr. Eva Jarosz generously provided their observational datasets those I used in this study.

To my friends, in Bologna, Maria del Mar, Paola, Andrea, Eleni, Miriam, Tomas, Vivianna, Giulia... They made it more fun to live in this nice city. Special thanks to Özgür, Claudia, Alessia, Utku, Leone, Marianna and Antonio also for tolerating me when I was sad or got mad.

To my friends, in Turkey, Erman, Mustafa, Erçin, Özge, Gaye ... for their life-long friendship.

And to my family, my mother Şerife, my father Tuncay, my sister Zeynep and my brothers Yusuf and Okan, for their patience. To my nephew, Meriç, with my apologies for not being able to spend enough time with him to date.

Finally, my dedication to my grandmother, Emine Aydoğdu, with the hope that when she has gone she knew how much she did for me.

Babaanneme,

Abstract

The design of the observing systems has become an important research area in the atmosphere and ocean communities. Some methodologies have been proposed to decide an optimal design for the existing or future observing systems. In this study, we apply the Observing System Experiments (OSE) and Observing System Simulation Experiments (OSSE) in the Adriatic Sea and the Marmara Sea. A fishery observing system (FOS) has been examined in the Adriatic Sea. The assimilation of temperature observations shows that the FOS is capable of improving the analysis. Moreover, the results of the OSE have proposed that the present FOS design may become optimal by reducing the number of fishing vessels close to each other while focusing more around the seasonal thermocline depth. The synthetic salinity observations are assimilated in the OSSE in addition to the temperature to test a possible impact of CTD sensor in place of the existing one. The assimilation of salinity didn't have impact significantly at least during the mixing season. The application of the OSE in the Marmara Sea is more challenging since no sustainable monitoring network exists yet. Before examining the impact of a ferrybox monitoring network in the eastern Marmara Sea by OSSE, we performed two inter-annual simulations with a very high resolution three dimensional ocean model forced by the realistic atmosphere for what we believe is the first time in the Turkish Straits System (TSS). The two simulations show that a realistic simulation of the TSS is possible and that the model is capable to represent many of the qualitative characteristics of the system. Furthermore, the results demonstrate that the halocline and thermocline can be kept similar to observations and stable throughout the integration. The comparison of the two simulations revealed the sensitivity of the TSS to the surface salinity. The wind work in the Marmara Sea is shown to be high which attributes an important role to wind on energizing the circulation. This highly energetic small basin has two main inter-annual surface circulation structures. First structure is form under relatively weaker wind forcing. The Bosphorus outflow moves to the south and then turns westward to exit from the Dardanelles. Second type of surface circulation is formed by the intensification and the extension of wind over the Marmara Sea. It consists of a cyclonic gyre in the middle of the basin. Using the model configuration of these two simulations we performed an OSSE in the Marmara Sea by mimicking a ferrybox network in the eastern basin to see the impact of temperature and salinity assimilation along the outflow of the Bosphorus. We have shown that assimilation improves the analysis significantly. Moreover, the reduction in errors propagates to the western basin where no data is assimilated. Therefore, we concluded that ferrybox network would be an initial sustainable observing system on the way to design an observation array in the Marmara Sea.

TABLE OF CONTENTS

[1] This chapter was published as Aydoğdu, A., Pinardi, N., Pistoia, J., Martinelli, M., Belardinelli, A., and Sparnocchia, S. (2016). Assimilation experiments for the Fishery Observing System in the Adriatic Sea. Journal of Marine Systems, 162:126-136. Progress in marine science supported by European joint coastal observation systems: The JERICO-RI research infrastructure. http://dx.doi.org/10.1016/j.jmarsys.2016.03.002

LIST OF FIGURES

LIST OF TABLES

General Introduction

Since Munk and Wunsch [1982] argued the possible developments in 1990s, our capability of monitoring the ocean has increased significantly in the last four decades. They suggested the basin-wide ocean observing systems as a precondition on the way to understand the dynamics of the ocean and its role in the climate and weather systems. In the last decades, a wide network of ocean observation systems has been established including satellites and in-situ arrays [Haines, 2010]. Many regional ocean observing systems from most part of the world are connected under a global ocean observing system (GOOS). However, large areas of the world ocean such as the deep open ocean and coastal zones are still not covered by the present observing systems despite the ongoing efforts.

A common approach to extend our knowledge about the ocean is blending the observations with model estimates in an optimal way using data assimilation techniques. The developments in the data assimilation made it possible to study the observed and unobserved ocean together. Besides all the other benefits, data assimilation allows to evaluate the design of the existing observing systems and test possible future developments by using Observing System Experiments (OSE) and Observing System Simulation Experiments (OSSE) methodologies. These methodologies have been intensively used by the atmospheric community for the impact assessment of new instruments and design of their implementation since last four decades [Atlas, 1997; Masutani et al., 2010]. In the ocean, the applications of OSSE have been increased in the last decade [Alvarez and Mourre, 2014; Halliwell Jr et al., 2015, 2014; Masuda, 2014; Raicich, 2006].

In this thesis, the first goal is to assess the impact of a new type of observing called Fishery Observing System (FOS) in the Adriatic Sea. A fully-coupled NEMO/3D-Var ocean data assimilation system is used to apply OSE and OSSE methodologies. We evaluate the impact of the temperature observations collected by the fishing vessels in the western coast of the Adriatic Sea. The experiments are conducted by a year of dataset gathered in 2007. The present design of the network has been evaluated and an optimal design has been proposed. Moreover, possible impacts of a CTD sensor have been examined by assimilating the synthetic salinity observations in addition to the temperature. The manuscript of this study is already published and presented in Chapter 1.

Another aim of the study is to perform a similar OSSE in the Marmara Sea. The Marmara Sea is a component of a water passage known as Turkish Straits System (TSS). The TSS connects the Black Sea and the Mediterranean by two narrow straits, namely, Bosphorus and Dardanelles and the Marmara Sea. The hydrological differences between the Black Sea and the Mediterranean

sustain a highly stratified two-layer flow system. Together with the very complex topography, it constitutes a challenging natural ocean laboratory [Ünlüata et al., 1990]. So far, the understanding of the system relied on the observations which makes it difficult to see the whole picture. Until recently, the modeling studies considered the separate compartments of the integral system because of the demand for high-resolution in the straits [Chiggiato et al., 2012; Hüsrevoğlu, 1998; Oguz et al., 1990; Sözer, 2013]. However, the model implementations for the integral system started to arrive with the increasing computational capacity. Sannino et al. [2015] and Gürses [2016] developed two different models including both the straits and the Marmara Sea.

Gürses [2016] implemented an unstructured mesh model in the TSS and performed a year of simulation of the whole system forced by the atmospheric variables for the first time. In this study, we continue to use the same model for further assessment. The second part of this thesis presents two six year long simulations of the TSS. The simulations demonstrate the inter-annual variability of the integral system for the first time by using a three dimensional ocean circulation model with atmospheric forcing. The hydrological aspects of the results are shown in Chapter 2. The dynamical aspects of the system and the circulation in the Marmara Sea are presented in Chapter 3.

The TSS model is coupled with an ensemble-based data assimilation system to perform the OSSE in the Marmara Sea. We propose a sustained monitoring system for the Marmara Sea based on the ferries which already operate for transportation between different cities. We examined a ferrybox array by loading temperature and salinity sensors to some of the ferries in the eastern Marmara Sea. The details and results of the OSSE are shown in Chapter 4.

In the last chapter, we give an overall summary and conclusions of the thesis.

Chapter 1

Assimilation experiments for the Fishery Observing System in the Adriatic Sea [1]

[1]This chapter was published as Aydoğdu, A., Pinardi, N., Pistoia, J., Martinelli, M., Belardinelli, A., and Sparnocchia, S. (2016). Assimilation experiments for the Fishery Observing System in the Adriatic Sea. Journal of Marine Systems, 162:126-136. Progress in marine science supported by European joint coastal observation systems: The JERICO-RI research infrastructure. http://dx.doi.org/10.1016/j.jmarsys.2016.03.002

Abstract

An impact assessment of a Fishery Observing System (FOS) network in the Adriatic Sea was carried out with an ocean circulation model fully-coupled with a data assimilation system. The FOS data are single point vertical values of temperature collected in 2007. In this study, we used the Observing System Experiment (OSE) and Observing System Simulation Experiment (OSSE) methodologies to estimate the impact of different FOS design and sensors implementation. OSEs were conducted to evaluate real observations and they show that the FOS network improves the analysis significantly, especially during the stratification season. Root mean square (RMS) of temperature errors are reduced by about 44% and 36% in the upper and lower layers respectively. We also demonstrated that a similar impact can be obtained with a reduced number of vessels if the spatial coverage of the data points does not change significantly. In the OSSE, the impact of the implementation of a CTD (conductivity-temperature-depth) sensor in place of the existing temperature sensor was tested with identical twin approaches between January and April 2007. The results imply that the assimilation of salinity does not improve the analysis significantly during the winter and spring seasons.

1.1 Introduction

Integrating new types of coastal observing systems into high resolution shelf and coastal ocean models is important for forecasting and obtaining best estimates of the essential marine variables in the shelf and coastal areas of the world's oceans. Since the real time global ocean observing system has become a reality in support of ocean forecasting in the open ocean regions [Dombrowsky et al., 2008], the challenge is now to define the strategy of the observing system for shelf and coastal areas.

There are various methods to analyze the impact of observing systems [Oke and OKane, 2011] on ocean dynamical field reconstructions. One of these is the Observing System Experiment (OSE) which is widely used in the atmospheric and oceanic community. It is a data-denial approach evaluating the impact of the excluded set of observations with a reference to a best estimate that assimilates all the data.

Another methodology is the Observing System Simulation Experiment (OSSE). The rationale is similar to the OSE but the OSSE evaluates the possible impact of a future observing system or various design strategies of the existing system together with new ones. In atmospheric research, the OSSE methodology has been used for the last three decades [Arnold Jr and Dey, 1986; Masutani et al., 2010]. For the Mediterranean Sea, Raicich [2006] used an identical twin approach in which a model simulation was used as the truth or nature run from which the synthetic observations are generated, and a perturbed model simulation is generated that differs from the nature run. Synthetic observations are assimilated in the perturbed model simulation and the estimated field variables are inter-compared with the nature run. Masuda [2014] studied the effectiveness of concentrated observations for an ocean state estimation in a region remote from the observation site in the North Pacific with the same approach. On the other hand, Alvarez and Mourre [2014] studied the design of a glider network with a fraternal twin approach, in which the nature run and the forecast model are the same but with different physical configurations. Finally, Halliwell Jr et al. [2015, 2014] used the fraternal twin approach and extensively validated their OSSE by comparing it with the reference OSEs.

We focus on the Adriatic Sea where a Fishery Observing System (FOS) has been developed to collect in-situ environmental data using fishing vessels [Falco et al., 2007]. The FOS is one of the most notable vessels of opportunity networks along with the RECOPESCA program [Leblond et al., 2010]. Designing a ship-of-opportunity optimal network is challenging and alternative

strategies for collecting vertical temperature profiles on fishing vessels in the coastal and open ocean are being evaluated [Kourafalou et al., 2015].

In this study, we use a high-resolution ocean circulation model coupled to a data assimilation system in order to assess the impact of specific FOS observations. In our case, FOS data are single vertical point measurements rather than profiles, and it is important to evaluate their impact on quality analysis since this ship-of-opportunity measurement system is cheap and does not impact on fishing activities. We performed Fishery Observing System Experiments (FOSE) to evaluate the impact of the geographical network and the temperature measurement depth distribution. We then designed a Fishery Observing System Simulation Experiment (FOSSE) to estimate the impact of the implementation of a CTD sensor instead of the temperature-only sensor that currently exists.

The paper is organized as follows: Section 2 introduces the model and data assimilation system and the FOS observations provided in 2007 are detailed. Section 3 presents the FOSE design and results. Section 4 is devoted to FOSSE, and the overall results are discussed in Section 5.

1.2 Materials

1.2.1 Model description

The model configuration is described in detail by Gunduz et al. [2013] and will only be outlined here. The model uses the NEMO (Nucleus for European Modeling of the Ocean, Madec [2008]) code in its explicit free surface, linear formulation. It has a constant horizontal grid resolution of 1/48° corresponding to 1.8 and 2.3 km in longitudinal and latitudinal directions, respectively, and 120 unevenly spaced z-levels with partial cells at the bottom. The vertical grid is 1 m in the top 60 m, increasing to 9 m at a depth of 100 m and to 50 m at the deepest point in the Adriatic Sea. The largest spacing of 70 m is in the Ionian Sea at the deepest point (2800 m, Fig. 1.1).

Atmospheric surface momentum, heat and water fluxes are computed using European Centre for Medium-Range Weather Forecasts (ECMWF) ERA-Interim surface fields and bulk formulas. However, precipitation is taken from the Merged Analysis of Precipitation (CMAP) observational dataset [Xie and Arkin, 1997]. The ERA-Interim atmospheric forcing fields are available at a 6-hour frequency and horizontal resolution of 0.25°.

The model domain has one open boundary that communicates with the Mediterranean Sea positioned south of the Otranto Strait (Fig. 1.1). The boundary conditions for temperature,

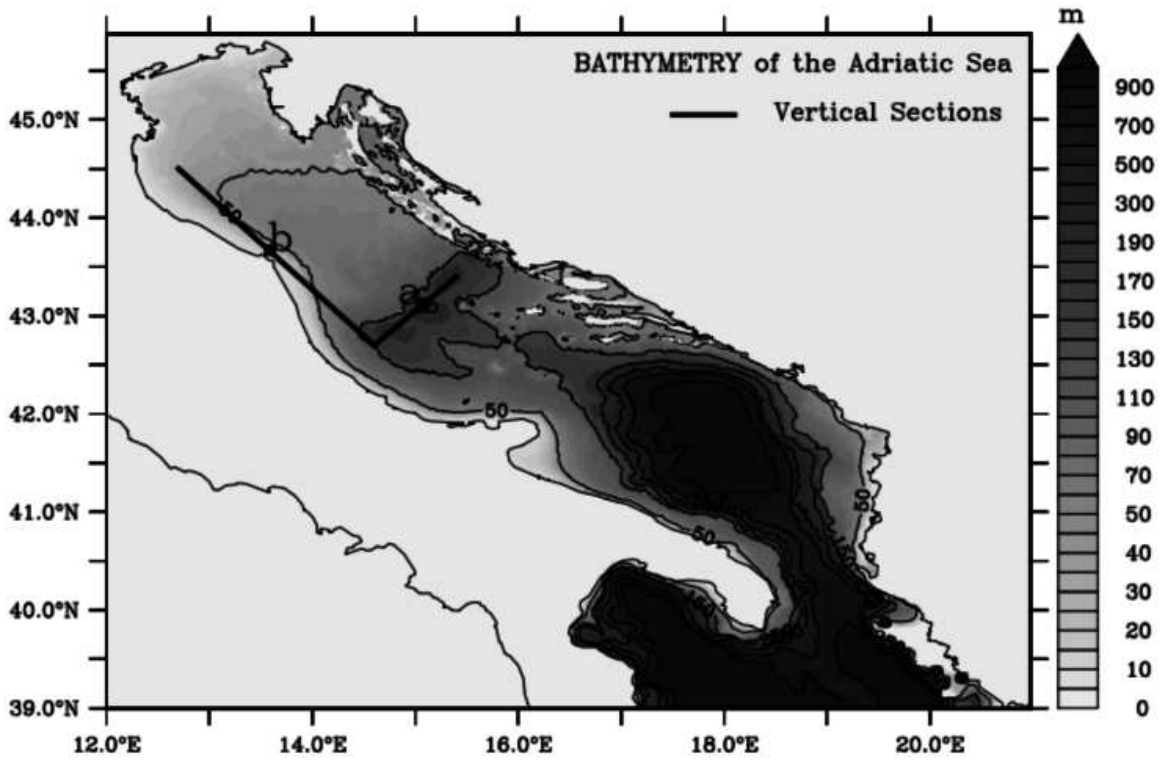

Fig. 1.1. Bathymetry of the Adriatic Sea. The section indicated with the line segments are used for studying vertical structure of the water column. The locations (a) and (b) are the reference points for the black and green lines, respectively, in the vertical cross-sections.

salinity, sea surface height, zonal and meridional currents are provided daily from the large-scale MFS [Pinardi and Coppini, 2010].

The initial conditions of the model were taken from the simulation by Gunduz et al. [2013] in order to coincide with 1 January 2007, and the simulation period is up to December 2007.

1.2.2 Data assimilation scheme

The OceanVar data assimilation scheme [Dobricic and Pinardi, 2008] is implemented in the Adriatic Sea using a new description of the vertical background error covariances. As described in Dobricic et al. [2005], part of the background error covariance is represented by vertical multivariate Empirical Orthogonal Functions (EOFs) for temperature and salinity. In our study the vertical EOFs were calculated at each model grid point and monthly, using a 10 year-long sim-

ulation [Gunduz et al., 2013], and the salinity and temperature variances as a departure from a monthly mean seasonal climatology.

The horizontal part of background error covariance is assumed to be Gaussian isotropic, depending only on distance. It is modeled by the successive application of the recursive filter in longitudinal and latitudinal directions, which provides a high computational efficiency in each iteration of the algorithm. The rapidly evolving part of the background error covariance, consisting of the sea level and they barotropic velocity components, is modeled using a barotropic model forced by the vertically-integrated pressure innovations resulting from temperature and salinity variations. The assimilation scheme of Dobricic and Pinardi [2008] is multivariate, i.e. temperature, salinity and sea surface height observations produce corrections not only in the corresponding state variables but also in the vertically correlated state variables, in particular the velocity fields. The assumption that the horizontal error correlation structure is homogeneous and isotropic is an important limitation of the scheme. This correlation structure is not adequate for strongly anisotropic flow fields as they exist along the western boundary of the Adriatic Sea and this might be responsible for some reduced impact of observations in the analysis quality.

1.2.3 The Fishery Observing System

The FOS data used in this study consists of seven different vessels from five different fleets [Falco et al., 2007]. The fleets are located in Chioggia, Rimini, Ancona, San Benedetto del Trento and Giulianova from north-west to mid-west Adriatic Sea, respectively (Fig. 1.2). StarOddi sensors are installed on the nets of the pelagic pair trawlers and purse seine fishing vessels. Sensors measure the temperature with an accuracy of $\pm 0.1^{\circ}$C. The depth is calculated from the pressure with a minimum accuracy of approximately ± 0.2 m. Profiles taken during the release and hauling of the net were excluded due to a stabilization problem of the sensor. Only the measurements taken at the fishing depth were used. This means that temperature is measured at a specific single vertical point. The sensor remains at that depth for approximately 23 h along the vessel track for the pelagic pair trawlers. The temperature doesn't change significantly along the track once the sensors get stabilized at depth as shown in Fig. 1.3 (upper panel). Thus the observations used in the assimilation are the average of the temperature values measured during the vessel drifting time. The result is the dataset of single vertical point measurements illustrated in Fig. 1.2 and 1.3 (lower panel).

The measurement points reach a maximum depth of 160 m however most stay within the first

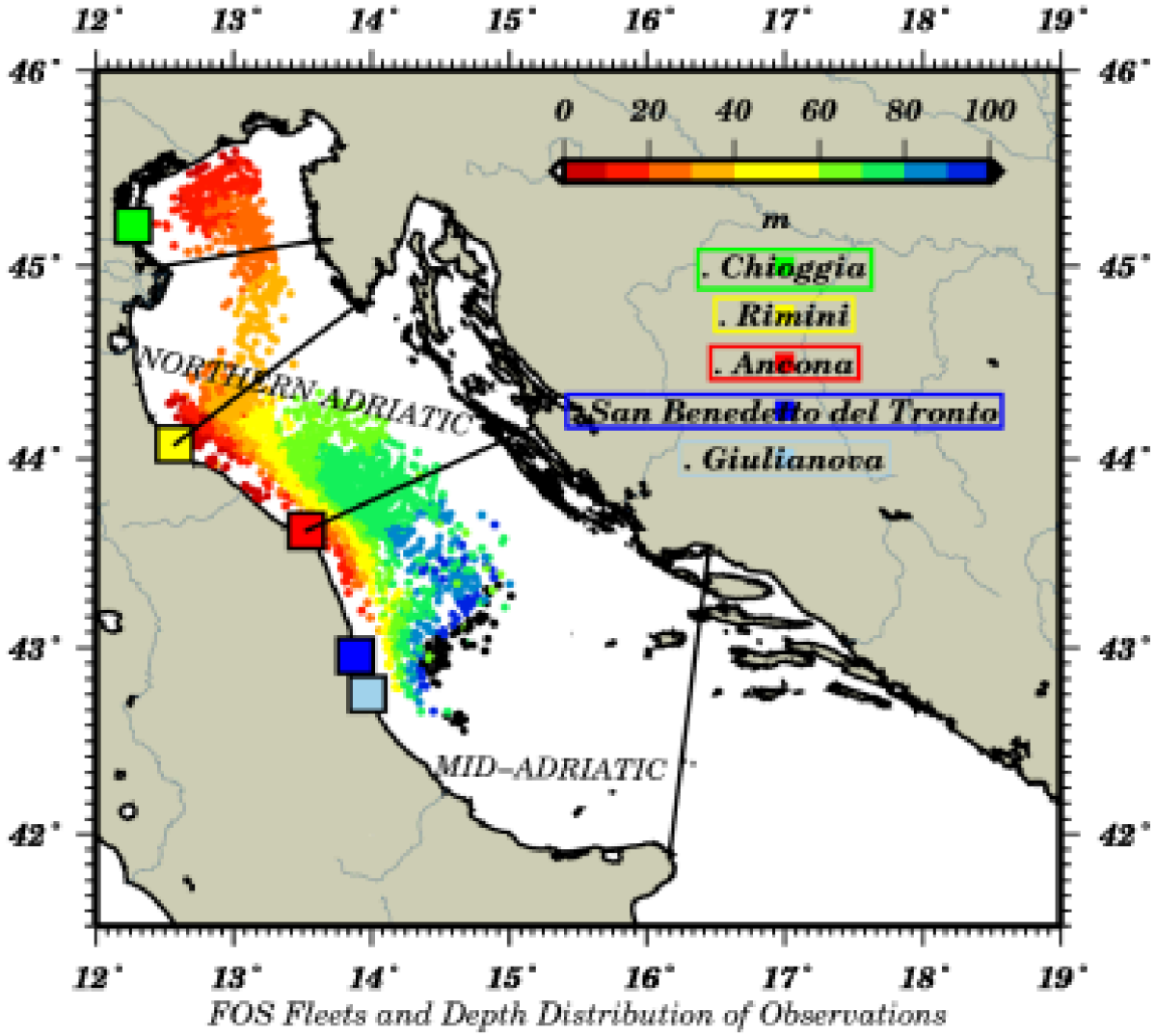

Fig. 1.2. FOS observations distribution and their nominal depth for the year 2007. The squares show the locations of fleets in the Adriatic Sea involved in collecting the data.

100 m. The largest amount of data was collected by the Ancona and Rimini fleets (Fig. 1.3) because two vessels were used for these fleets whereas only one vessel was available in each of the other three fleets. The least amount of data was collected in August due to the restrictions in fishing activities.

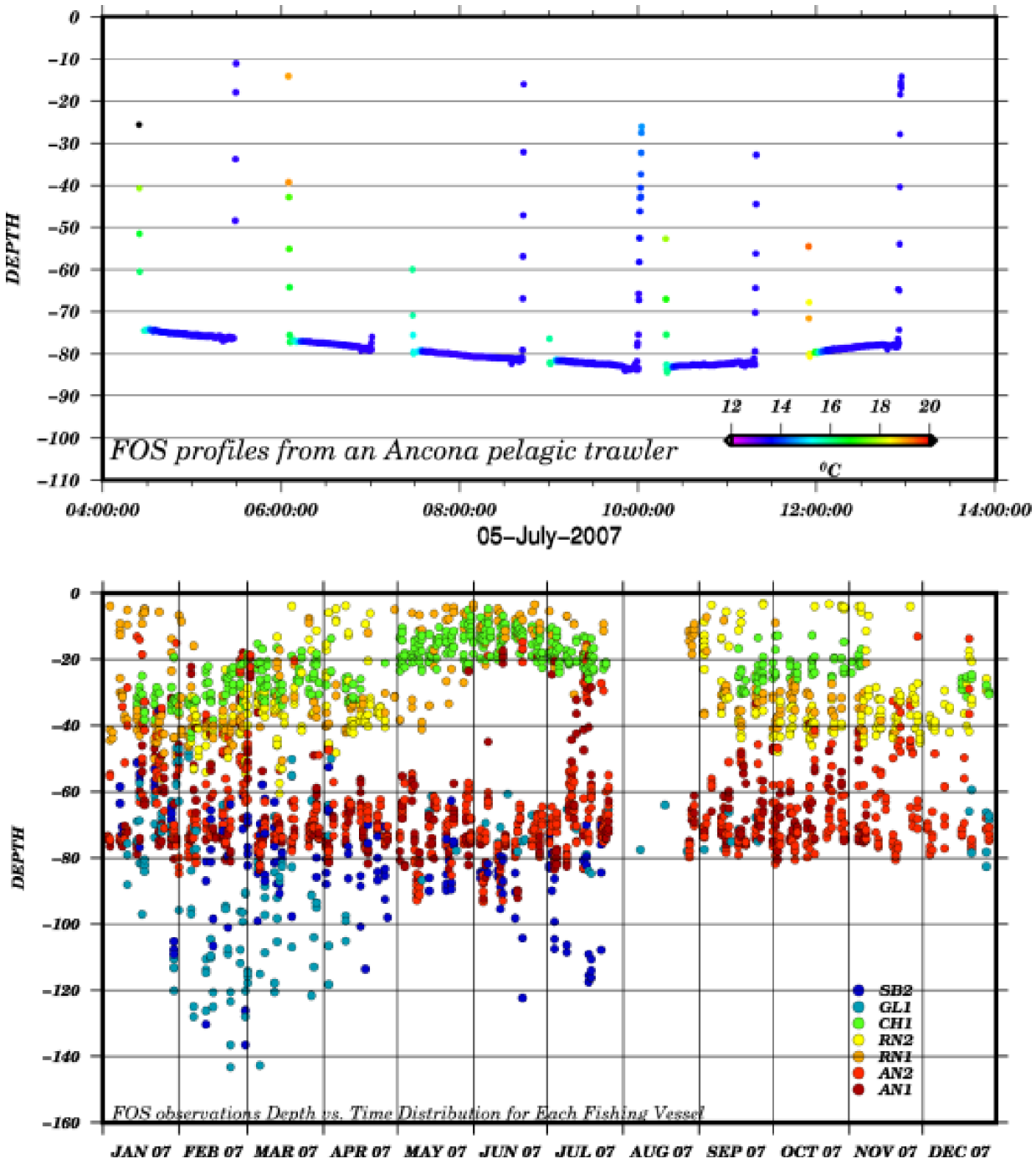

Fig. 1.3. Temperature of sample profiles from an Ancona pelagic trawler in 5 July, 2007. Time axis shows the hour of the day (upper panel). Distribution of FOS observations with depth and months of 2007 (lower panel). The data collected by each vessel are shown with a different color. The vessels from Ancona, Rimini, Chioggia, Giulianova and San Benedetto del Tronto are plotted as red, yellow, green, light blue and blue circles, respectively.

1.3 Fishery Observing System Experiments (FOSEs)

1.3.1 Design of the FOSEs

The FOSEs were designed to show the impact of the FOS measurements described in Section 2.3 on the quality of analysis with respect to simulations and to check the impact of a lower number

of fishing vessels on the quality analysis. All the experiments are listed in Table 1.1.

Experiment	Type	Assimilation
Control run	Simulation	NO
Best estimate	Assimilation	ALL FOS
OSE01	Assimilation	Four vessels
OSE02	Assimilation	All vessels except Ancona

Table 1.1: Fishery Observing System Experiment (FOSE) design.

Experiment	Chioggia	Rimini	Ancona	Guilianova	S. Benedetto
Control run	0	0	0	0	0
Best estimate	1	2	2	1	1
OSE01	1	1	1	1	0
OSE02	1	2	0	1	1

Table 1.2: Number of fishing vessels used in experiments from each fleet.

It would be interesting to see the impact of the FOS along with other observations but given the specific area we decided not to consider complementary satellite observations. To our knowledge FOS is the only systematic large scale in situ observing system for the Adriatic Sea shelf areas. Only satellite data could be considered at the same level, in particular altimetry and sea surface temperature (SST). However, in shelf areas of the Adriatic Sea satellite altimetry consists only of few tracks and, due to the closeness of coastlines, the accuracy of the retrieved signal is low. For SST, accuracy is also low due to the low seawater coastal temperatures which interfere with the cloud detection algorithm. Thus it was decided to concentrate only on FOS observations which are at the moment the only systematic in situ observing component for the Adriatic Sea shelf areas with a reasonable accuracy.

The control run was performed without assimilation as a reference experiment to assess the impact of the assimilation. All of the observations were then assimilated to produce an analysis or 'best estimate'. Two other experiments were designed: the first, OSE01, used the observations only from four of the vessels, while OSE02 completely neglected the Ancona fleet.

In OSE01 the observations collected by one of the two fishing vessels from Ancona and Rimini fleets were excluded (AN2 and RN2 in Fig. 1.3, respectively). The observations from the San Benedetto fleet were not used since the fleet was close to the Giulianova fleet. OSE01 was performed with four vessels to assess the impact of observations covering all regions but with fewer vessels (see Table 1.2).

Most of the data collected by the Ancona fleet, which amounts to 45% of the total data, was under a depth of 30 m which is approximately the depth of the surface Ekman layer and also

the T,S mixed layer [Artegiani et al., 1997]. OSE02 was therefore performed without using the Ancona data in order to evaluate the impact of the shallower observations alone.

1.3.2 Evaluation methodology for the FOSEs

The FOSEs were compared using misfits and analysis residuals. The misfit, also called innovation, is the difference between the observation and the background state at the location of the observation. It can be written as $m = y - H(x_b)$ where x_b is the background state, H is the observation operator mapping the background from model space to the observation space and y is the observation. The root mean square of the temperature misfits (hereafter, RMS error) are calculated weekly in two different layers of the water column as follows:

$$RMS = \sqrt{\frac{1}{N}\sum_{i=1}^{N}(y - H(x_b))_i^2} \tag{1.1}$$

where N is the number of observations in a week in the averaging layers, chosen to be 0-40 m and 40-100 m. Since the misfits are calculated before the assimilation of the FOS data, they can be considered as quasi-independent observations.

The RMS of misfits are evaluated by using the entire FOS data set regardless of the excluded observations in OSEs. The impact of data is considered to be positive if the RMS error is reduced in the assimilation experiments compared to the control run.

1.3.3 Results of the FOSEs

In Fig. 1.4, the RMS of temperature misfits are shown for all the FOSEs. In the control run, the RMS error shows a significant seasonality in the upper 0-40 m layer reaching up to 2.5°C during the stratification season and then decreasing again in autumn. On the other hand, in the 40-100 m layer the maximum error is achieved in autumn due to the deepening of the surface mixed layer after the summer [Artegiani et al., 1997]. The mean control run RMS temperature error throughout the year is 1.3°C for the upper layer and 0.5°C for the lower layer.

When we assimilate all the FOS observations in the best estimate experiment, the RMS error falls significantly and does not exceed 2°C throughout the year. During the stratification season, when the misfit between the data and model is higher, the reduction in the RMS error is bigger than the annual mean. The mean RMS error of the best estimate throughout the year is 0.74°C in the upper layer, which corresponds to a reduction of 44% compared to the control run. In the

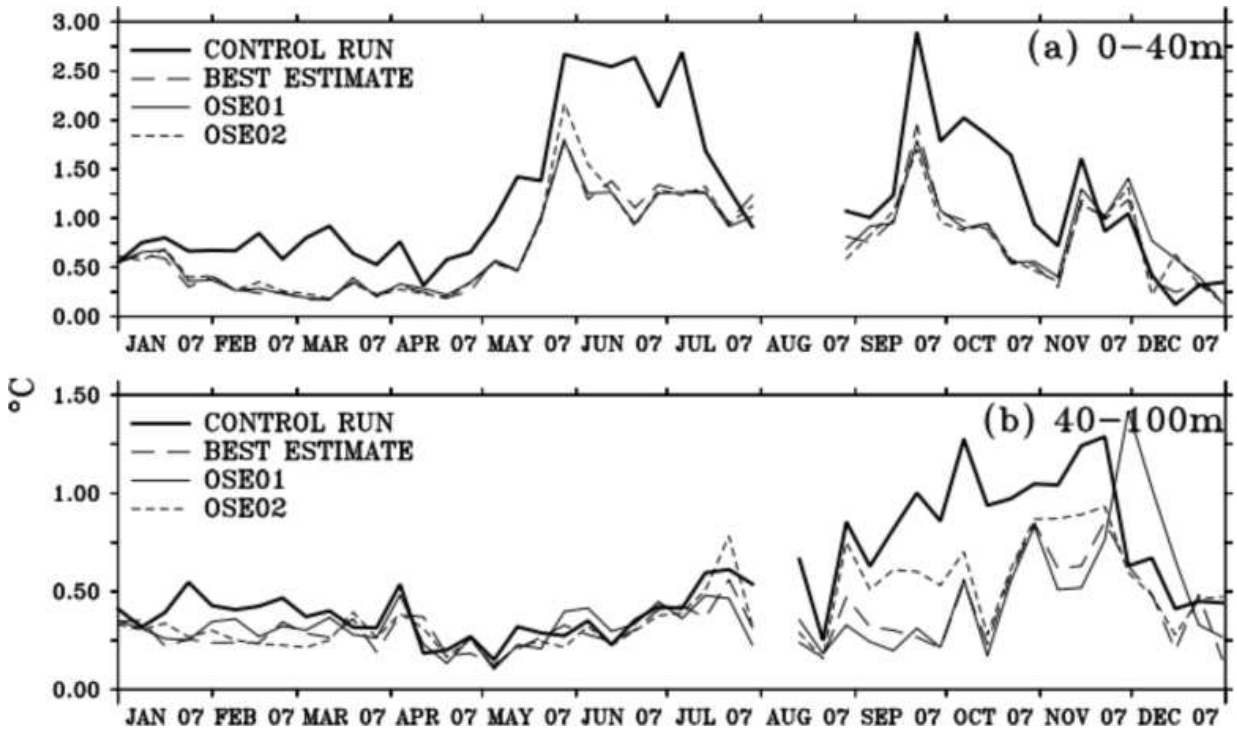

Fig. 1.4. Time series of weekly RMS of temperature misfits for all the FOSEs, the control run, the best estimate, OSE01 and OSE02 for a) the 0-40 m layer and b) 40-100 m layer. Symbols corresponding to each experiment are shown in the legend.

lower layer, it is 0.3°C which means a 36% reduction in the error. In addition to the improvement in the RMS error, the bias in the best estimate is 79% and 88% less than the control run in the upper and lower layers, respectively (Table 1.3).

	RMS error			Bias		
	Control run	Best estimate	Reduction	Control run	Best estimate	Reduction
0-40 m	1.3	0.7	44	0.5	0.1	79
40-100 m	0.5	0.3	36	0.2	0.03	88

Table 1.3: Estimates of yearly mean RMS temperature errors and bias for the control run and the best estimate experiments. The last column shows the reductions in RMS error and bias after the assimilation in the best estimate are also listed.

	Best estimate	OSE01	OSE02
March	340	191 (57%)	207 (62%)
July	292	174 (60%)	129 (44%)

Table 1.4: Number of assimilated observations for March and July in each of best estimate, OSE01 and OSE02. Ratios of the assimilated observations to the whole dataset are given in percentages.

In the best estimate, 76% of the data passed the quality check of the data assimilation system, i.e. the difference between the model and the observations was less than 5°C and the depth is less than the bathymetry. The amount of assimilated data decreased by about 40% in OSE01 and 50% in OSE02. The decrease of data in the different experiments is given in Table 1.4: we present

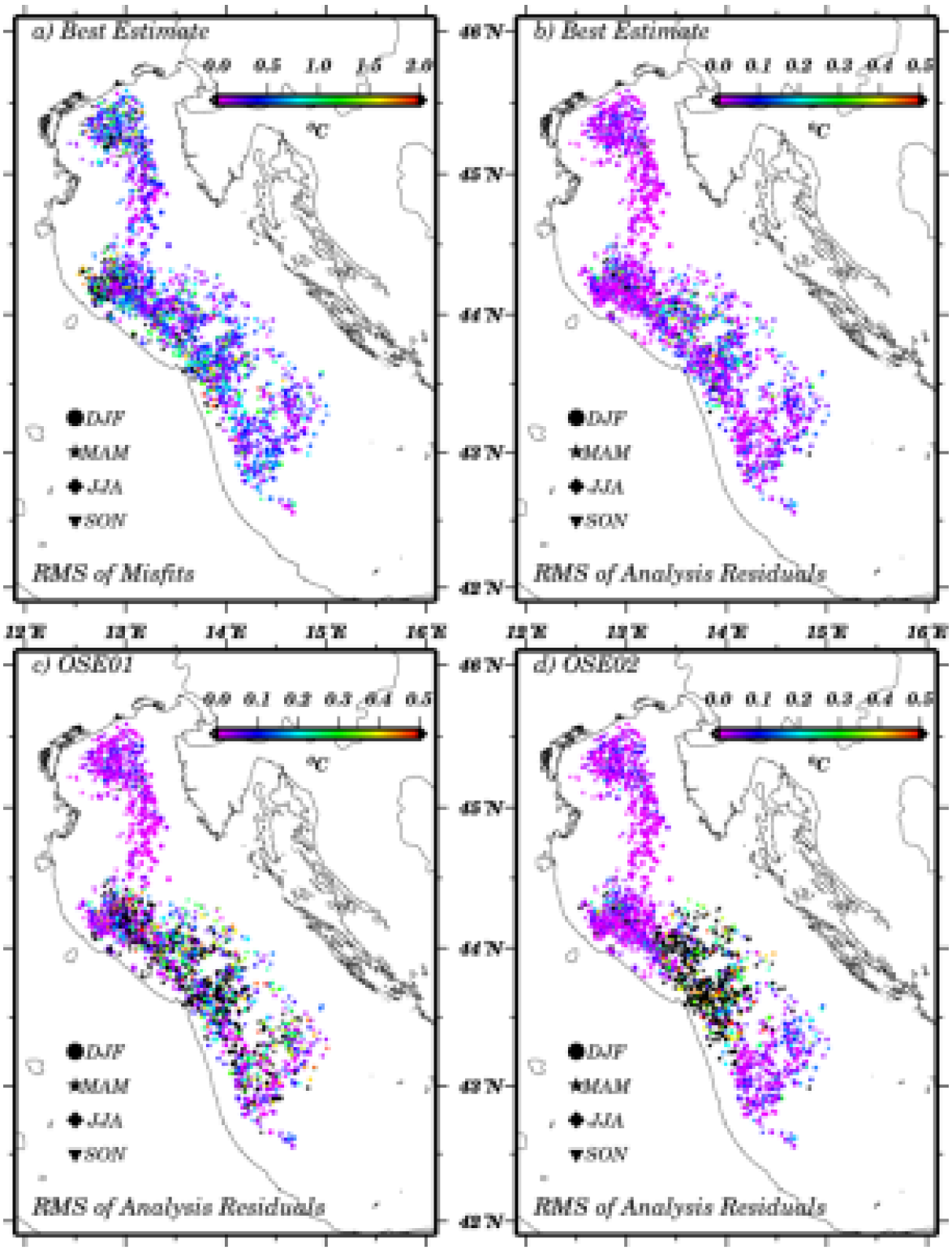

Fig. 1.5. Spatial distribution of temperature a) misfits and b) analysis residuals for the best estimate (top two panels). The bottom two panels illustrate the analysis residuals for c) OSE01 and d) OSE02. The data of different seasons are represented by different symbols such that circles for DJF, stars for MAM, diamonds for JJA and inverted triangles for SON months of 2007. Color scales are different for each figure.

only March and July because they are representatives of the mixing and stratification seasons. In both OSEs, the denial of a subset of data doesn't degrade significantly the solution in terms

of temperature misfit RMS error (Fig. 1.4). The OSE01 shows that the impact of decreasing to four fishing vessels is negligible because the four vessels chosen sample almost the same horizontal areas as the full fleet, only with fewer repeated measurements. If we exclude the Ancona fleet, in OSE02 the impact is again similar to the best estimate for most of the time. Since the samples provided by the Ancona vessels were mostly below a depth of 40 m, we conclude that fewer data are sufficient to increase the deep layer quality analysis with respect to the simulation. However, there is a degradation of RMS in both OSE01 and OSE02 at the end of November and in December. Similarly, OSE02 shows a larger RMS during the whole September. We think that these larger RMS values are caused by the same dynamics will be discussed at the end of this section.

In Fig. 1.5, the spatial distribution of errors are shown. In Fig. 1.5a and b, the RMS of temperature misfits and RMS of temperature analysis are compared. Moreover, the analysis RMS of OSE01 and OSE02 are presented in Fig. 1.5c and d, respectively. The RMS of misfits for the best estimate are higher in the north-western part of the basin, mainly due to the impact of PO river. The errors exceed 3°C along the coast of Rimini. On the other hand the errors are reduced in that area as well as the other regions in the analysis. (Fig. 1.5b). In the OSE01 and OSE02, the analysis errors are larger in the areas where we decreased the number of assimilated observations, as expected (Fig. 1.5c and d). Beside that the analysis RMS are similar where we assimilate in all experiments such as the northern-most Adriatic Sea.

The variational data assimilation algorithm produces a correction that is added to the background state variables. In Fig. 1.6, we show the vertical structure of the temperature corrections due to the assimilation of the FOS data for March and July. It is evident that the best estimate has the largest corrections to the background field with respect to OSE01 and OSE02 but the shape is largely the same since it is due to the vertical structure of the error covariance matrix. Fig. 1.6 shows that the single point vertical observations can correct the whole water column during the well-mixed season, while during the stratification season, the corrections are centered around the measurement layer that coincides with the seasonal thermocline.

In Fig. 1.7, we show the standard deviation around weekly mean temperature calculated by the background temperature values for all the experiments. The standard deviations in the assimilation experiments are getting smaller when the water column is well-mixed between January and May. However, following the thermocline formation during the summer, the standard deviation gets higher in the upper layer when the data is assimilated. Moreover, the deepening of the

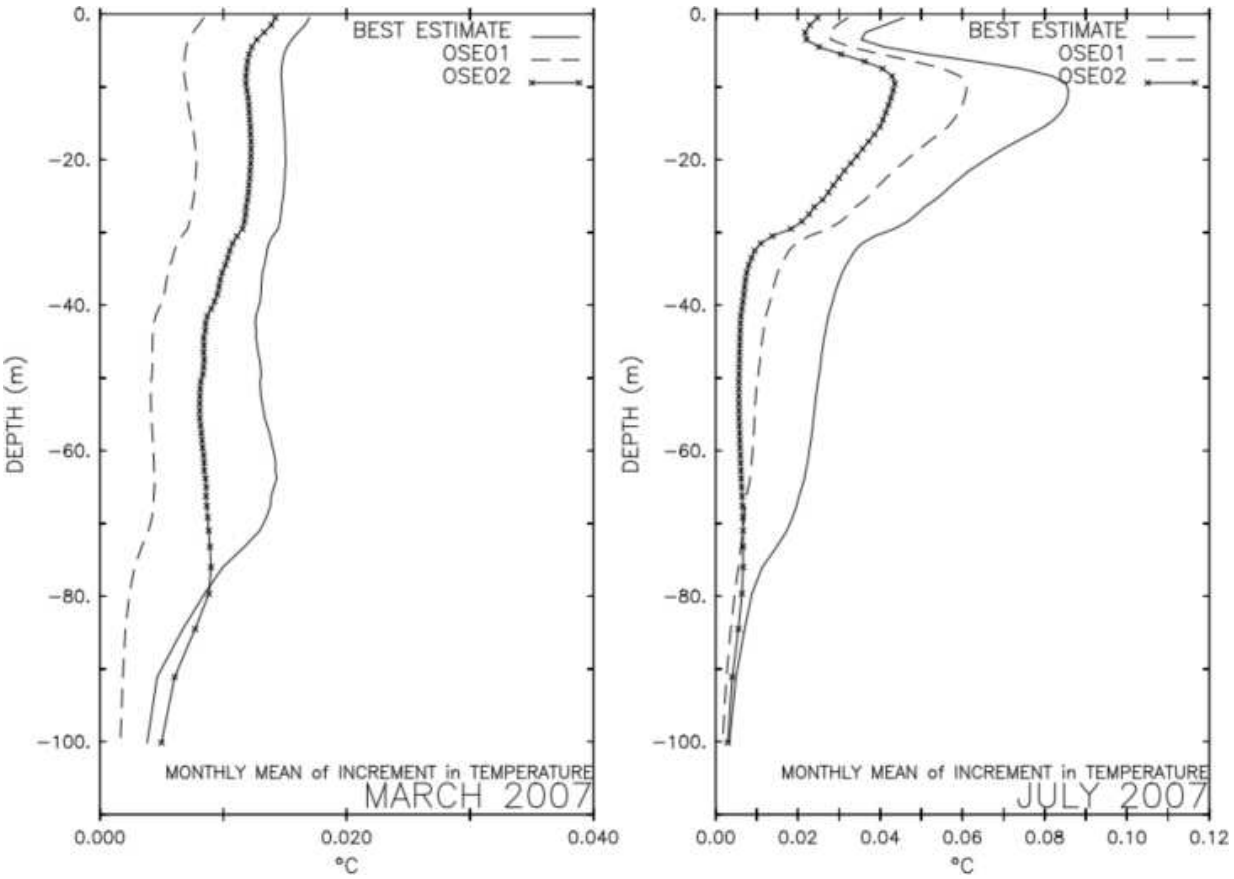

Fig. 1.6. Monthly basin mean of increments in the best estimate (full line), OSE01 (dashed line) and OSE02 (crossed line). In March (left), the profiles are almost uniform until 70 m whereas in June (right) the correction is larger around the seasonal thermocline.

surface mixed-layer in September carries higher standard deviation to the lower layer. Therefore, we conclude that the assimilation of FOS increases the variance around the thermocline.

In order to show the impact of temperature assimilation experiments on the other non-observed variables, the mean SSH time series for the region between 42N-46N and 12E-16E and for all the experiments assimilating only FOS temperature is shown. In Fig. 1.8 the SSH is reproduced for all the experiments and the difference is small but visible and it is larger in the November and December periods where it was shown that OSE1 and OSE2 has a larger RMS error.

We compared the model mean sea surface temperature for each experiment with the OISST (Optimum Interpolation Sea Surface Temperature) 1/4° daily analysis product of NOAA. The analysis is constructed by combining observations from different platforms such as satellites, ships and buoys on a regular global domain [Reynolds et al., 2007]. We used only the AVHRR-only product which involves satellite SST only from AVHRR.

The assimilation-free control run SST (not shown) already agrees with the OISST except in

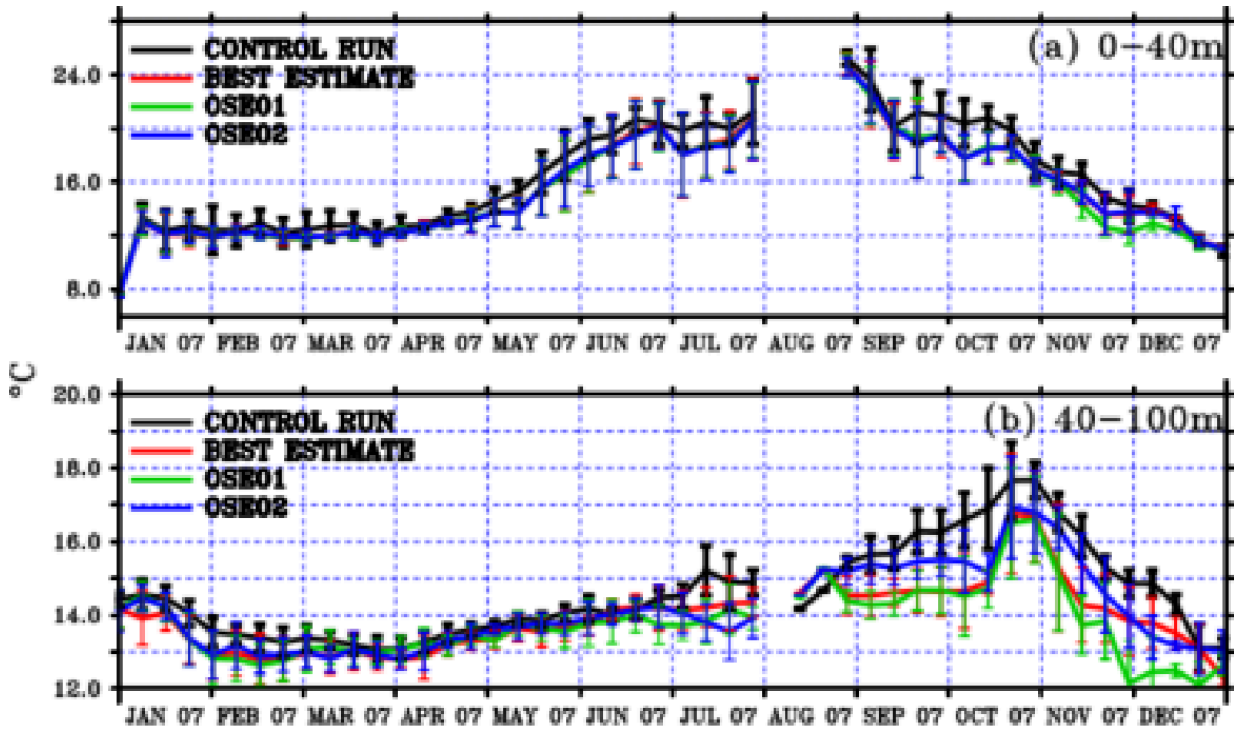

Fig. 1.7. Time series of weekly mean temperature calculated by the background values for the FOS dataset for all the FOSEs. The Control run, the best estimate, OSE01 and OSE02 are represented by black, red, green and blue lines, respectively a) for the 0-40 m depth layer and b) 40-100 m layer. Error bars show the standard deviation around mean

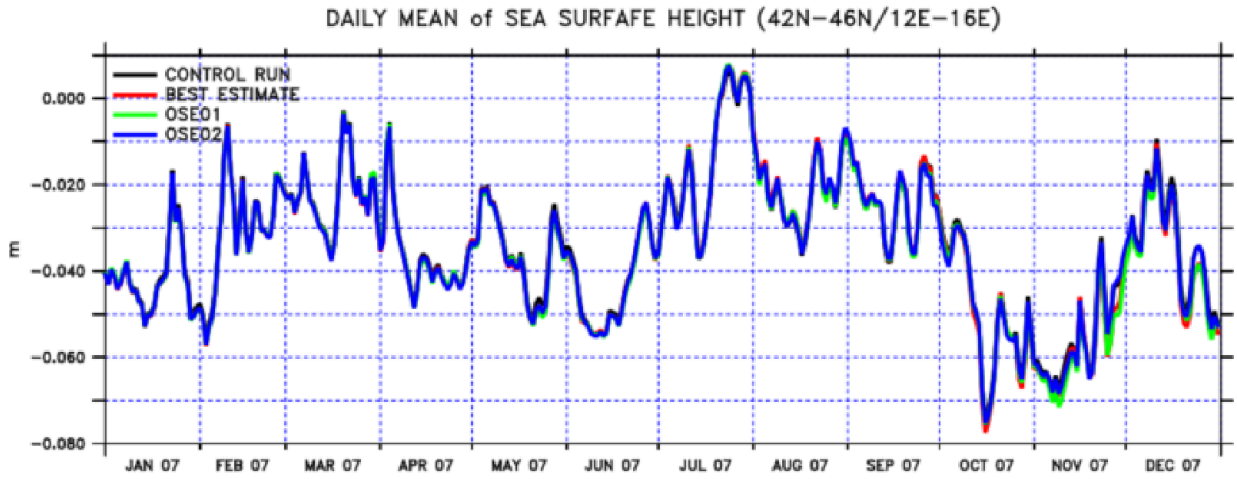

Fig. 1.8. Time series of daily mean sea surface height between the region 42N-46N and 12E-16E for all the FOSEs. The control run, the best estimate, OSE01 and OSE02 are represented by black, red, green and blue lines, respectively.

June and July. The free-model overestimates the SST in these two months as well as December. In the assimilation experiments, the impact of FOS on the SST seems very small. That is not surprising since the FOS is by design a subsurface observing system and the SST is generally restricted by the heat fluxes forcing the ocean model at the surface boundary.

The time series of RMS of misfits in Fig. 1.4 and mean temperature in Fig. 1.7 show a temperature minimum in OSE01 which is significantly different from the other experiments at

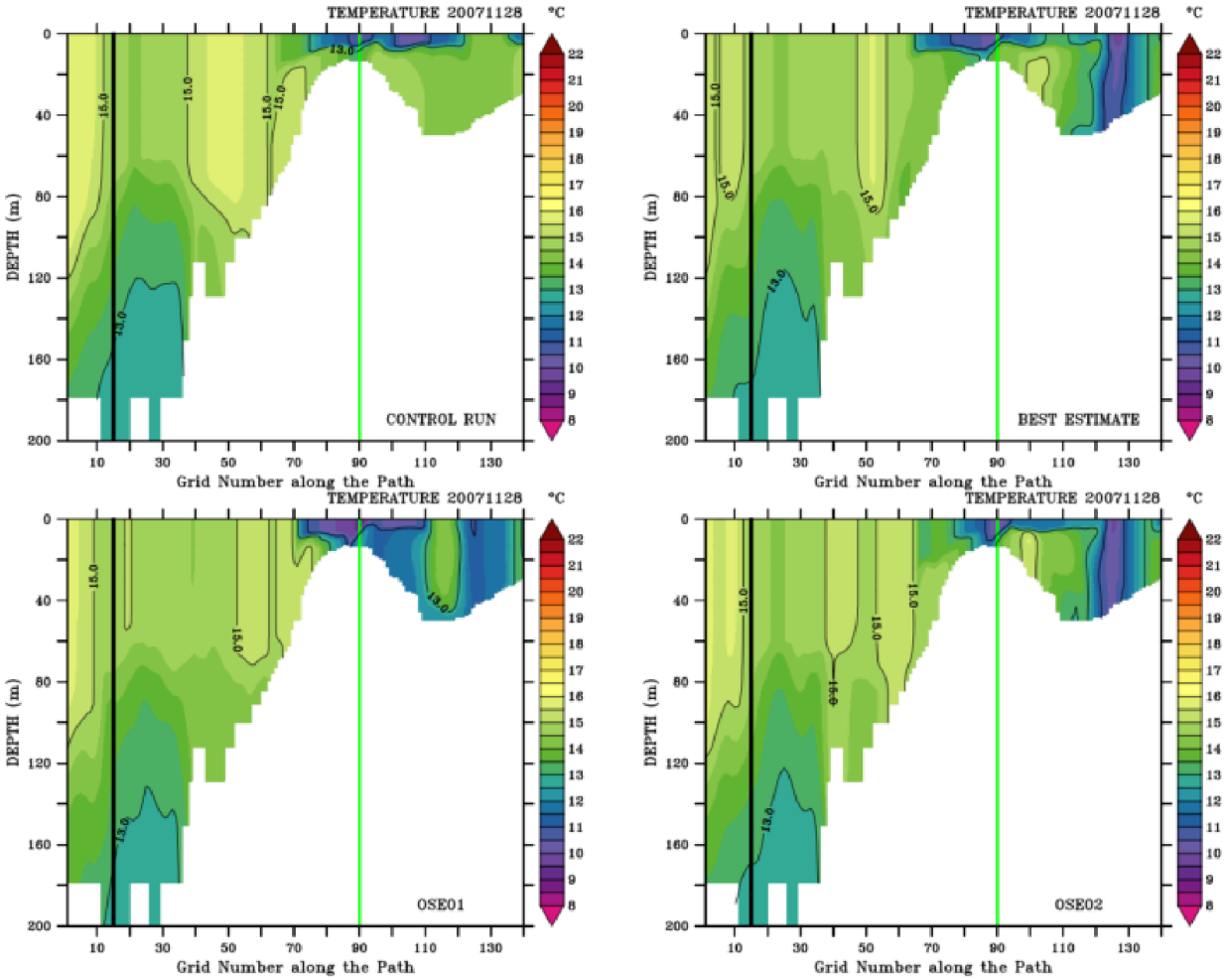

Fig. 1.9. Vertical structure of the water column following the section represented in Fig. 1.1 for 28 November 2007. Black and green lines correspond to the locations of the grid points (a) and (b), respectively shown in Fig. 1.1. The control run, the best estimate, OSE01 and OSE02 are shown from top left to bottom right, respectively.

the end of November 2007. We believe that this error is a result of the western Adriatic dynamics related to the Po river discharge and the jet along the western coast. As we described in Section 3.1, the OSE01 excludes the data from RN2 and AN2 vessels (see Fig. 1.3). When the data is assimilated, the temperature in the Po river impact area is corrected and decreases as compared to the control run in the subsurface layers. The resulting cold water masses are transported southward by the Western Adriatic Coastal Current [Artegiani et al., 1997] towards Ancona. If we stop to assimilate the data, as in the case of OSE01, the water reaching Ancona will be still cold (see Fig. 1.9) and will lead to larger errors. If we continue to assimi- late as in the best estimate (RN2 and AN2 are assimilated) and OSE02 (RN2 assimilated) we correct the fields and the RMS statistics become better compared to the control run. In the control run, however, since we never assimilate the path of the jet is already warmer than the other experiments, therefore the error is smaller compared to OSE01. As a result, we conclude that a FOS design with fewer observations

as in OSE01 or OSE02 may perform similar to the available FOS network. However, the deficit of data along the Western Adriatic Coastal Current for some period may degrade the analysis. Therefore, continuous monitoring in time may be more crucial than repeated observations in the same area.

Thus in conclusion, the assimilation of FOS temperature observations improves the analysis especially during the stratification season, despite being single point measurements. OSE01 also shows that the quality of the analysis does not change dramatically provided that the geospatial data coverage stays similar, while the number of observations is reduced given that a continuous data in time is provided. Finally, a similar improvement in the analysis below the seasonal thermocline can be achieved with fewer data.

1.4 Fishery Observing System Simulation Experiments (FOSSEs)

1.4.1 Design of the Fishery Observing System Simulation Experiments (FOSSE)

FOSSE uses the identical twin methodology, considering two experiments, one called truth and the other, the perturbed experiment. The control run outlined in Section 3.3 is chosen to be the truth from which to sample synthetic temperature and salinity observations.

The perturbed experiment is produced by adding a perturbation to the temperature and salinity fields and then letting it grow due to flow field nonlinearities. The perturbation was applied on June 1, 2006 using the thermocline intensified random perturbation (TIRP) method introduced by Pinardi et al. [2008]:

$$\begin{aligned} T_p(x,y,z) &= T_0(x,y,z) + p(x,y)\sum_{i=1}^{N} e_i f_i(z) \\ S_p(x,y,z) &= S_0(x,y,z) + p(x,y)\sum_{i=1}^{N} e_i g_i(z) \end{aligned} \tag{1.2}$$

where T_0 and S_0 are the unperturbed temperature and salinity fields; $p(x,y)$ is a random number between (0, 1.8) for temperature and (0, 0.4) for salinity; and f_i and g_i are 20 vertical empirical orthogonal functions computed from the model statistics and e_i are their eigenvalues.

The perturbed run uses the 2005 wind fields until December 31, 2006 in order to increase the perturbation growth. The difference between the truth and the perturbation run on January 1, 2007 is shown in Fig. 1.10. The perturbation is large particularly on the shelf areas of both the Croatian and Italian coasts where the nonlinear dynamics of the Western Adriatic coastal current [Zavatarelli and Pinardi, 2003] and the northward flowing eastern Adriatic current are capable of

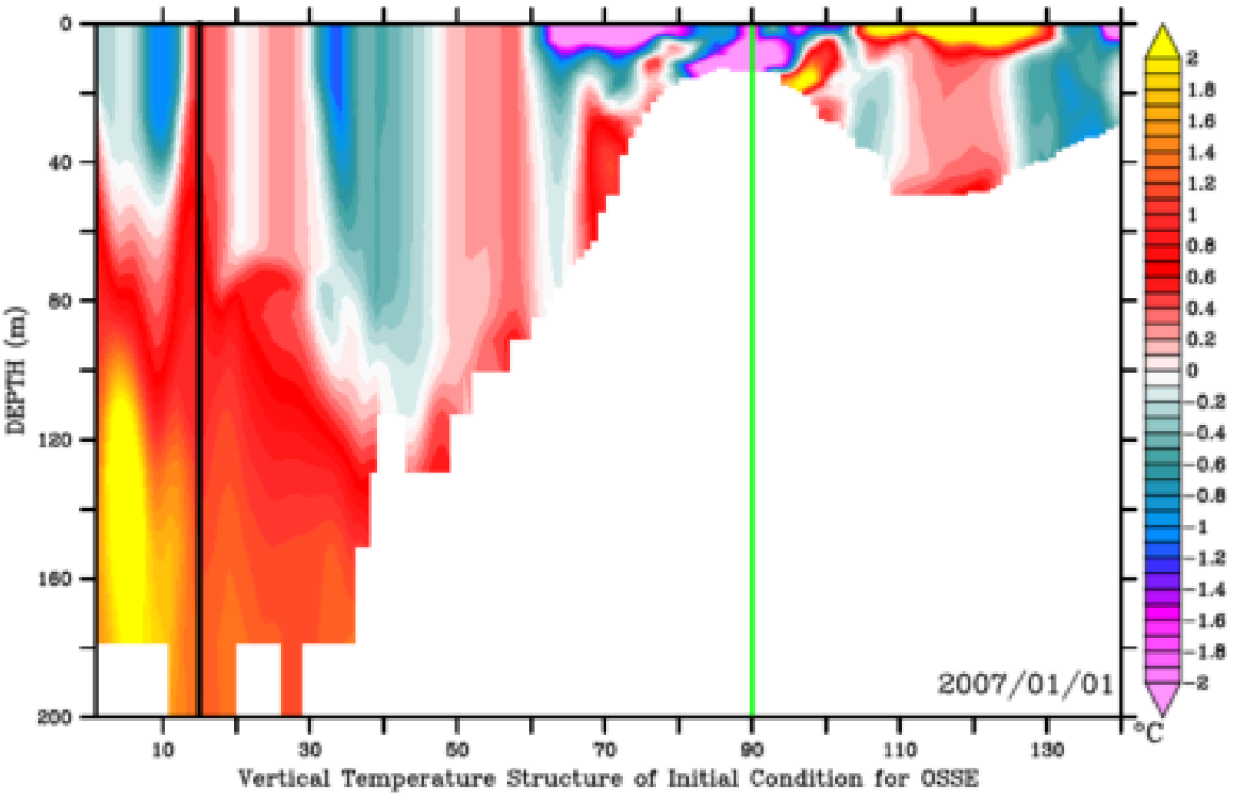

Fig. 1.10. Vertical structure of the temperature field differences between the initial conditions of the truth and the perturbation run along the section shown in Fig. 1.1. Black and green lines indicate the vertical sections below the reference points (a) and (b), respectively shown in Fig. 1.1. Horizontal axis is the number of grid points along the transect. The depth is in meters.

amplifying the initial perturbations. Starting from January 1, 2007 synthetic observations were inserted into the perturbation run.

Two FOSSEs were designed using this perturbation run (Table 1.5). In OSSE01 we only assimilated the synthetic temperature observations, while in OSSE02 both temperature and salinity synthetic observations were assimilated.

Experiment	Type	Assimilation	Variable
Truth	Nature run	No	
Perturbation	Simulation	No	
OSSE01	Assimilation	All synt. FOS#1	Temp
OSSE02	Assimilation	All synt. FOS#1	Temp + Salt

Table 1.5: Fishery Observing System Simulation Experiment (FOSSE) design.

1.4.2 Synthetic observations and evaluation methods

The distribution of the synthetic observations from January to April 2007 is shown in Fig. 1.11 for all the existing fishing vessels. The horizontal coverage of the measurements for this period is similar to the whole year distribution (Fig. 1.2). The temperature and salinity values were

sampled from the truth run at the realistic FOS positions using a random instrumental error parametrization. For the temperature, a random error is added to the samples by fitting a Gaussian distribution with mean equal to 0°C and a std. of 0.1°C. For salinity errors, a random Gaussian distribution is used with mean equal to 0 psu and a std. of 0.04 psu.

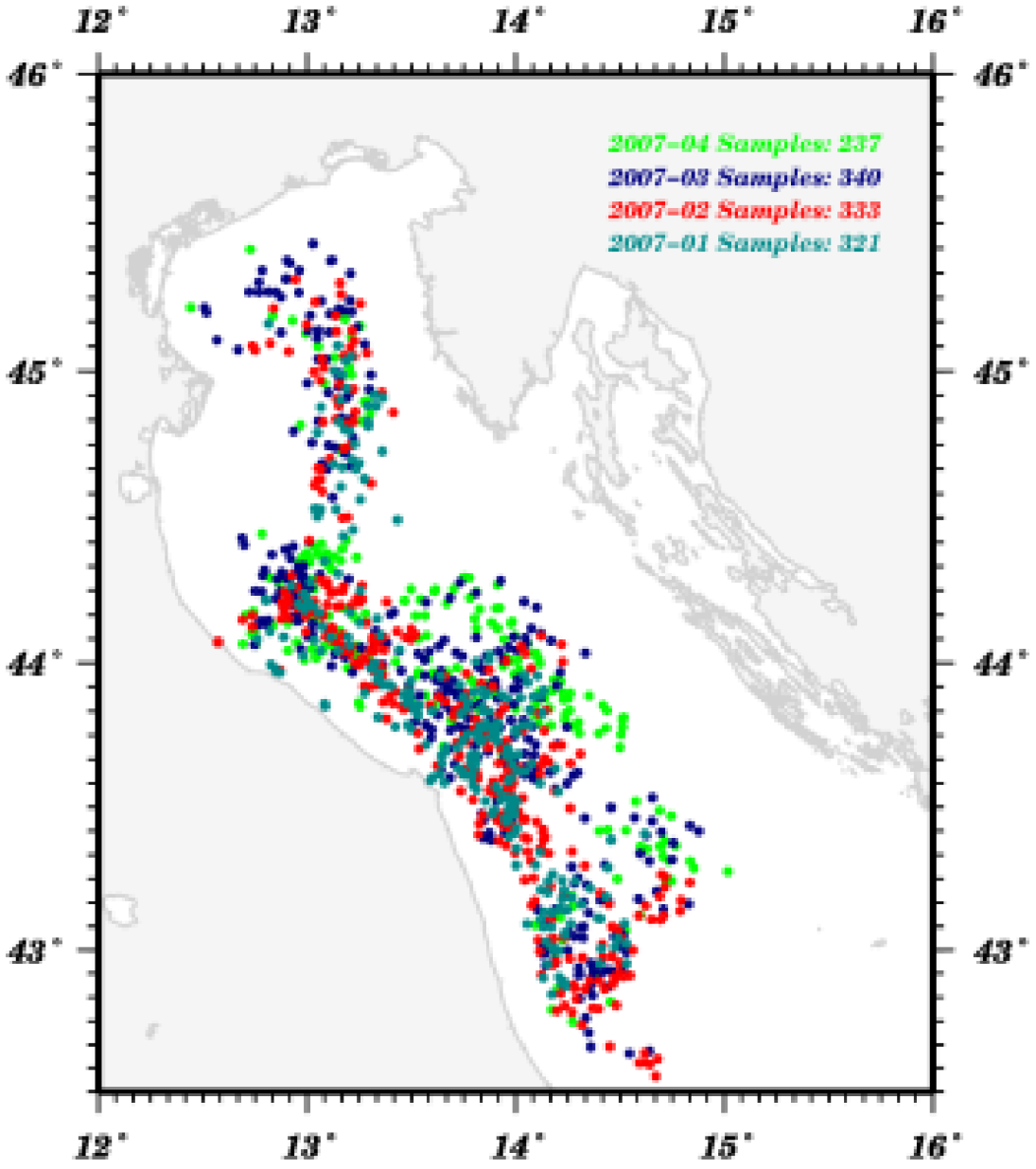

Fig. 1.11. Monthly distribution of the synthetic observations from January to April 2007.

In order to evaluate our FOSSE results, we compare the misfit RMS error with FOSE best estimate error statistics. This highlights whether the perturbed run produces errors that are statistically similar to the real observation assimilation case, so that the FOSSE results will be

credible. In FOSSE, we only use the period between January 2007 and April 2007 because after this time, the perturbation run converges to the truth and the impact of the assimilation is not similar to the corresponding FOSEs.

1.4.3 FOSSE results

The RMS temperature error in this period is less than 1°C for all the experiments (Fig. 1.12). The control run reaches 0.9°C RMS errors in the upper layer in March, whereas the maximum error in the perturbation run is 0.65°C. The mean RMS error of the control run in this period is 0.68°C in the upper layer, and 0.46°C for the perturbation run (Table 1.6). In the lower layer, the mean RMS temperature errors are 0.34°C and 0.27°C for the control run and the perturbation run, respectively. The mean RMS error of the best estimate is 0.31°C and for the OSSE01 is 0.35°C in the upper layer. For the lower layer, this is 0.27°C and 0.23°C for the best estimate and the OSSE01, respectively. Thus in synthesis, the error statistics between FOSE and FOSSE experiments are similar, and thus the OSSE experiments are a credible experimental tool to evaluate new characteristics of the observing systems.

	FOSE			FOSSE		
	Control run	Best estimate	Reduction	Perturbation	OSSE01	Reduction
0-40 m	0.68	0.3	54	0.46	0.35	24
40-100 m	0.34	0.27	21	0.27	0.23	15

Table 1.6: Comparison of mean RMS temperature error of FOSE and FOSSE in January-April 2007. Upper 0-40 m and lower 40-100 m are considered separately. Error reductions after temperature assimilation are also listed.

The OSSE02 is designed to test the possible impact of installing a CTD sensor on the fishing vessels in place of the existing one. The synthetic salinity observations are assimilated in addition to the synthetic temperature observations. Fig. 1.13 compares the OSSE02 with the perturbation run and OSSE01.

In both layers, the impact of salinity assimilation is negligible as shown in Table 1.7. The mean RMS salinity errors in the upper and lower layers are practically equal in all the experiments.

In Fig. 1.13a, the biggest errors appear in January and April when there are few data in the first 20 m of the water column (Fig. 1.3). These observations are generally in the coast of Rimini where there is the highly dynamic western Adriatic coastal jet. When the RMS salinity error is calculated in the 20-40 m depth, excluding those misfits in the first 20 m, although the performance of the analysis does not improve (Table 1.8), it is not degraded (Fig. 1.14).

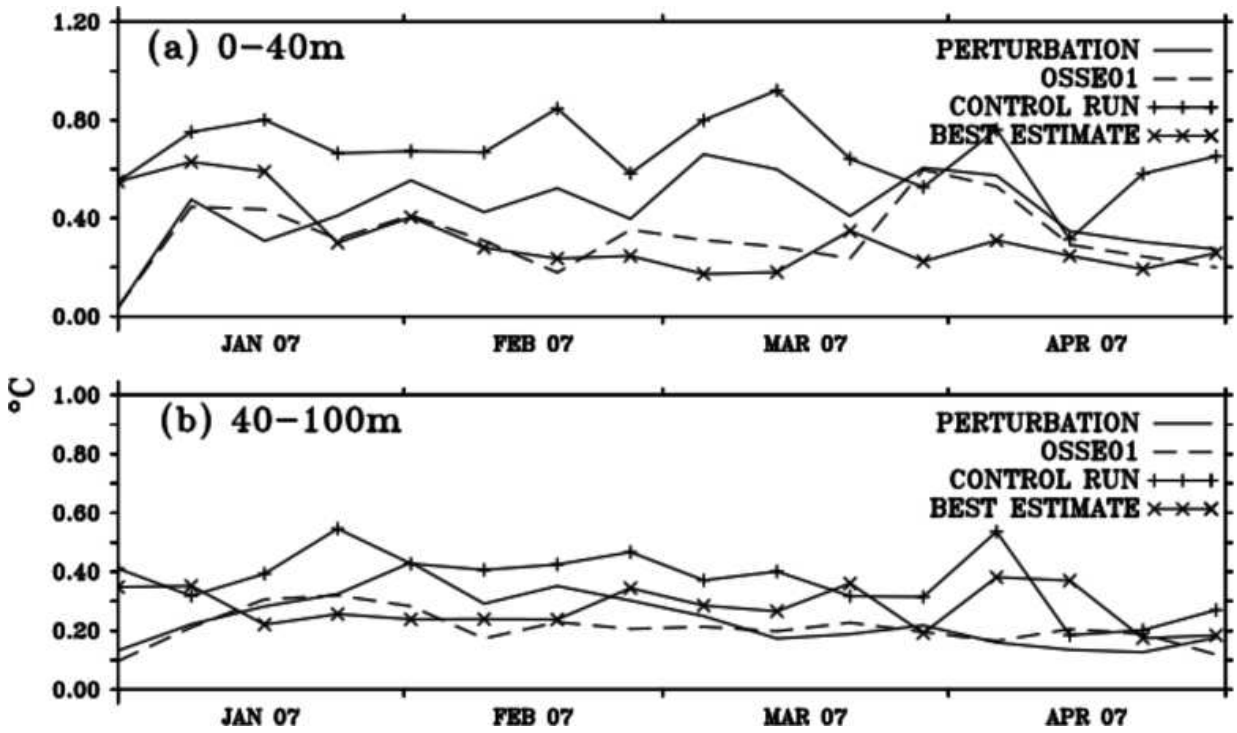

Fig. 1.12. RMS of temperature misfits comparison of the OSE and the OSSE. The perturbation run in OSSE corresponds to the control run of OSE. Similarly, OSSE01 corresponds to the best estimate of OSE since we assimilated all the temperature data between January and April 2007.

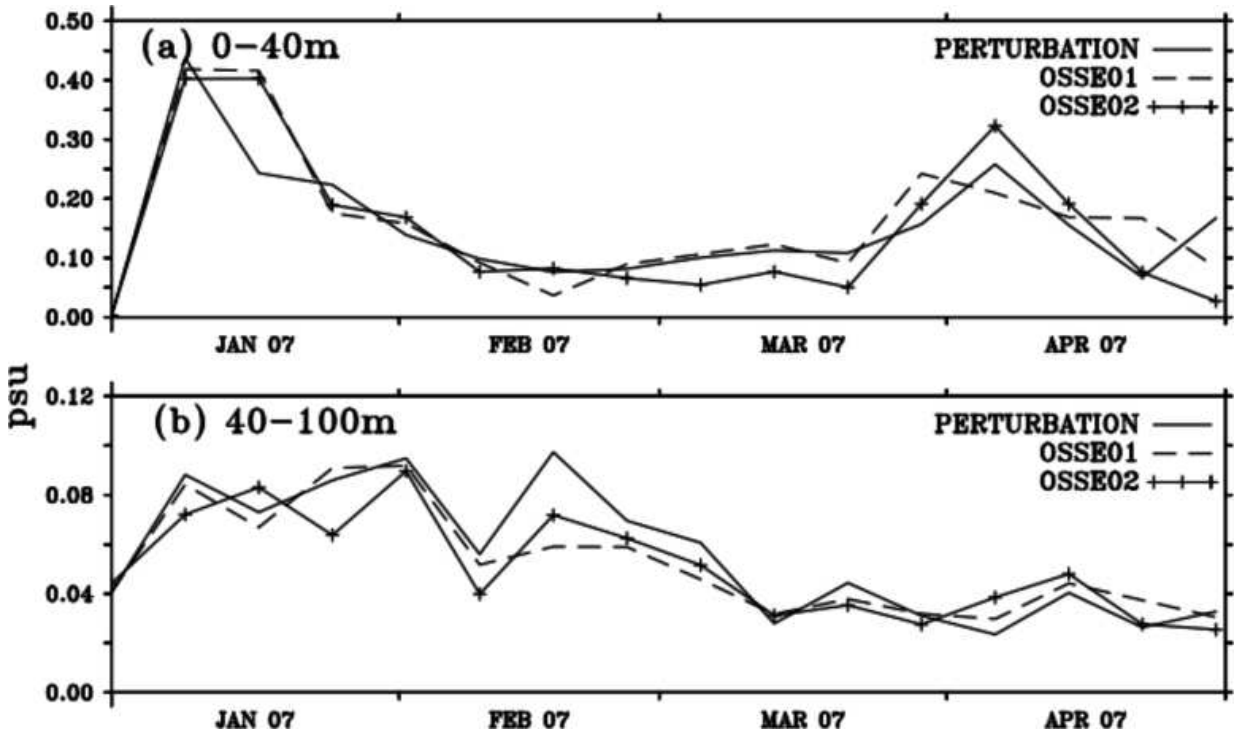

Fig. 1.13. The RMS salinity error comparison of perturbation run, the OSSE01 and the OSSE02 (a) 0-40 m depth (b) 40-100 m depth. The scales are different in the upper and lower layer.

Several publications in the past have shown that the data assimilation system used in this paper has been successful to assimilate temperature and salinity observations from different observing systems such as XBT [Dobricic and Pinardi, 2008], gliders [Dobricic et al., 2010] and Argo

[Nilsson et al., 2011] in the Mediterranean Sea and its sub-basins.

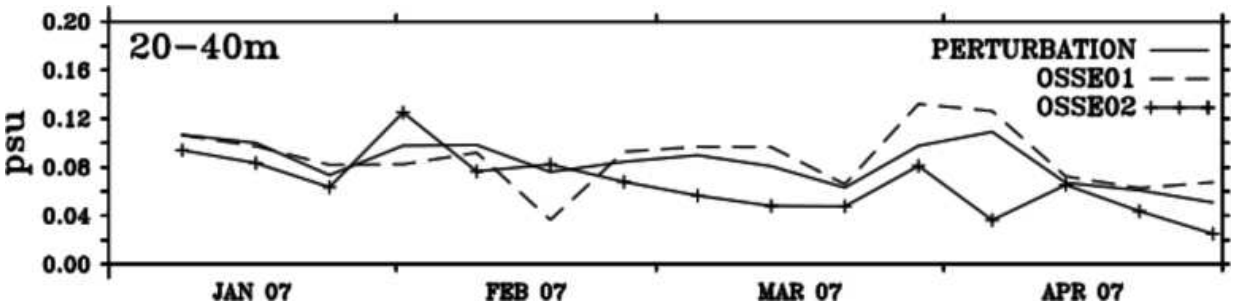

Fig. 1.14. Same as Fig. 1.13 but RMS salinity errors are calculated between 20 and 40 m.

The difference of our study case is that we apply the large scale data assimilation scheme to a shelf and rapidly evolving coastal area. Our results show that corrections are rapidly advected towards the Southern Adriatic Sea by the rapidly flowing western Adriatic coastal current thus impacting negatively the quality of the field downstream of the assimilation. Therefore, we argue that for narrow coastal jet streams we may not be able to assess the real impact of the assimilation of salinity data.

	Perturbation Run	OSSE01	OSSE02
0-40 m	0.16	0.18	0.16
40-100 m	0.06	0.06	0.05

Table 1.7: The mean RMS salinity error for the perturbation run, the OSSE01 and the OSSE02 in the 0-40 m depth and the 40-100 m depth.

	Perturbation run	OSSE01	OSSE02
20-40 m	0.08	0.09	0.07

Table 1.8: The mean RMS salinity error for the perturbation run, the OSSE01 and the OSSE02 in the 20-40 m depth.

In conclusion, we believe that the net gain for CTD single vertical value measurements near coastal areas might be of limited benefit to the quality of analysis during winter and spring seasons, although our experiments are not conclusive in this respect.

1.5 Summary and discussion

The paper examines a special fishery vessel of opportunity observing system in the Adriatic Sea using the OSE and OSSE methodologies. The FOS observations used are only single value temperature measurements averaged over the fishing net hauling period and covering all of 2007. FOSE experiments tested the impact of the number of fishing vessels used, while the FOSSE tested the impact of introducing CTD salinity and temperature measurements.

The FOSE results indicate that decreasing the number of vessels by leaving the coverage unaltered, and decreasing the number of measurements does not have a critical impact on the quality of the analysis. Our work shows that FOS improves the RMS of temperature misfits by a factor of 35-43% with respect to the simulation RMS error. The impact is bigger during the stratification season around the thermocline where the errors are larger.

We designed an identical twin FOSSE system to assess the possible impact of salinity in addition to temperature observations.

Our results demonstrate that the salinity assimilation does not change the quality of the analysis significantly. We argue that this is because our data assimilation scheme is not suitable for the fast advecting dynamics of the coastal flow field that requires non-homogeneous and non-isotropic horizontal correlation function. This is a limitation of our data assimilation system and thus we believe that our FOSSE experiments are not conclusive. More work and a different assimilation scheme would be required to finally establish the impact of CTD single value measurements in the FOS.

Chapter 2

Numerical simulations of the Turkish Straits System for the 2008-2013 period

Part I: Model Setup and Validation

Abstract

We present two six-year simulations of the Turkish Straits System (TSS) using a high-resolution three dimensional unstructured mesh ocean circulation model with realistic atmospheric forcing. The difference between the two simulations is the surface salinity boundary condition that is left free to decide since the model domain is closed. The results suggest a sensitivity of the system to the surface salinity boundary conditions. The depth of the interface between the upper and lower layers remains stationary after six years of integration showing that even with the limitations of the closed domain numerical solutions it can be kept realistic for several years. The water mass structure in the Marmara Sea is compared with the observations and results show a qualitative agreement between model and observations and relatively good skill scores. The experimtent with boundary condition that considers also the water fluxes seems to reproduce the data better.

2.1 Introduction

The Turkish Straits System (hereafter TSS) is composed of the Bosphorus and the Dardanelles Straits and the Marmara Sea connecting the Black Sea and the Mediterranean. The exchange of brackish Black Sea surface water and salty North Aegean Sea subsurface water through the TSS generates a strongly stratified marine environment [Ünlüata et al., 1990] with a pycnocline about 25 m in the Marmara Sea [Beşiktepe et al., 1994]. The upper layer above the pycnocline has the characteristics of the Black Sea with low salinity flowing towards the Aegean Sea. The lower layer is occupied by dense Mediterranean waters reaching to the Black Sea in the reverse direction.

The topography of the TSS is very complex as it is composed of two elongated narrow straits and an internal basin with deep bottom depressions and large shallow shelf areas (Fig. 2.1). The morphology of each separate compartment has been reported by Ünlüata et al. [1990] in detail. Under the influence of the atmosphere, the two-layer exchange flow and complex topography in TSS together have created a natural oceanographic laboratory.

This unique laboratory has attracted the attention of the scientists for several centuries [Marsigli, 1681]. Contemporary investigations date back to Nielsen [1912]. In the last four decades, several surveys have been organized to explore the hydrography and circulation of the Marmara Sea [Beşiktepe et al., 1994; Chiggiato et al., 2012; Latif et al., 1991; Özsoy et al., 1988]. Others have focused on understanding the flow and volume fluxes as well as the mixing in the straits [Gregg and Özsoy, 2002; Jarosz et al., 2011a,b, 2012, 2013; Latif et al., 1992; Ozsoy et al., 1998]. The volume exchange between the Marmara Sea and the Black Sea through the Bosphorus has also been studied because it is the only oxygen and nutrient supply for the Black Sea bottom layers [Altiok et al., 2012; Özsoy et al., 2001; Tugrul et al., 2002]. The water budget of the Black Sea has always been of great importance since it is the main driver of the barotropic flow through the straits [Kara et al., 2008; Peneva et al., 2001] and the resulting sea level differences between different compartments have been intensively studied [Alpar et al., 2000; Bogdanova, 1969; Büyükay, 1989; Tutsak, 2012]. The impact of the Dardanelles outflow to the Aegean Sea has been another research interest [Kourafalou and Barbopoulos, 2003; Zervakis et al., 2000; Zodiatis, 1994].

The complexity of the topography requires advanced modeling approaches in the TSS to further deepen the understanding and provide overall picture of the system. To date, modeling

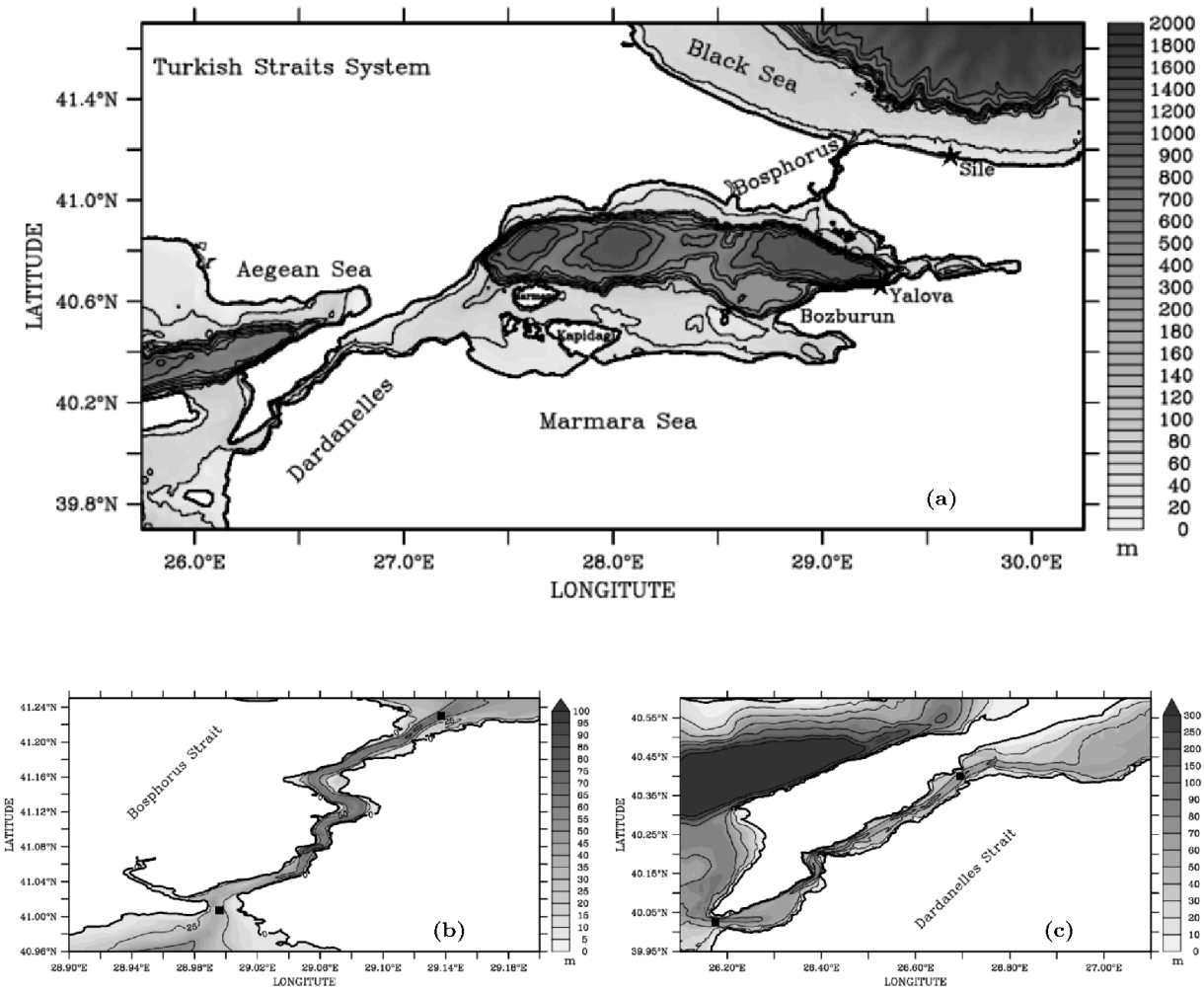

Fig. 2.1. a) Bathymetry of the Turkish Straits System. Contour interval is 50 m between 0-200 m, 100 m between 200-500 m and 250 m between 500-1000 m. b) Bosphorus Strait c) Dardanelles Strait. The locations used for analysis at the exits of the straits are marked by squares.

efforts have focused on studying the compartments of the system separately. Johns and Oguz [1989] studied the exchange flow through the Bosphorus by a two-layer model of a variable rectangular cross-section. A two-layer model of the Dardanelles was developed by Oguz and Sur [1989] with simplified topography. The same model has also been applied to the Bosphorus by Oguz et al. [1990]. Hüsrevoğlu [1998] introduced a three dimensional ocean model in the Dardanelles. The Bosphorus is then investigated by Sözer [2013] using a three dimensional model with realistic topography. Recently, Chiggiato et al. [2012] modeled the Marmara Sea using realistic atmospheric forcing and open boundaries in the straits. Gündüz and Özsoy [2015] implemented a relatively low resolution model of the TSS to estimate the Dardanelles volume fluxes and cor-

relate the blocking events to the fish catches in the Aegean Sea. All these models are built on regular grid structures in which resolving the Marmara Sea and the straits at the same time is difficult due to their computational cost. The inter-annual variability of the Marmara Sea has been examined by Demyshev et al. [2012] using open boundary conditions in the strait exits. Maderich et al. [2015] employed a chain of models to simulate the inter-annual variability of the water exchange through the TSS.

Recently, two different studies took up the challenge of modeling the integral system [Gürses, 2016; Sannino et al., 2015] as a whole. Sannino et al. [2015] used a very high-resolution version of the MIT-GCM with a non-uniform grid. They investigated the impact of different barotropic flows through the Bosphorus without any atmospheric forcing. The other study [Gürses, 2016] uses an unstructured triangular mesh model, namely FESOM, with very high resolution in the straits.

In this study, we extend the work of [Gürses, 2016] from annual to multi-year time scales. For what we believe is the first time, we demonstrate the inter-annual variability of the TSS with a three dimensional model using realistic atmospheric forcing and also considering the water budget.

The study consists of two parts. In this part (PART I), the model setup and experiments are described. The evolution of temperature, salinity and density is also demonstrated and validated. In the second part (PART II), we focus on the dynamics of the system and the circulation in the Marmara Sea.

Part I is organized as follows: In the next section, the materials and methodologies are presented and the details of the experiments are outlined. In section 2.3, the results of the study are presented. The final section summarizes and discusses the results.

2.2 TSS Modeling Environment and Experiment Design

In this study, the general ocean circulation model is the Finite Element Sea-ice Ocean Model (FESOM). FESOM is an unstructured mesh ocean model using finite element methods to solve the hydrostatic primitive equations with Boussinesq approximation [Danilov et al., 2004; Wang et al., 2008]. It is the first global model using an unstructured mesh and adapted to many application areas with a complex topography such as the Canadian Arctic Archipelago [Wekerle et al., 2013] or with strong dynamics such as the Southern Ocean [Timmermann and Hellmer, 2013] by refining the mesh for the area of interest in a global configuration. In Gürses [2016],

FESOM is applied to the TSS as a first regional application to resolve the straits with a finer mesh resolution compared to the neighboring seas, namely the Black Sea and Aegean Sea. The TSS implementation has been reported by Gürses [2016]. It was tested for different applications such as lock-exchange simulations, various parameterizations and forcing by a realistic atmosphere.

The TSS model domain extends from 22.5°E to 33°E zonally and from 38.7°N to 43°N meridionally covering a total surface area of 1.52 x 10^{11} m^2 (Fig. 2.2). The mesh resolution increases up to 65 m and 150 m in the Bosphorus and Dardanelles, respectively. In the Marmara Sea, the resolution is always finer than 1.6 km and is not coarser than 5 km in the Black Sea and the Aegean Sea. The water column is discretized by 110 vertical z-levels. Vertical resolution is 1 m in the first 50 m depth and decreases to 65 m at the bottom boundary layer in the deepest part of the model domain.

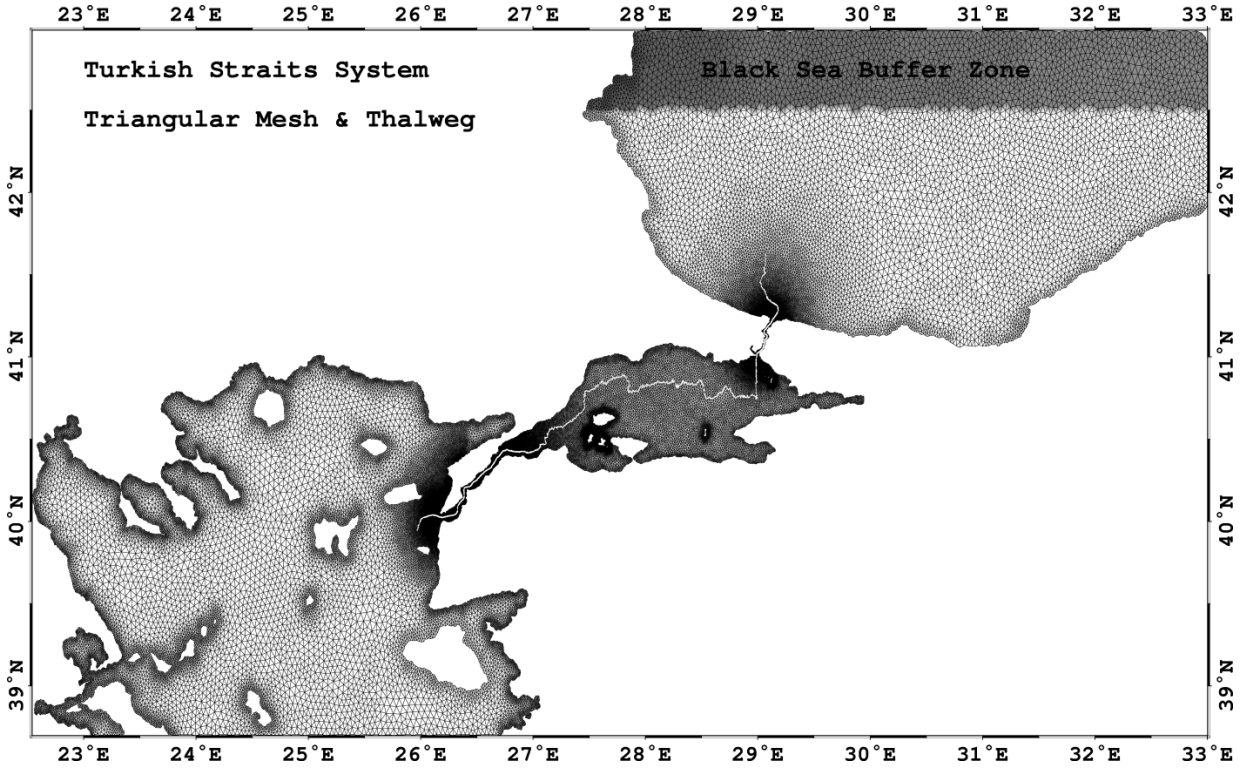

Fig. 2.2. Triangular mesh representation of the study area. The white transect shows the thalweg path used for computations for the vertical structure. The Black Sea buffer zone is shaded in dark gray.

The model equations are presented in section 2.2.1. The current model implementation considers closed lateral boundaries. Therefore, volume conservation and volume salinity conservation are required to prevent a significant excess or deficit in long simulations. The approach in FESOM for salinity and volume conservation is described in section 2.2.2.

For this study, two realistic simulations were performed over a six-year period from 2008 to 2013. The simulations have almost identical model configurations except for different surface salinity boundary conditions. The differences are outlined in section 2.2.1 and detailed in section 2.2.3.

A surface area, approximately 2.22 x 10^{10} m^2, in the north of 42.5°N in the Black Sea functions as a buffer zone. In this zone, the model is forced by the Black Sea runoff which is an important component of the Black Sea fresh water balance that drives the barotropic flow through the Bosphorus [Peneva et al., 2001]. Surface salinity is relaxed to a climatology in the same zone to prevent a dramatic reduction in local salinity due to an excessive amount of fresh water input. Details of all the external forcing are in section 2.2.4.

2.2.1 Model Equations

FESOM solves the standard set of hydrostatic primitive equations with Boussinesq approximation [Wang et al., 2008].

The momentum equations are:

$$\partial_t \vec{u} + \vec{v} \cdot \nabla_3 \vec{u} + f\hat{k} \times \vec{u} = -\frac{1}{\rho_0}\nabla p \ - g\nabla\eta - \nabla A_h \nabla(\nabla^2 \vec{u}) + \partial_z A_v \partial_z \vec{u} \tag{2.1}$$

where $\vec{u} = (u, v)$ and $\vec{v} = (u, v, w)$ are 3D and 2D velocities, respectively, in the spherical coordinate system, ρ_0 is the mean density, p is the hydrostatic pressure, g is the gravitational acceleration, η is the sea surface elevation, f is the Coriolis parameter and $\hat{k}$ is the vertical unit vector. ∇ and ∇_3 stand for 2D and 3D gradients or divergence operators, respectively. The lateral and vertical viscosities are denoted by A_h and A_v. Finally, ∇^4 is the biharmonic operator.

It is known that the Laplacian viscosity is generally too damping and strongly reduces the eddy variances of all fields compared to observations when the model is run at the eddy resolving resolution [Wang et al., 2008]. Therefore, biharmonic viscosity is used in the momentum equations. Here, A_h is scaled by the cube of the element size with a scale factor A_{h0} of 2.7×10^{13} m^4/s (Table 2.1) which is set for the reference resolution of 1 degree.

The continuity equation is used to diagnose the vertical velocity w:

$$\partial_z w = -\nabla \cdot \vec{u} \tag{2.2}$$

and the hydrostatic equation is:

$$\partial_z p = -g\rho \tag{2.3}$$

where ρ is the deviation from the mean density ρ_0.

Tracer equations (2.4) and (2.5)

$$\partial_t T + \vec{v} \cdot \nabla_3 T - \nabla \cdot K_h \nabla T - \partial_z K_v \partial_z T = 0 \tag{2.4}$$

$$\partial_t S + \vec{v} \cdot \nabla_3 S - \nabla \cdot K_h \nabla S - \partial_z K_v \partial_z S = 0 \tag{2.5}$$

are solved for the potential temperature, T, and salinity, S where K_h and K_v are the lateral and vertical diffusivities, respectively. K_h is again scaled as A_h but by the element size with a scale factor of $2.0 \times 10^3\ m^2/s$. These values are set following the convergence study of Wallcraft et al. [2005].

The density anomaly ρ is computed by the full equation of state (2.6).

$$\rho = \rho(T, S, p) \tag{2.6}$$

The surface and bottom momentum boundary conditions are, respectively, as:

$$A_v \partial_z \vec{u} = \tau \tag{2.7}$$

$$A_v \partial_z \vec{u} + A_h \nabla H \cdot \nabla \vec{u} = C_d \vec{u} \mid \vec{u} \mid \tag{2.8}$$

where τ and C_d are the wind stress and the bottom drag coefficient, respectively.

The surface kinematic boundary condition is:

$$w = \partial_t \eta + \vec{u} \cdot \nabla \eta + (E - P - R) + W_{corr} \tag{2.9}$$

where E (m/s), P (m/s) are evaporation and precipitation, respectively. R (km^3/yr) is runoff and converted to m^3/s before it is normalized by the area of the buffer zone in the Black Sea (see Fig. 2.2). Finally, W_{corr} is a correction applied to conserve the volume of the model as described later.

The sea surface height equation can now be derived from equations 2.2 and 2.9 as:

$$\partial_t \eta + \nabla \cdot \int_{z=-H}^{z=\eta} \vec{u} dz = -(E - P - R) - W_{corr} \tag{2.10}$$

The upper limit of integration in (2.10) is set to η in this version of FESOM and is different from Wang et al. [2008] for a non-linear free surface solution.

The bottom boundary condition for the temperature and salinity are

$$(\nabla T, \partial_z T) \cdot \mathbf{n}_3 = 0 \tag{2.11}$$

$$(\nabla S, \partial_z S) \cdot \mathbf{n}_3 = 0 \tag{2.12}$$

where $\mathbf{n}_3$ is the 3D unit vector normal to the respective surface.

The surface boundary condition for temperature is

$$K_v \partial_z T \big|_{z=\eta} = \frac{Q}{\rho_0 C_p} \tag{2.13}$$

where $C_p = 4000 J/(kg\ K^\circ)$ and Q (W/m^2) is the surface net heat flux into the ocean.

The available surface salinity boundary condition in FESOM is a relaxation (restoration)

condition (2.14a). In global applications, surface salinity is generally relaxed to a climatology to prevent a drift. In our regional application the relaxation term is applied only in the Black Sea buffer zone since we want to impose that the Black Sea salinity is kept low. As a second solution, we implemented the mixed boundary condition (2.14b) to enable the water fluxes to modify the surface salinity.

$$K_v \partial_z S\big|_{z=\eta} = \gamma(S^* - S_0) - S_{corr} \tag{2.14a}$$

$$K_v \partial_z S\big|_{z=\eta} = S_0(E - P - R) + \gamma(S^* - S_0) - S^*_{corr} \tag{2.14b}$$

In the boundary conditions (2.14a) and (2.14b), S_0 and S^* are the surface salinity and the reference salinity, respectively, γ is the relaxation coefficient (Table 2.1). Finally, S_{corr} and S^*_{corr} are the counterpart of W_{corr} for salinity conservation corresponding to boundary conditions (2.14a) and (2.14b), respectively, which will be defined in the following section.

PARAMETER	DESCRIPTION	VALUE	UNIT
A_D	Model Domain Area	1.52×10^{11}	m^2
A_B	Black Sea Buffer Zone AREA	2.26×10^{10}	m^2
R_B	Black Sea Runoff	Table 2.3	
S_0	Sea Surface Salinity		psu
S^*	Salinity relaxed in the Black Sea Buffer Zone	Table 2.3	psu
γ	Salinity relaxation coefficient	5.79×10^{-6}	m/s
W_{corr}	Water flux correction		m/s
S_{corr}	Salinity flux correction		$psu\ m/s$
A_{h0}	Horizontal eddy viscosity scale factor	2.7×10^{13}	m^4/s
K_{h0}	Horizontal eddy diffusivity scale factor	2.0×10^{3}	m^2/s
A_{v0}	Vertical background viscosity	1.0×10^{-5}	m^2/s
K_{v0}	Vertical background diffusivity	1.0×10^{-6}	m^2/s

Table 2.1: Parameters used in the model equations, surface boundary conditions and budget corrections.

2.2.2 Salt Conservation Properties

Since our model domain is closed we need to enforce salt conservation. Volume salinity conservation requires the time rate of the change in the volume salinity term in equation (2.15) to be zero. A balance must be satisfied between the surface integral terms.

$$\frac{\partial}{\partial t} \iiint_V S dV = - \iint_A S_0(E - P - R - W_{corr}) dA + \iint_A (K_v \partial_z S\big|_{z=\eta}) dA = 0 \tag{2.15}$$

In FESOM, this balance is achieved by applying a correction for each term separately. The amount of water flux by evaporation, precipitation and runoff is integrated over the surface every

time step (Equation 2.16). After normalizing by the domain area as in (2.17), the surplus or deficit is added to or subtracted from the total water flux equally from each node of the mesh with the W_{corr} terms in equations (2.9) and (2.10).

$$\Delta_{(E-P-R)} = \int_{x,y} (E - P - R) dxdy \tag{2.16}$$

$$W_{corr} = \frac{\Delta_{E-P-R}}{A_D} \tag{2.17}$$

The salinity flux is corrected in a similar manner for the boundary condition (2.14a):

$$\Delta S = \int_{x,y} \gamma(S^* - S_0) dxdy \tag{2.18}$$

$$S_{corr} = \frac{\Delta S}{A_D} \tag{2.19}$$

and boundary condition (2.14b):

$$\Delta S^* = \int_{x,y} (S_0(E - P - R) + \gamma(S^* - S_0)) dxdy \tag{2.20}$$

$$S^*_{corr} = \frac{\Delta S}{A_D} \tag{2.21}$$

After applying these corrections, we get a surplus of water corresponding to ∼1 mm of sea surface height increase a year which we believe that is due to the random numerical errors. Correspondingly, the volume-mean salinity decreases by an order of 10^{-5} psu a year. Although these errors may be significant in climate scales, they are acceptable for our six-year experiments.

2.2.3 Experiment Design and Initialization

In this paper (i.e. Part I), two simulations integrated for six years between 1 January 2008 and 31 December 2013 are presented (Table 2.2). The availability of both the high-resolution atmospheric forcing and in-situ observations for validation are taken into account in order to determine the simulation period. The two experiments are performed by imposing different surface salinity boundary conditions, above all to investigate the impact of the surface salinity on the general structure of the water masses throughout the system. Simulation BLK01 is performed with a relaxation boundary condition (2.14a) for salinity whereas simulation BLK02 uses a mixed salinity boundary condition (2.14b) [Huang, 1993].

EXPERIMENT	Start Date	End Date	Salinity SBC	Relaxation Time
$BLK01$	01-JAN-2008	31-DEC-2013	Eq'n (2.14a)	∼2 days
$BLK02$	01-JAN-2008	31-DEC-2013	Eq'n (2.14b)	∼2 days

Table 2.2: Summary of the experiments

The initial conditions used in this study were obtained after a three-month integration of a lock-exchange case which was initialized from different temperature and salinity profiles in each

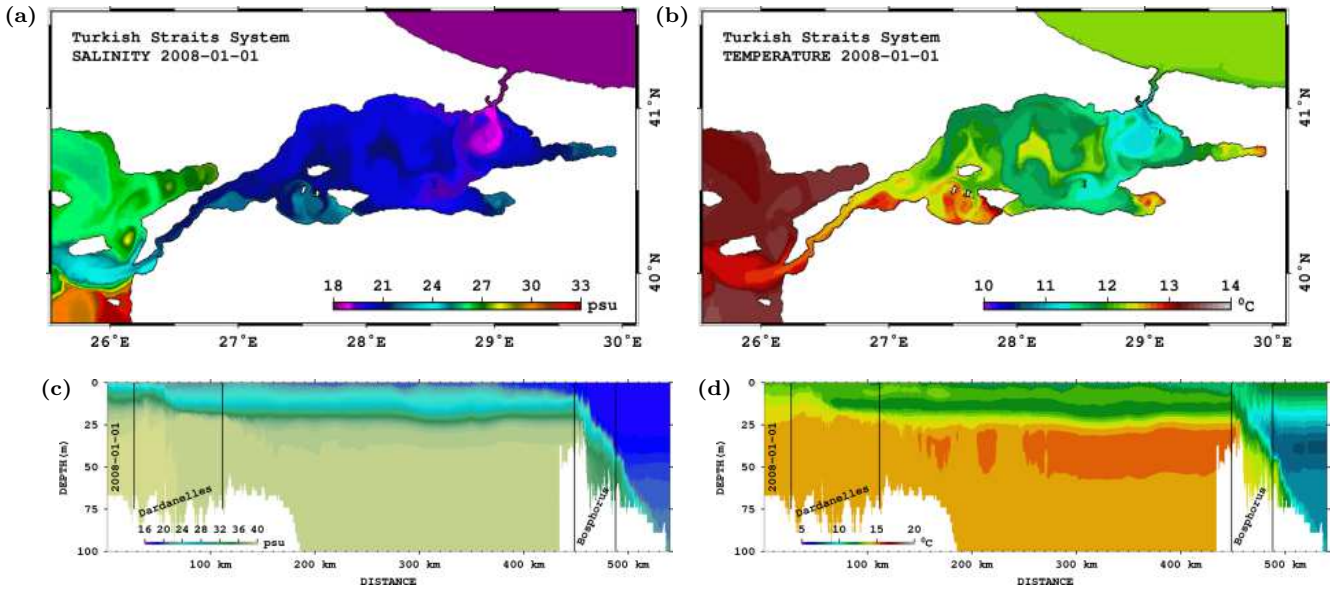

Fig. 2.3. Initial fields in 1 January 2008 a) sea surface salinity b) sea surface temperature c) salinity along the thalweg and d) temperature along the thalweg. See Fig. 2.2 for the path of the thalweg.

basin [Gürses, 2016]. The initial horizontal and vertical salinity fields are shown in Fig. 2.3a and 2.3c, respectively, for 1 January 2008. The system has already evolved and we can easily differentiate the outflows of the Bosphorus and the Dardanelles towards the Marmara and Aegean Seas, respectively (Fig. 2.3a). In the sea surface temperature horizontal field, the cold buoyant plume can also be distinguished from the surrounding water (Fig. 2.3b). In the Marmara Sea, the southern coast is warmer and more saline as is the Izmit Bay in the eastern basin. Both the halocline and thermocline are around 25 m depth in the Marmara Sea (Fig. 2.3c and 2.3d).

Fine mesh resolution and energetic flow structures in the straits require small time steps not to violate the CFL condition. Therefore, the time step is set to 12 s throughout the integration.

2.2.4 Surface Forcings

The simulations were forced by atmospheric fields provided by ECMWF with 1/8° resolution. The forcing data cover the whole experiment period with a frequency of six hours. However, precipitation was obtained from monthly CPC Merged Analysis of Precipitation (CMAP, Xie and Arkin [1997]) and interpolated to the ECMWF grid as daily climatology.

The monthly runoff climatology was obtained from Kara et al. [2008] for all the six years. In addition, surface salinity at the buffer zone was relaxed to a monthly climatology computed from a 15-year simulation of Copernicus Marine Environment Monitoring Service Black Sea circulation model [Storto et al., 2016]. The salinity relaxation time is approximately 2 days. Although this

MONTH	JAN	FEB	MAR	APR	MAY	JUN
$R(km^3/y)$	260.3	281.7	333.9	404.1	417.6	353.6
$S^*(psu)$	18.97	18.96	18.91	18.88	18.74	18.74
MONTH	JUL	AUG	SEP	OCT	NOV	DEC
$R(km^3/y)$	292.5	231.2	198.7	196.2	223.0	254.2
$S^*(psu)$	18.87	18.98	18.90	18.92	18.94	19.02

Table 2.3: Monthly Black Sea river discharges and salinity relaxation values.

is a strong constraint, it is needed to prevent the surface salinity from decreasing in the buffer zone due to the excessive amount of fresh water input. Climatological values used for runoff and salinity relaxation are shown in Table 2.3.

2.3 Results

2.3.1 Surface Heat and Water Fluxes

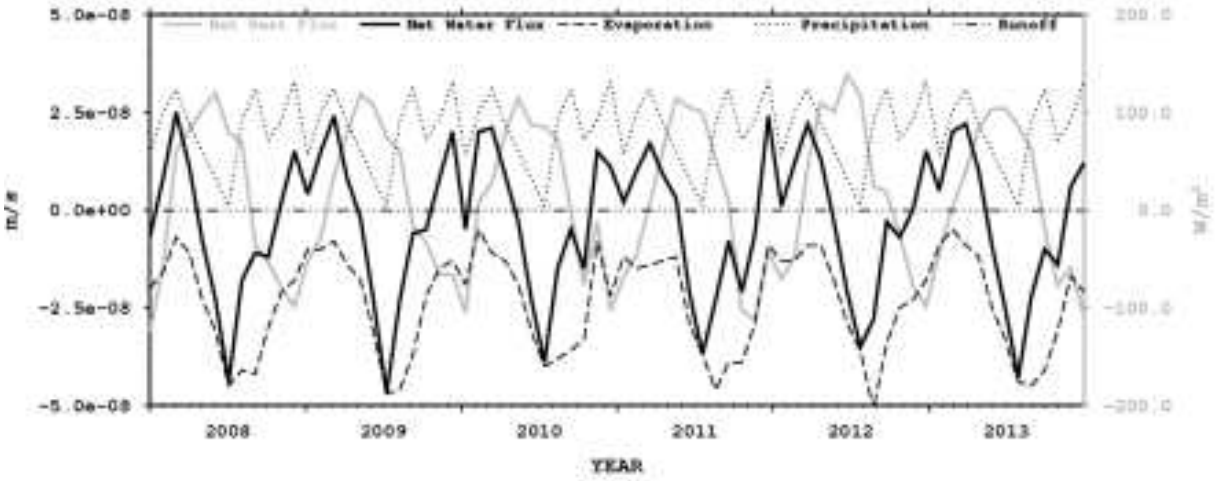

Fig. 2.4. Monthly averaged net heat (gray) and water fluxes (black) in the Marmara Sea are shown. Evaporation (dashed) and precipitation (dotted) are also overlaid. Runoff is zero in the Marmara Sea. The gray vertical axis (right) is for heat flux and black vertical axis (left) is for water fluxes.

The monthly averages of water fluxes and net heat flux in the Marmara Sea are shown in Fig. 2.4 for BLK02. The runoff is identically zero in the Marmara Sea. Evaporation fluctuates between -5.1x10^{-8} m/s and -5x10^{-9} m/s with an absolute minimum in March and maximum in July. Minimum precipitation is 1x10^{-9} m/s in July whereas maximum is 3.3x10^{-8} m/s in December. The resulting net water flux E - P varies between -4.7x10^{-8} and 2.5x10^{-8}. The net heat flux in the Marmara Sea is calculated as -123.3 W/m^2 and 138.4 W/m^2 with minimum and maximum in December-January and May-June, respectively.

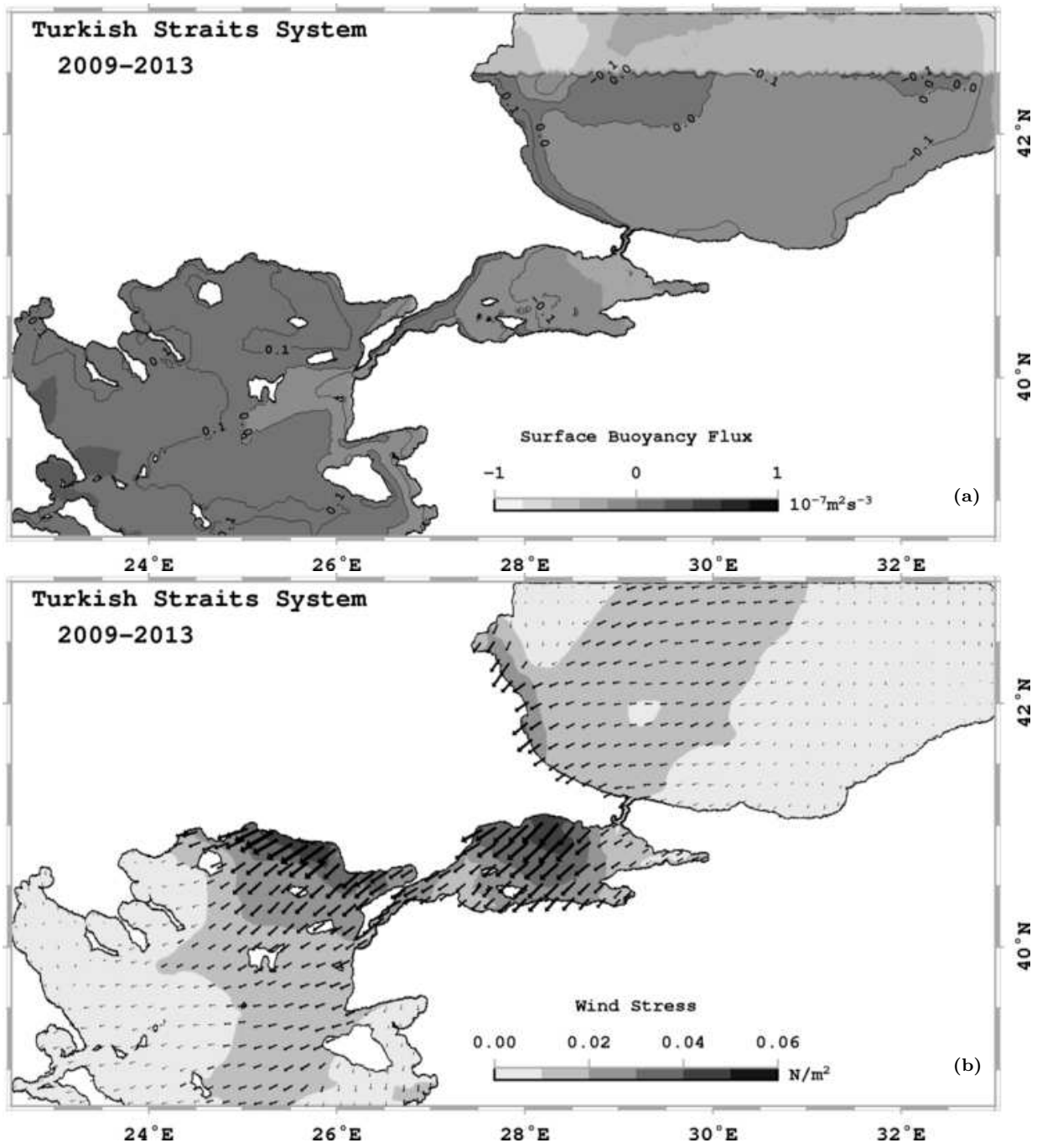

Fig. 2.5. Mean of a) surface buoyancy fluxes (negative down to the ocean) and b) true stress in Turkish Straits System for the 2009-2013 period. Vectors show the direction of the true stress in b).

Throughout this section, time averages of the simulations are computed for the 2009-2013 period. The first couple of months of the 2008 is considered as a spin-up period since the initial conditions are from a simulation without atmospheric forcing.

The daily buoyancy and momentum fluxes were averaged for 2009-2013 and are shown for

BLK02 in Fig. 2.5. The buoyancy flux was computed using the formula (2.22):

$$Q_b = \frac{g\alpha}{\rho_0 C_w} Q_H - \beta S_0 g(E - P - R) \tag{2.22}$$

where α and β are thermal and haline expansion coefficients, Q_H is the heat flux, C_w is the specific heat capacity, S_0 is the surface salinity and $E - P - R$ is the water flux.

The Black Sea and the Marmara Sea gain buoyancy except for a small area near their western coasts (Fig. 2.5a). On the other hand, the Aegean Sea has a buoyancy loss except near the Dardanelles exit and the Anatolian coast. The average buoyancy flux changes between -7x10^{-8} and 3.4x10^{-8} over the domain. It does not show significant spatial differences inter-annually but the gradient between the Aegean and Black Seas was stronger in 2011 compared to the other years (not shown).

The true stress which is computed as:

$$\tau = \rho_0 C_d \mid \mathbf{u}_d \mid \mathbf{u}_d \; where \; \mathbf{u}_d \; is \; \mathbf{u}_w - \mathbf{u}_o \tag{2.23}$$

is maximum in the northern coasts of the Aegean and Marmara Sea and exceeds 0.05 N/m^2 in the five-year mean (Fig. 2.5b). The main pattern is favourable for upwelling and downwelling in the northern and southern coasts.

2.3.2 Comparison of the Experiments

The comparison of the surface salinity in the two simulations reveals the impact of the different surface salinity boundary conditions (Fig. 2.6). The surface salinity in BLK02 ranges from 16 psu to 38 psu over the whole domain (Fig. 2.6a). The surface waters exit the Bosphorus with a salinity about 21 psu and the Dardanelles with a salinity about 30 psu. In the northern Marmara Sea, the surface salinity is less than 23 psu and it increases to 25 psu in the south. Fig. 2.6b shows the difference between BLK02 and BLK01. BLK02 is about 1 psu less saline than BLK01 in the Black Sea. On the contrary, the surface water becomes saltier in BLK02 in the Aegean Sea since evaporation is higher than precipitation. In the Marmara Sea, the difference between the simulations is about 0.6 psu. Long-term measurements from 1986 to 1992 in the Marmara Sea assert a surface salinity ranging between 23±2 psu [Beşiktepe et al., 1994] satisfied by both simulations.

The impact of the difference in surface salinity boundary conditions is also pronounced in the subsurface waters of the Aegean Sea entering the Marmara Sea through the Dardanelles. In Fig. 2.7a and 2.7b, the mean temperatures in the last year of the simulations is shown for BLK01 and BLK02, respectively, along the thalweg (see Fig. 2.2). In BLK01, the subsurface waters

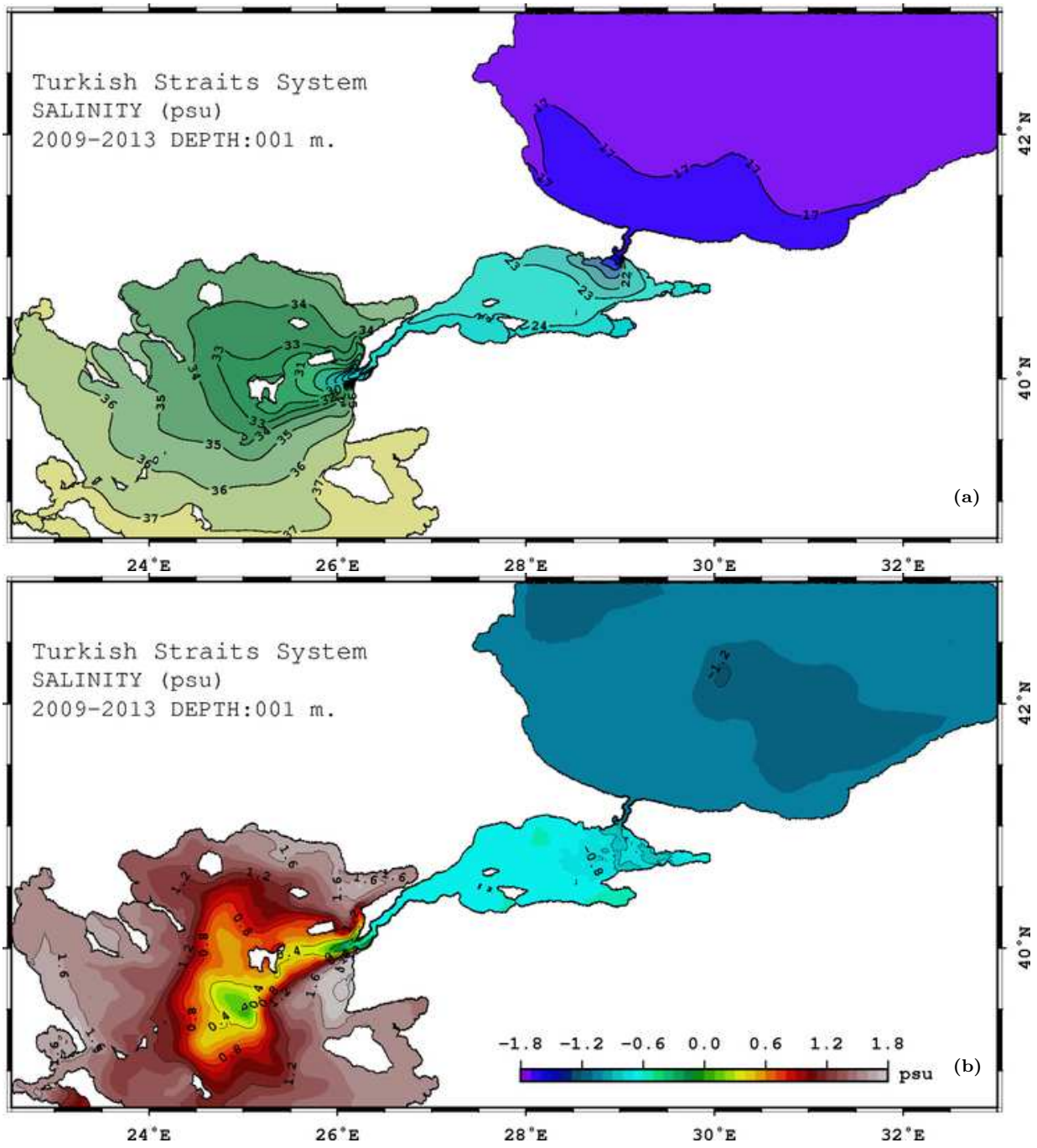

Fig. 2.6. The mean of surface salinity for 2009-2013. a) BLK02 b) difference between BLK02 and BLK01.

with temperatures around 9°C are about 25 m deep in the Dardanelles and its Aegean exit while they are absent in BLK02. The cold water masses developed in the Aegean side during winter periods are trapped in the subsurface in a different way in BLK01 and BLK02. The subsurface salinity is also different in two simulations (Fig. 2.7c and 2.7d). BLK01 is more stratified in the Dardanelles and Marmara Sea whereas BLK02 is almost homogeneous in the Marmara Sea below 25 m. Moreover, less saline surface waters reach to 20 m in the Black Sea and Bosphorus in

BLK02. These water mass differences generate different density structures at the Dardanelles with denser water in BLK02 below the pycnocline (Fig. 2.7e,f).

The difference in the water mass structure of the two experiments also appears in the Hovmoller diagram of daily salinity and temperature profiles at the strait exits (Fig. 2.8). Subsurface salinity starts to differ after the first year of the simulations at the southern exit of the Dardanelles (upper panels). The winter of 2009 is the beginning of appearance of the cold water in the Dardanelles in BLK01 and it is accumulated every year thereafter. This water mass moves to the northern exit and sinks to a lower layer (Fig. 2.8c) after 2012. In BLK02, however, water below the thermocline is more homogeneous (Fig. 2.8b,d).

The stratification at the Bosphorus side of the Marmara Sea is more similar in BLK01 and BLK02 (Fig. 2.7). Altiok et al. [2012] reported a cold tongue in the Bosphorus extending to the Marmara Sea with a temperature about 11-12°C in June-July between 1996-2000. In the Marmara Sea, this cold tongue emerges as a cold intermediate layer (CIL) between the thermocline and the Mediterranean waters of 14°C. This water mass was also observed by Altiok et al. [2012] and reproduced in both simulations (Fig. 2.7a,b). However, the Mediterranean waters below the CIL are modified by the cold water which propagates from the Dardanelles in BLK01.

In general, salinity decreases from south to north and the halocline deepens from 8-9 m to 45-46 m. The thermocline is shallower in the southern exits of the straits and reach a 25 m depth in the northern Bosphorus. Altiok et al. [2012] gives a temperature range of between 6-26°C in the northern exit of the Bosphorus while temperatures below 3°C have also been observed during the winters of 1944 and 1954 [Acara, 1958]. A minimum temperature of approximately 3.5°C occurred in 2012 which is an anomalous year for the winter season with strong cold events over Europe [Luo et al., 2014]. The impact of the temperature anomaly in 2012 has been studied for the Adriatic Sea [Benetazzo et al., 2014] showing a strong cooling in two weeks but no similar study has yet been carried out for the Black Sea.

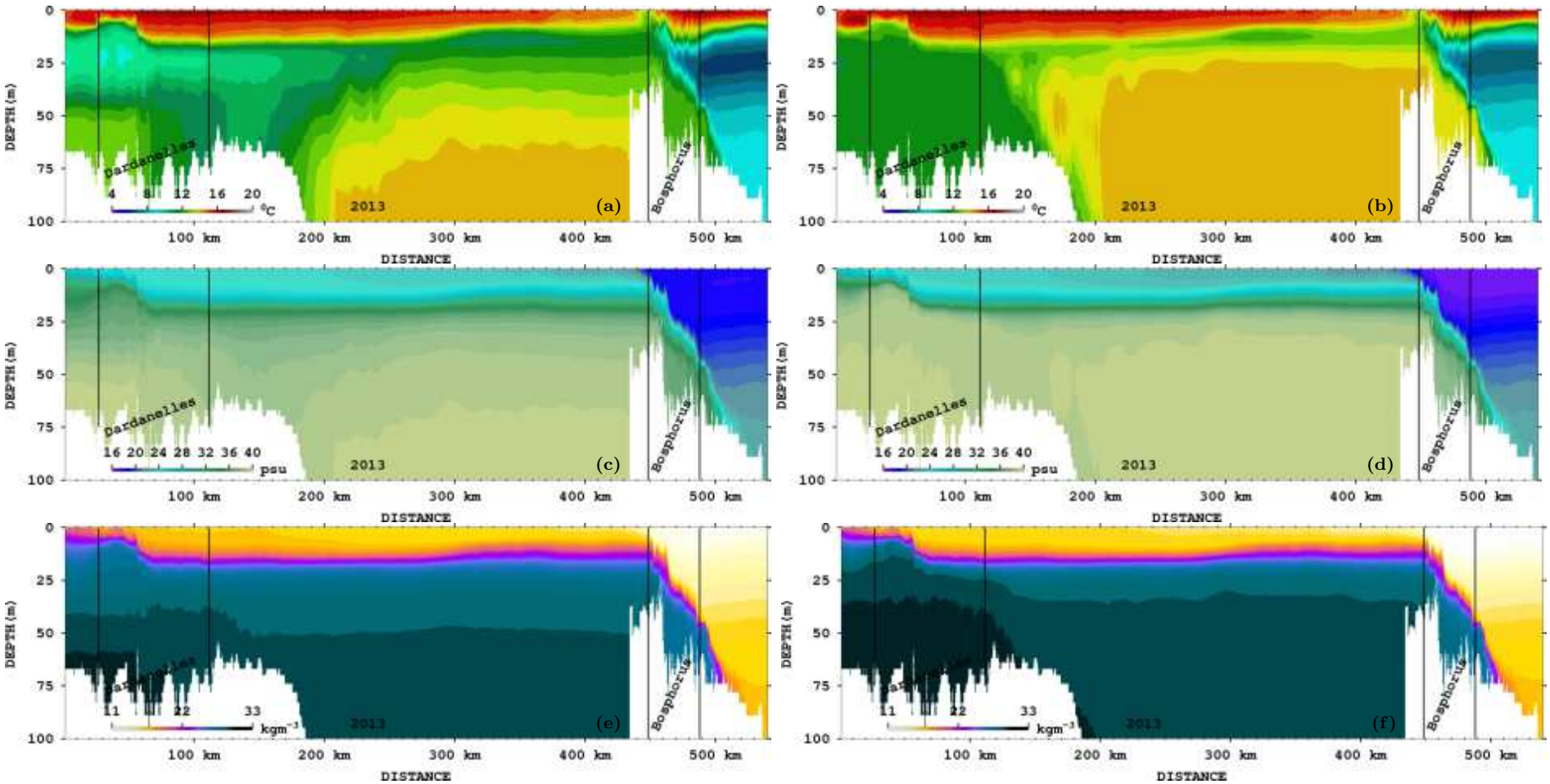

Fig. 2.7. Annual mean of temperature (top), salinity (middle) and density (bottom) along the thalweg for BLK01 (left) BLK02 (right) for 2013.

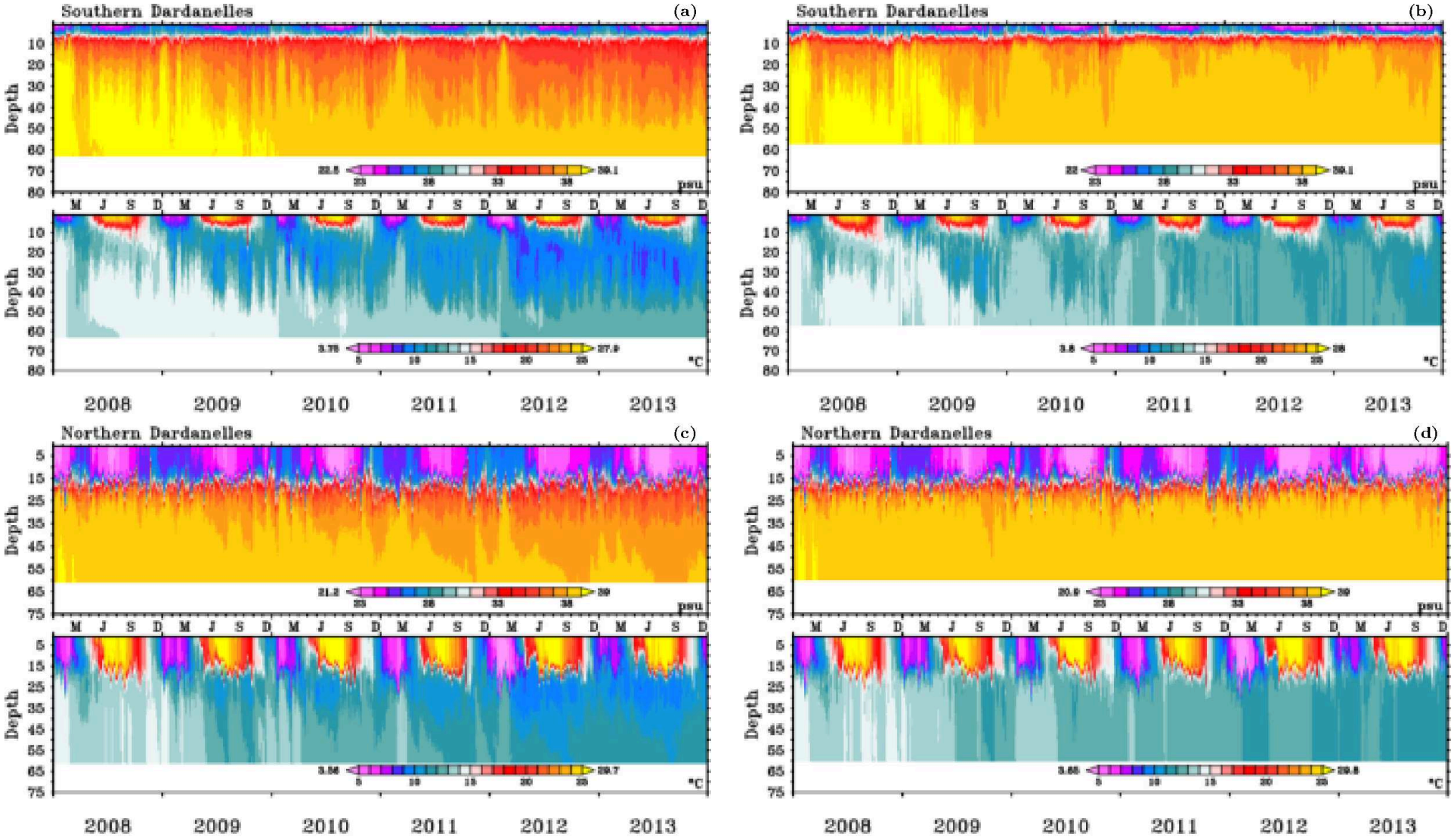

Fig. 2.8. Hovmoller diagram of daily salinity (upper panel) and temperature (lower panel) profiles for BLK01 (left) and BLK02 (right) at Southern Dardanelles (top) and Northern Dardanelles (bottom). Extrema are printed on the color bars.

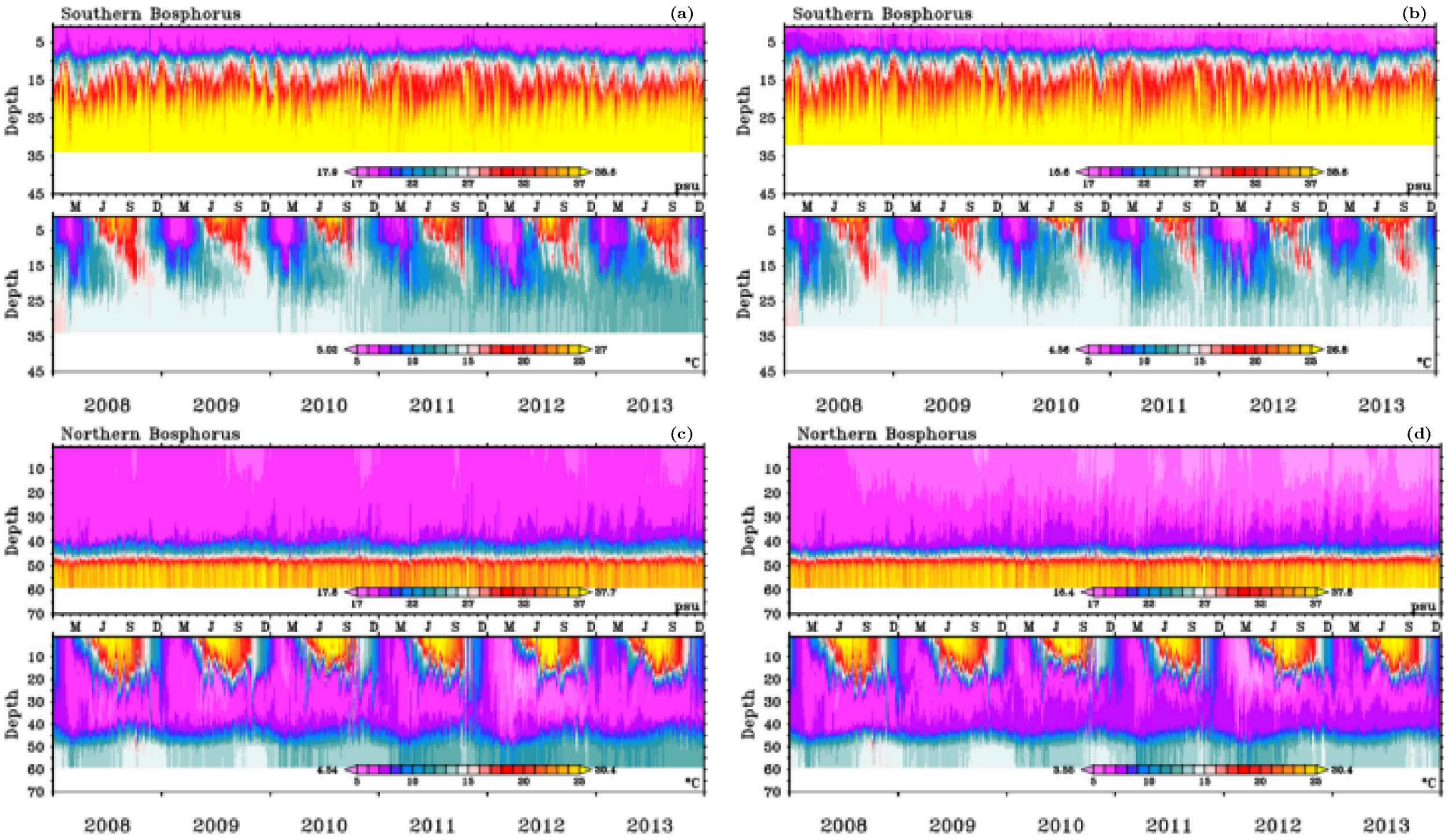

Fig. 2.9. Same as Fig. 2.8 but for Southern and Northern Bosphorus.

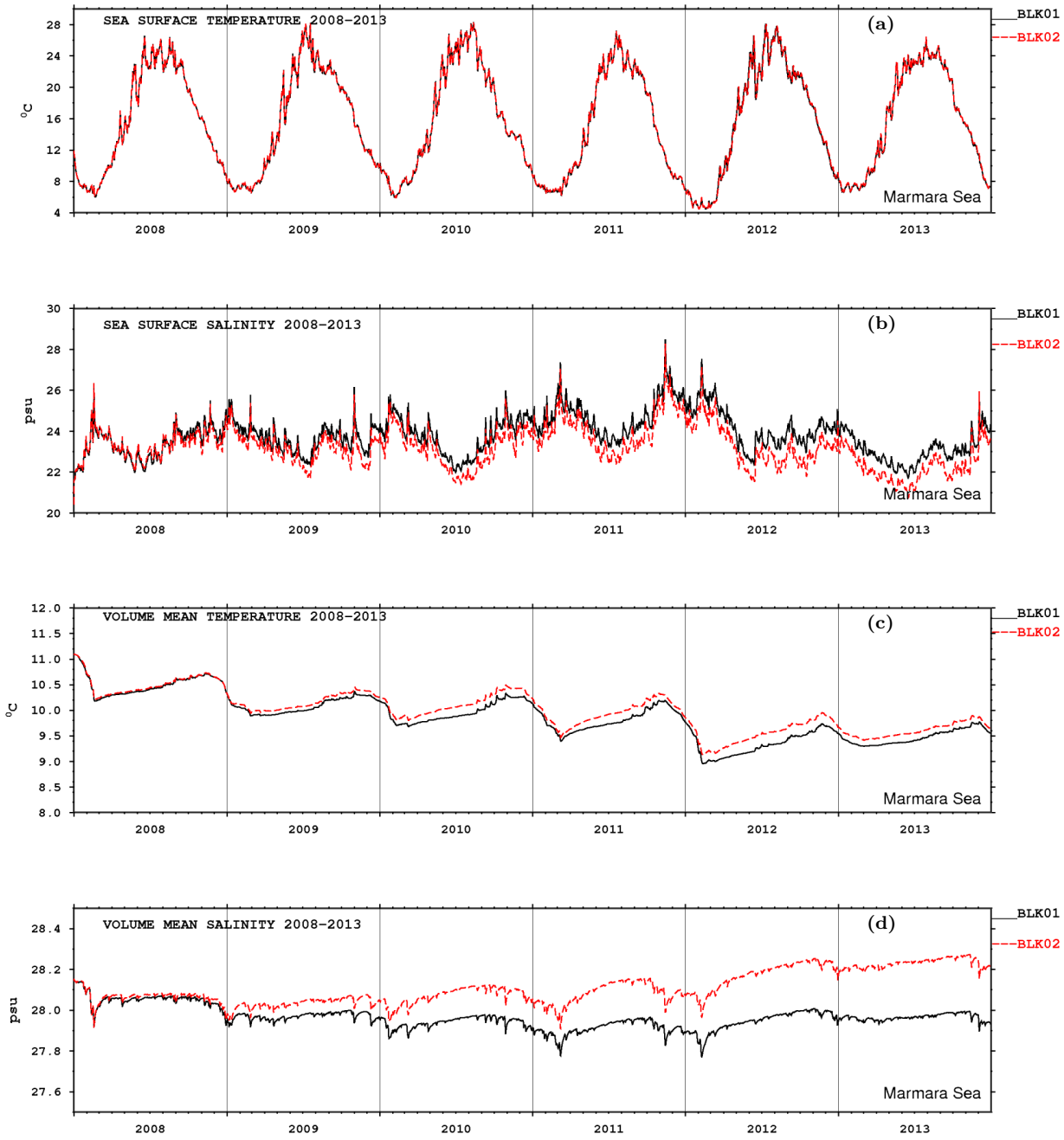

Fig. 2.10. Timeseries of daily averages of a) surface salinity b) surface temperature c) volume salinity d) volume temperature in the Marmara Sea for BLK01 (black) and BLK02 (red).

The mean sea surface temperature in the Marmara Sea fluctuates between 4.4 - 28.3°C in both experiments (Fig. 2.10a). Surface mean salinities are in phase and BLK02 is approximately 1 psu less saline than BLK01 at the end of the simulations (Fig. 2.10b). Volume mean salinity and temperature in BLK01 and BLK02 start to diverge in time by winter 2009. The volume averages show that the intermediate and bottom layers of the Marmara Sea still continue to adjust after six years of integration. As shown above, more saline water masses enter from the

Dardanelles in BLK02 increasing the salinity in the Marmara Sea. At the end of the integration there is more than 0.2 psu difference between the volume averages of the two solutions. Volume mean temperatures start from 11°C and decrease to 9-10°C interval varying seasonally. The range of temperature and salinity averages in the Marmara Sea for both experiments are listed in Table 2.4.

	SSS	VMS	SST	VMT
BLK01	20.42-28.48 psu	27.76-28.15 psu	4.46-28.28 $^{\circ}C$	8.85-11.09 $^{\circ}C$
BLK02	20.42-28.26 psu	27.90-28.27 psu	4.43-28.24 $^{\circ}C$	9.13-11.09 $^{\circ}C$

Table 2.4: Range of mean sea surface salinity (SSS), volume mean salinity (VMS), mean sea surface temperature (SST) and volume mean temperature (VMT) during the simulations.

2.3.3 Comparison with observations and skill assessment

In this section, the temperature and salinity of the simulations are evaluated with observations in the Marmara Sea. We use two datasets of in-situ CTD observations collected by R/V Bilim2 from the Institute of Marine Sciences (IMS/METU[1]) from 4-11 April 2008 and 1-4 October 2008 and 18-23 June 2013.

Fig. 2.11 compares the mean profiles between simulations and observations for April 2008, October 2008 and June 2013. In April and October 2008, there are very small differences between BLK01 and BLK02. The simulated salinity in the surface layers is ∼1.5 psu less than observed for both simulations and the halocline thickness is about ∼15 m (Fig. 2.11a,b). After six years of integration (Fig. 2.11c,f), in June 2013, the two simulations differ and BLK02 is closer to the observations for both temperature and salinity although the halocline is 10 m higher than in the observations.

The RMS errors of salinity and temperature corresponding to the profiles in Fig. 2.11 are depicted in Fig. 2.12. There are differences between BLK01 and BLK02 shown in June 2013 near the halocline and thermocline. The maximum RMS errors are approximately 8 psu and 5°C for salinity and temperature due to the difference in the thermocline and halocline positions as also shown in Fig 2.11.

In the following two figures (Fig. 2.13 and 2.14), the horizontal distribution of RMS errors with respect to the CTD observations averaged in the first 50 m depth are presented in order

[1]The first two datasets are from European SESAME-Southern European Seas: Assessing and Modeling Ecosystem Changes Integrated Project/ FP6. The last dataset is from the subsequent PERSEUS: Policy-oriented marine Environmental Research for the Southern European Seas Funded by the EU under FP7 Theme Oceans of Tomorrow OCEAN.2011-3 Grant Agreement No. 287600 project.

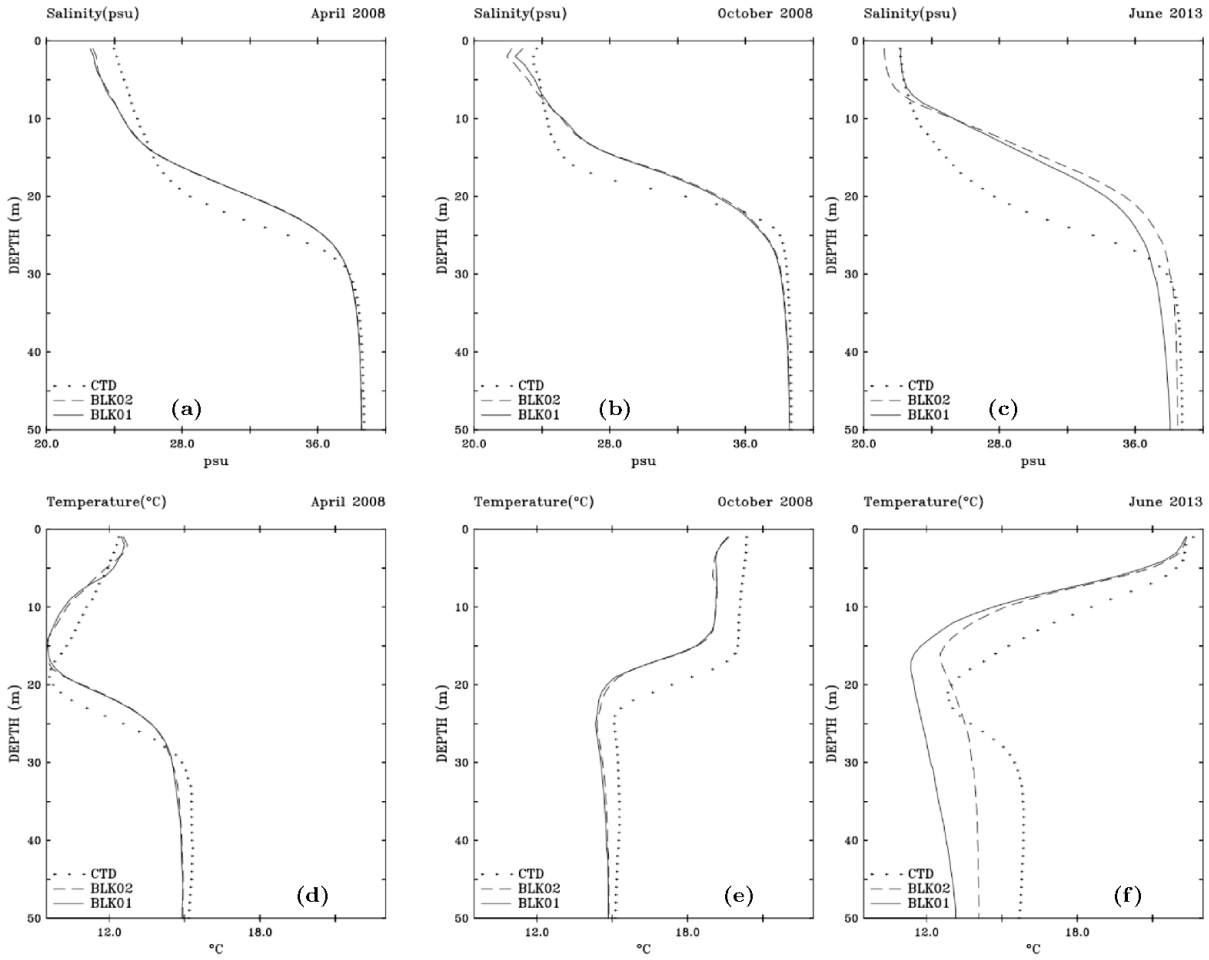

Fig. 2.11. Comparison of simulations with in-situ CTD observations at the top 50 m. of the water column in April 2008, October 2008 and June 2013 from left to right, respectively. Panels at the top and bottom refer to salinity and temperature, respectively.

	April 2008		October 2008		June 2013	
psu / °C	Salinity	Temperature	Salinity	Temperature	Salinity	Temperature
BLK01	1.31	0.81	1.61	1.10	2.75	2.78
BLK02	1.34	0.77	1.71	1.09	3.18	2.09

Table 2.5: Mean RMS error with respect to CTD measurements for BLK01 and BLK02

to see how well the model performs in different areas of the Marmara Sea. For 2008, we only show the validation of BLK02 (Fig. 2.13) because spatial error distributions are similar for both simulations.

In April 2008, the mean RMS error of salinity and temperature for BLK02 is computed as 1.34 psu and 0.77°C (Table 2.5), respectively. For both variables, the errors are higher in the regions under the influence of the Bosphorus. In October 2008, the salinity RMS error increases to 1.71 psu. The error is more pronounced in the Bosphorus exit and along the track in the middle of the Marmara Sea. Same conclusion is valid for temperature with a RMS error of 1.09°C.

In June 2013 (Fig. 2.14), there is an overall decrease in the performance of the model (note

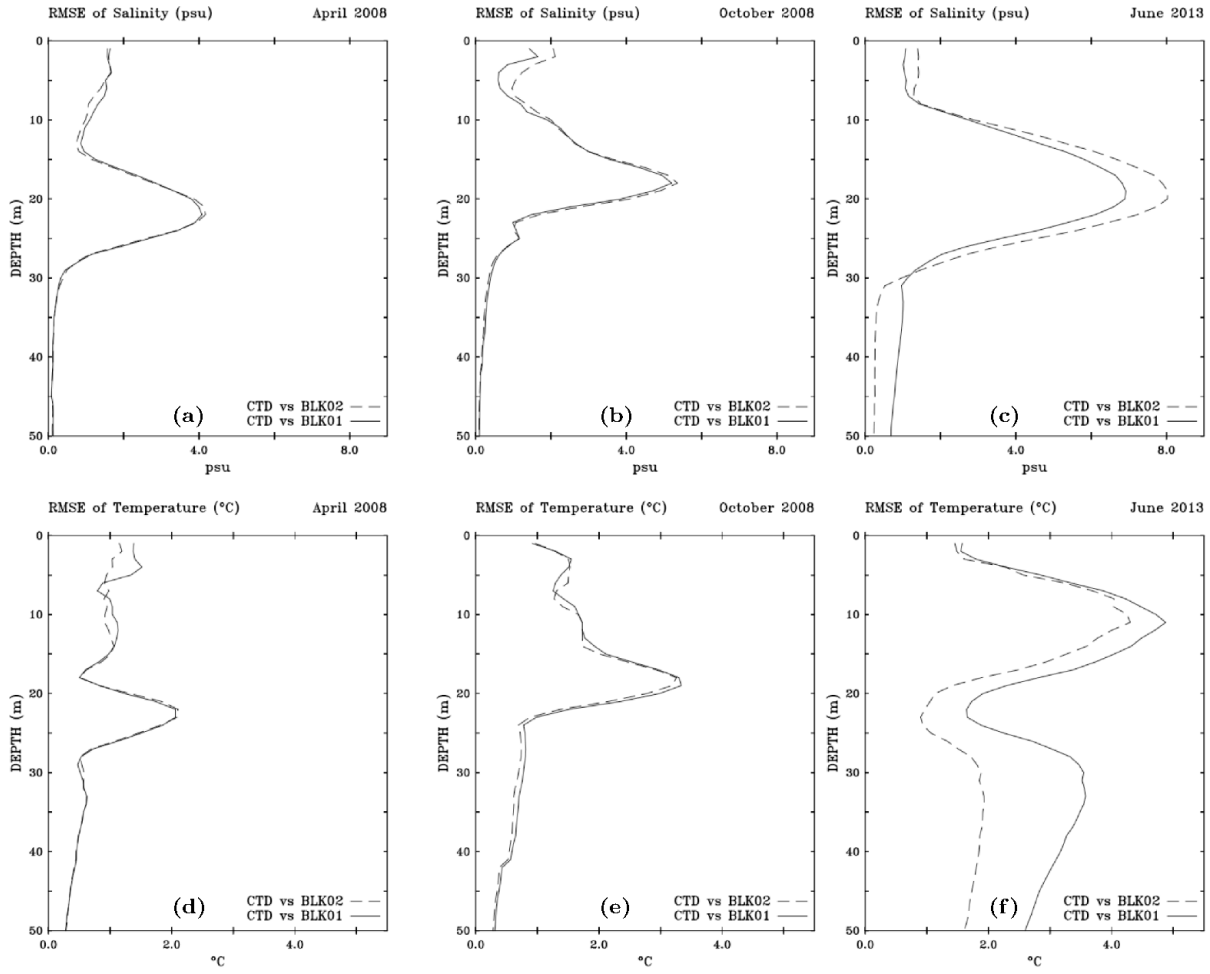

Fig. 2.12. Vertical distributions of salinity (top) and temperature (bottom) RMS errors in April 2008, October 2008 and June 2013 from left to right, respectively.

the difference in color scale with the previous figure). The mean RMS salinity error is higher for BLK02 (3.18 psu) than BLK01 (2.75 psu). Conversely, BLK02 performes better for temperature. The impact of the cold water intrusion from the Dardanelles is clearly detected in the temperature errors, especially in BLK01.

2.4 Summary and discussion

In this paper, which is the first of a two-part report, we have presented two simulations of the Turkish Straits System for a six-year period using realistic atmospheric forcing and different surface salinity boundary conditions.

The two simulations show that a realistic simulation of the TSS is possible and that the model is able to represent many of the qualitative characteristics of the system. Furthermore, the results demonstrate that the halocline and thermocline can be kept similar to observations and stable throughout the integration. The model is able to reproduce the historically reported water mass

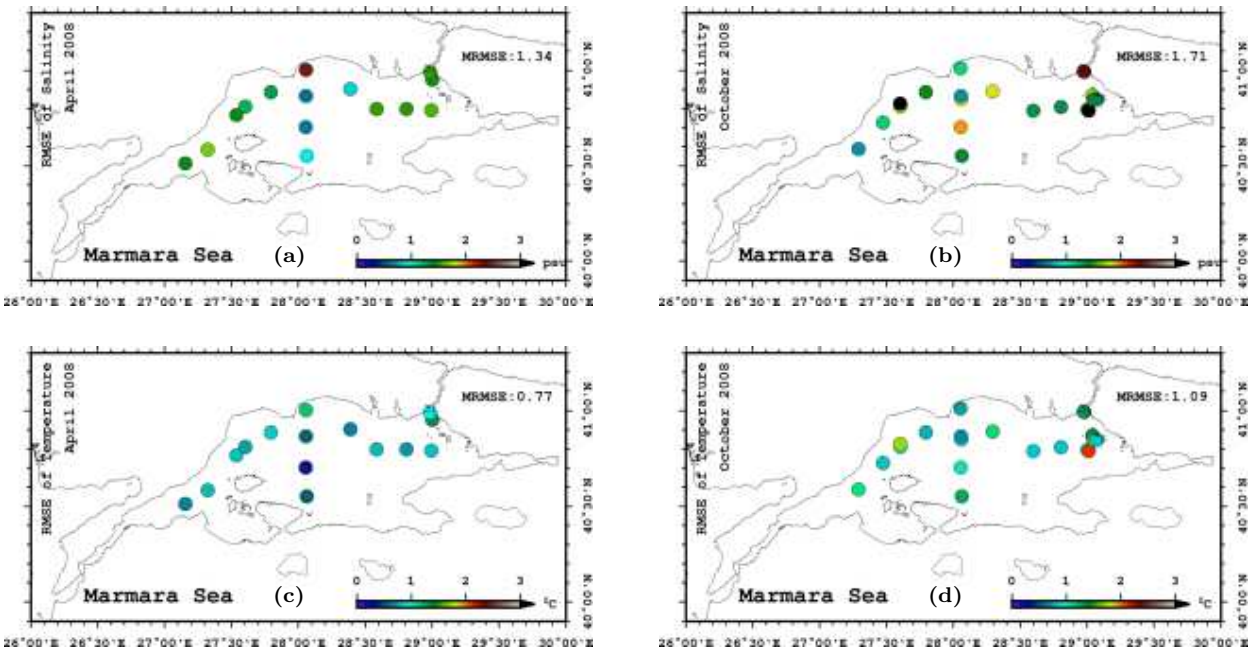

Fig. 2.13. Horizontal distribution of RMS errors computed at the top 50 m. of the CTD casts for BLK02 a) salinity in April 2008 and b) salinity in October 2008, c) temperature in April 2008 and d) temperature in October 2008.

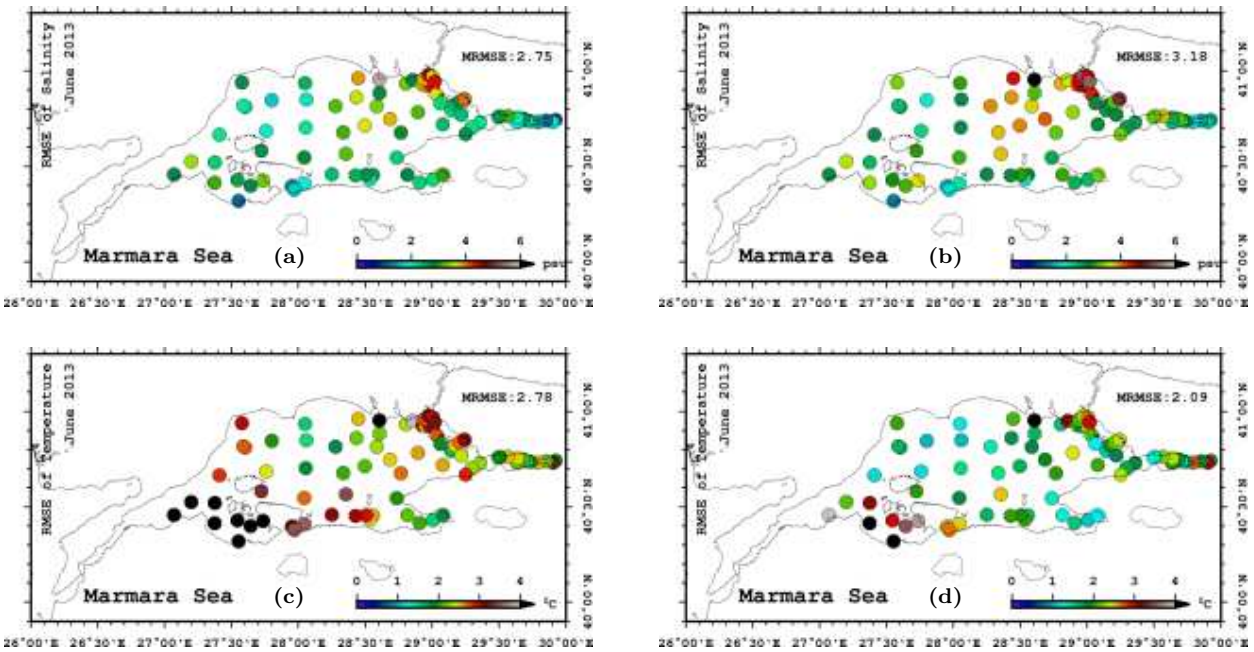

Fig. 2.14. Horizontal distribution of RMS errors of a) salinity in BLK01 b) salinity in BLK02 c) salinity in BLK01 and d) salinity in BLK02 computed at the top 50 m. of the CTD casts in June 2013. Note the different scales are from the those in Fig. 2.13

structure of the Marmara Sea. Model errors peak particularly in the mixed layer especially for salinity and in the halocline and thermocline depths. The largest error in June 2013 may be due to an insufficient water transport through the Bosphorus which is known to be maximum in

summer.

The importance of the surface salinity boundary condition for the Dardanelles inflow has been demonstrated. Strong stratification in BLK01 generated a cold intermediate layer in the Dardanelles similar to the one in the Bosphorus. The propagation of the CIL in the Dardanelles towards the Marmara Sea resulted in a different lower layer structure in the two simulations.

The results discussed this part are not independent of the dynamical aspects of the system and circulation in the Marmara Sea. We will support and enhance the conclusions established in this manuscript in Part II of this study.

Chapter 3

Numerical simulations of the Turkish Straits System for the 2008-2013 period

Part II: Inter-annual variability in circulation and dynamics

Abstract

In the first part of the study, we presented two six-year simulations of the Turkish Straits System. We showed that the model is able to reproduce the water mass structure of the system. In this second part, we focus on the dynamics and the circulation of the Marmara Sea and the volume fluxes through the Bosphorus and Dardanelles. The net volume flux through the Bosphorus compares well with the observations. However, the upper and lower layer fluxes are always less than the observed estimations. The wind work in the Marmara Sea is shown to be even higher than the Baltic Sea. The kinetic energy due to the wind can exceed the energy input due to the Bosphorus outflow in some years. The kinetic energy in the Marmara Sea strongly responds to the short-term atmospheric cyclone passages. We identified two circulation patterns in the annual averages. When the wind stress maxima is located in the central basin, the Bosphorus jet flows to the south and turns west after reaching the Bozburun peninsula. On the other hand, when the wind stress maxima increases and expands to the north, the jet deviates to the west after exiting the strait and forms a cyclonic gyre in the central basin.

3.1 Introduction

This paper is the second part of our study on the multi-year numerical simulation of the Turkish Straits System (hereafter TSS). For what we believe is the first time, the TSS has been simulated with a three dimensional ocean circulation model forced by realistic air-sea forcings for such a long period. In the previous part (hereafter PART I), we described the TSS model set-up and two six-year experiments between 2008-2013. We studied the impact of different surface salinity boundary conditions on the water mass structure of the Marmara Sea and the Straits in the TSS on multi-year timescales. The simulations were validated with available observations for temperature and salinity.

We first demonstrated that the model is capable of successfully simulating annual mean thermohaline state of the Marmara Sea. The variability of the salinity and temperature was represented qualitatively. The interface depth between the upper and lower layers was kept stable throughout the simulations. However, a comparison with the observations suggests that the slope of the interface between the upper and lower layers was not captured well in June 2013 whereas it was much better in April and October 2008.

A comparison of the two experiments revealed the importance of the surface salinity boundary condition for the lower layer of the Marmara Sea. The strong stratification in BLK01 experiment generated a cold intermediate layer (CIL) in the Dardanelles similar to the CIL of the Black Sea. The propagation of a CIL through the Dardanelles changes the lower layer structure of the Marmara Sea.

In this second part, we focus on the inter-annual variability of the dynamical aspects of the system and circulation in the Marmara Sea. The analysis is presented only for the BLK02 experiment since there are small differences between BLK01 and BLK02 in terms of dynamics and circulation.

In section 3.2, the dynamical initial conditions and relevant atmospheric forcing are presented. In the results section 3.3, the sea surface height differences and volume fluxes through the straits are demonstrated and compared with the observations. In addition, the mean circulation of the Marmara Sea in different years is analyzed together with the wind work and kinetic energy budgets. In the last section, we summarize and conclude the study.

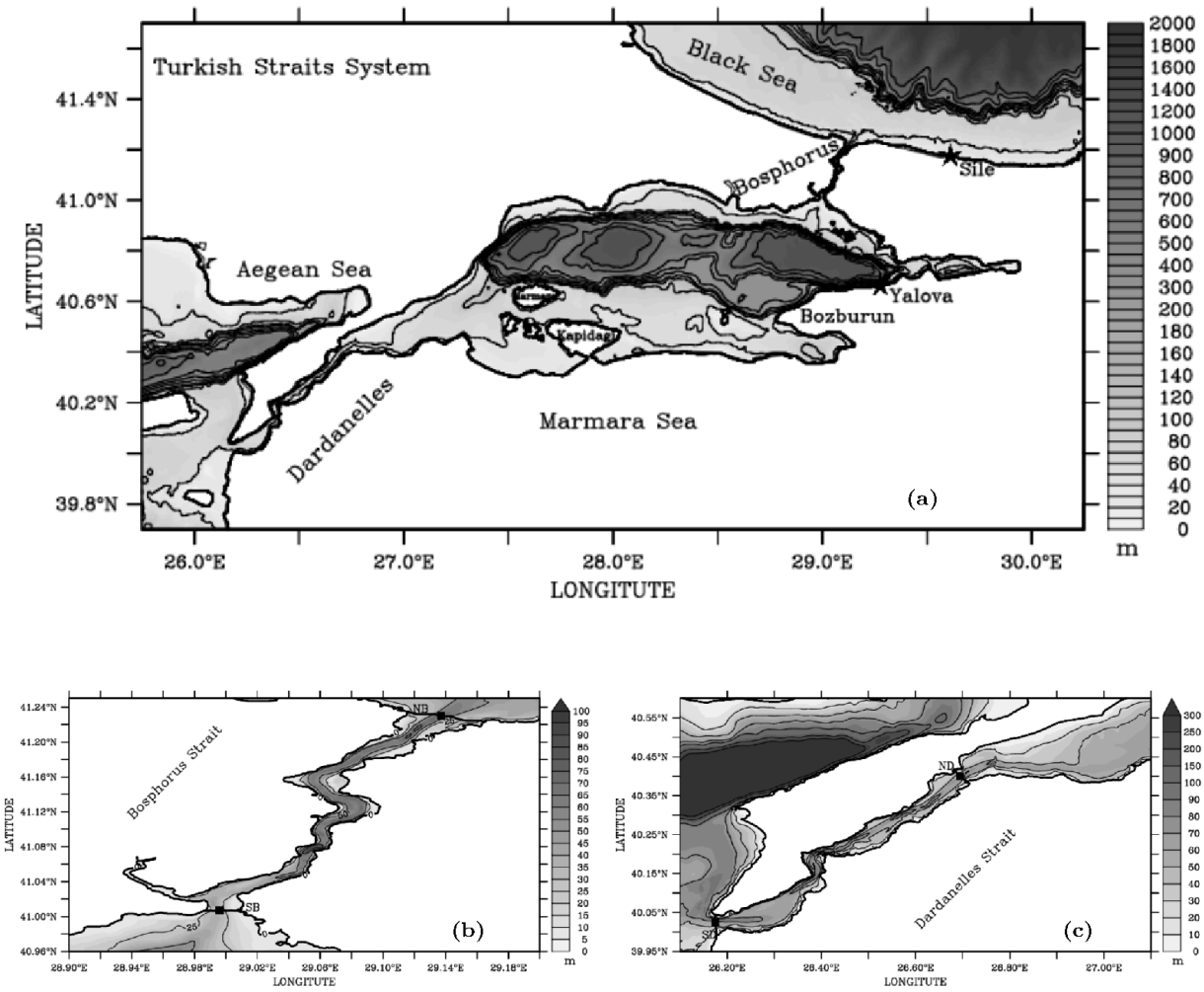

Fig. 3.1. a) Bathymetry of the Turkish Straits System. Contour interval is 50 m between 0-200 m, 100 m between 200-500 m and 250 m between 500-1000 m. b) Bosphorus Strait c) Dardanelles Strait. The locations used for the strait exits are marked by squares. The cross-sections for volume flux computations are shown by the straight lines for each exit of the straits.

3.2 Initialization and Surface Forcing

Figure 3.2 shows the initial sea surface height and surface velocity currents. In the initial state, the sea surface height difference between the Dardanelles and the Bosphorus is small since the net water fluxes have not yet been introduced in Gürses [2016] lock-exchange experiments which are integrated for three months starting from single vertical profiles in each basin. Two anti-cyclones have already formed one in the mid-basin and another due to buoyant Bosphorus jet. The circulation of the Marmara Sea is similar to the no barotropic volume flux - no atmospheric forcing case of Sannino et al. [2015]. The velocity of the Bosphorus and Dardanelles outflows

exceeds 0.5 m/s.

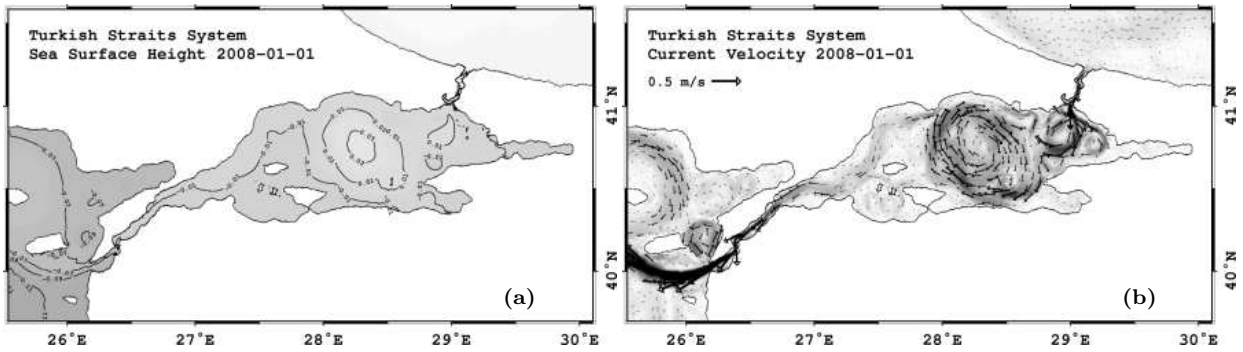

Fig. 3.2. Initial condition on 1 January 2008 a) sea surface height (m) b) surface current velocity (ms^{-1})

In PART I, we discussed the surface buoyancy fluxes in the Marmara Sea and found that overall there is a buoyancy gain as with the Black Sea. The annual mean of wind, wind stress and curl are shown for 2009 (Fig. 3.3a), 2011 (Fig. 3.3b) and 2013 (Fig. 3.3c). The annual mean wind fields are north easterlies which are strongest in 2011 and weakest in 2013. Wind stress is calculated as

$$\tau = \rho_0 C_d \mid \mathbf{u}_{wind} \mid \mathbf{u}_{wind} \; where \; C_d = 1.2 \cdot 10^{-3} \tag{3.1}$$

and is higher than 0.04 Nm^{-2} in the central-north Marmara Sea in 2009. It expands in north-south direction exceeding 0.05 Nm^{-2} in the central basin in 2011 and then weakens again in 2013. The wind stress curl is a dipole shaped by the north easterlies, negative in the north and west, and positive in the south and east Marmara Sea. In 2011, the wind stress curl intensifies compared to the other two years.

3.3 Results

3.3.1 Inter-annual variability of the strait outflows

The sea level difference of BLK02 between the Şile (Black Sea) and Yalova (Marmara Sea, see Fig. 3.1) are compared with measurements collected between 2008-2011 [Tutsak, 2012] (Fig. 3.4). The correlation with the measurements is 0.56. The mean sea level difference between the two stations is 0.12 m and 0.18 m for observations and simulation, respectively. However, the response of the model is weaker during atmospheric cyclone passages in which the sea level difference is amplified, or sometimes reversed, i.e. the eastern Marmara Sea sea level is higher than the southwestern Black Sea. The higher sea level in the Marmara Sea may result in a short term

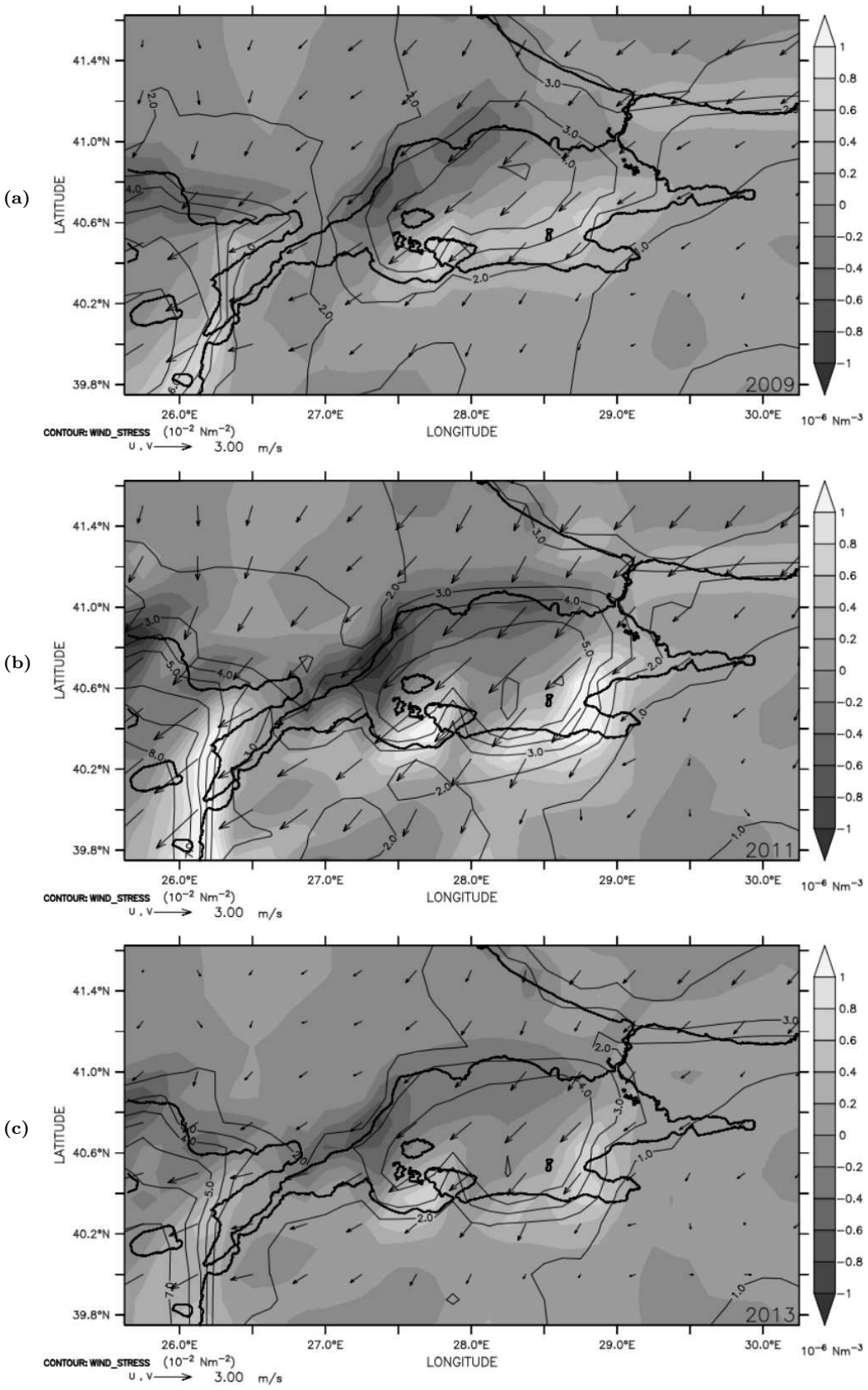

Fig. 3.3. Mean wind velocity (ms^{-1}, arrows), wind stress ($10^{-2}Nm^{-2}$, contour) and wind stress curl ($10^{-6}Nm^{-3}$, shades) in the Marmara Sea for a) 2009 and b) 2011 c) 2013

blocking or even reversal of the Bosphorus surface flow (locally called Orkoz). One such events was studied by Book et al. [2014] for 21 November 2008 in relation to the bottom pressure change during an atmospheric cyclone passage. The signal of this event is captured in the sea level difference measurements and successfully reproduced by the model, though with a smaller amplitude (Fig. 3.4).

The blocking events can also be investigated by along-strait velocities. Fig. 3.5 shows the Hovmoller diagram of the daily along-strait velocities from the surface to a 30 m depth at the southern exit of the Bosphorus. In addition to the reversal event in 21 November 2008, some other blocking or reversal events can also be identified such as those in October 2009, May 2010 and October 2011.

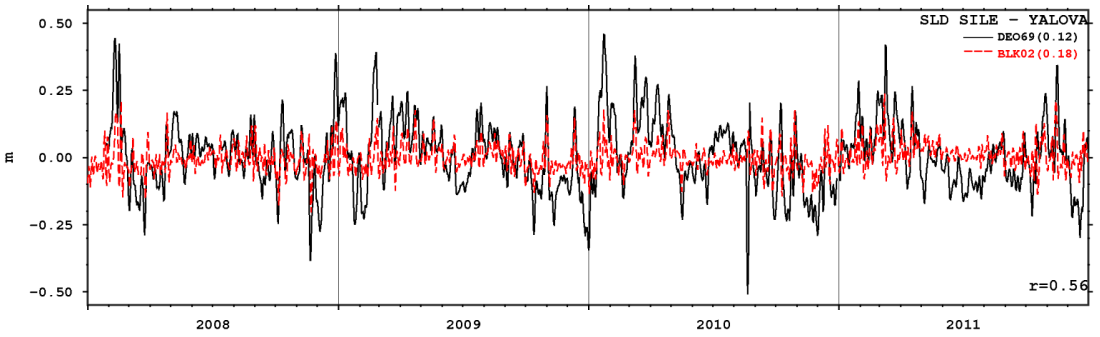

Fig. 3.4. Sea level differences (SLD) between Sile and Yalova (See Fig. 3.1) between 2008-2011 in meters. The in-situ observation DOE69 is plotted with black for daily averages. The BLK02 SLD is shown by red dashes. The four-year means subtracted from the time series are in the legend.

Upper layer velocities in the southern exits of both the Bosphorus (Fig. 3.5) and Dardanelles are generally higher than their northern exits due to hydraulic controls exerted at the constrictions in the middle of both straits and the expansion area in the mouth [Sözer, 2013]. Conversely, lower layer velocities have much higher maxima at the northern exits in both straits. In particular, the maximum along-strait velocity of the upper layer flow is ∼-0.35 m/s and the lower layer flow is ∼1.4 m/s in the northern Bosphorus. In the southern Bosphorus, the maximum velocity of the upper layer flow is ∼-1.85 m/s and the lower layer flow is 0.63 m/s. In the Dardanelles, the maximum upper layer along-strait velocities are ∼-1.0 m/s and ∼-1.8 m/s in the northern and southern exits, respectively. In the lower layer, the maximum along-strait velocities are ∼0.78 m/s and ∼0.5 m/s for the northern and southern exits of the Dardanelles, respectively. Lower layer velocities are roughly 0.2 m/s less than the measurements by Jarosz et al. [2011b, 2012] in both straits. At the northern exits of both straits, the upper layer maximum velocities

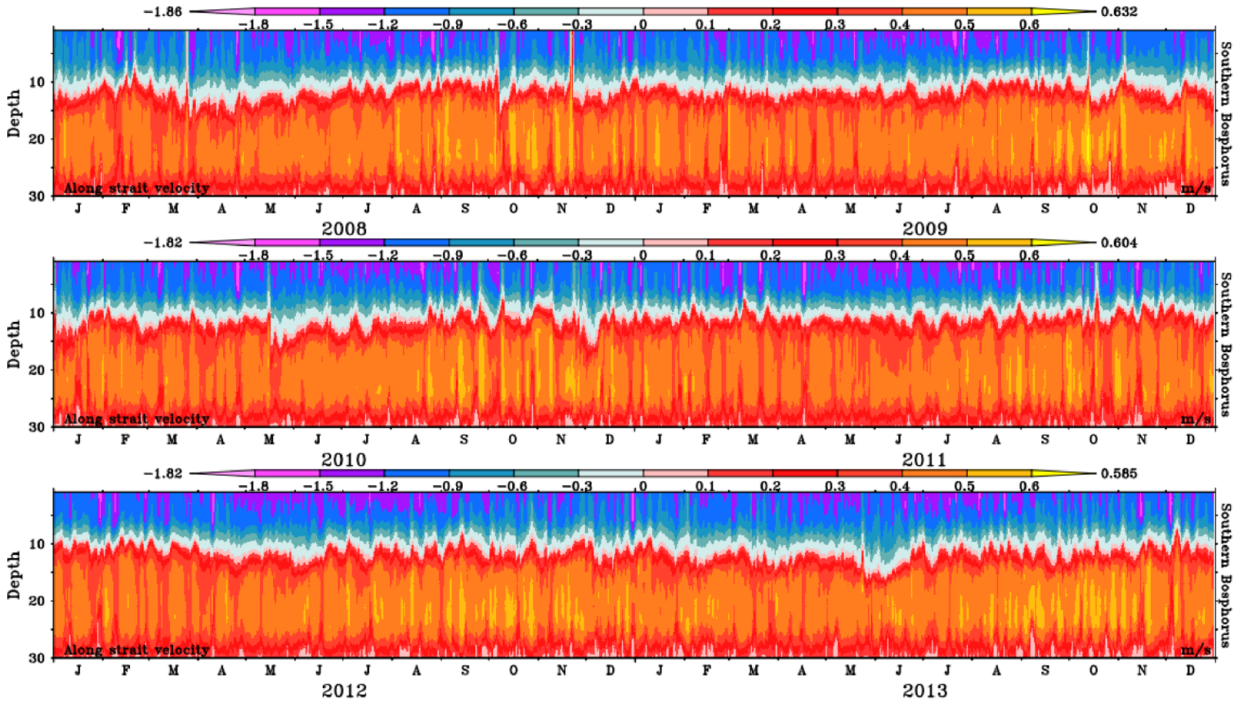

Fig. 3.5. Time series of along-strait velocity (ms^{-1}) in the southern Bosphorus. Each panel shows a two-years period. See the squares in Fig. 3.1b and c for the location of the profiles in the southern Bosphorus exit as well as in the other strait exits.

are in accordance with data. But in the southern Bosphorus, there are maximum velocities of 2.3 m/s during extreme atmospheric conditions. The model produces higher extrema also in the southern Dardanelles upper layer compared to the observations. However, this is probably because measurements are not available at the surface layer where the extrema are mostly confined.

The depth of the zero velocity level varies significantly in the straits. In the northern Bosphorus, the upper layer flow reaches a depth of 40 m, while in the southern Bosphorus, the upper layer depth decreases to approximately 10 m. In the northern Dardanelles, the interface is about 20 m depth and the upper layer flow at the southern Dardanelles reaches to 10 m depth. These approximate depths are consistent with the recent observations reported in Jarosz et al. [2011b, 2012] for northern Bosphorus, southern Bosphorus, northern Dardanelles and southern Dardanelles approximately as 39 m, 13.5 m, 22 m and 13 m, respectively.

The resulting upper layer and lower layer volume fluxes in both straits are lower than the previous estimates based on the observations, the differences being larger in the Dardanelles. The baroclinic and barotropic volume transports through the straits are computed and shown in Fig. 3.6 with the overlay of the estimates by Jarosz et al. [2011a, 2013].

In the northern Bosphorus, the time-mean of the upper and lower layer volume transports are -283 km^3/yr and 136 km^3/yr, respectively where positive sign is the flux from the Marmara Sea to the Black Sea (Fig. 3.6a). Jarosz et al. [2011b] estimated the upper layer flux as -375

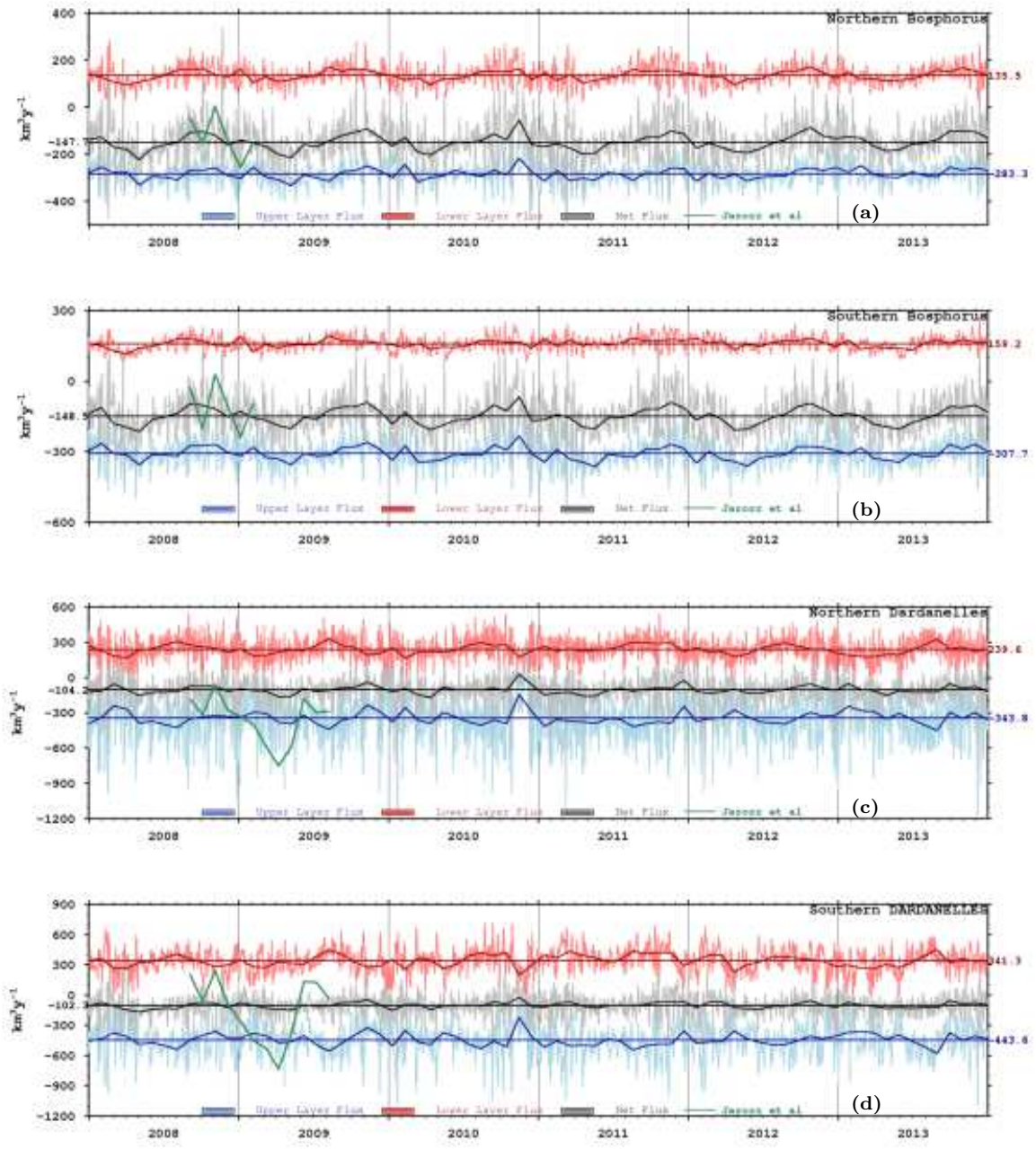

Fig. 3.6. Daily upper layer (blue), lower layer (red) and net volume fluxes (gray) through a) Northern Bosphorus b) Southern Bosphorus c) Northern Dardanelles d) Southern Dardanelles in km^3yr^{-1}. Monthly and five-year averages are overlaid with a darker color. The monthly means of volume fluxes for Jarosz et al. [2011a, 2013] are shown in green for the period of observations.

km^3/yr and lower layer flux as 253 km^3/yr between 2 September 2008 - 5 February 2009 (see Table 3.1). For the same period, the corresponding volume fluxes in simulation are ∼25% less than their estimates. However, the average net volume transport matches with the observations although the monthly variability is smaller.

Strait	Experiment	Net Flux	Upper Layer Flux	Lower Layer Flux
Jarosz et al. 2011 2 September 2008 - 5 February 2009 (km^3/yr)				
Northern Bosphorus	BLK02	-122	-272	150
	Jarosz	-122	-375	253
Southern Bosphorus	BLK02	-117	-282	165
	Jarosz	-111	-444	333
Jarosz et al. 2013 1 September 2008 - 31 August 2009 (km^3/yr)				
Northern Dardanelles	BLK02	-108	-351	242
	Jarosz	-367	-809	442
Southern Dardanelles	BLK02	-107	-436	329
	Jarosz	-158	-1156	998

Table 3.1: Volume Fluxes through the straits. Negative means volume flux is from the Black Sea to Marmara Sea in the Bosphorus and from the Marmara Sea to Aegean Sea in the Dardanelles.

In the southern Bosphorus, the rate of upper and lower fluxes are approximately 50% less than the observation based estimates. The upper layer transport during the same period above are -282 km^3/yr and -444 km^3/yr for the simulation and observation, respectively. Similarly, the lower layer fluxes are 165 km^3/yr and 333 km^3/yr. The net mean volume transports are as follows: -117 km^3/yr and -111 km^3/yr again in good agreement. The six-year average of the upper, lower and net volume fluxes through the Southern Bosphorus between 2008-2013 are computed as -308 km^3/yr, 160 km^3/yr and -149 km^3/yr, respectively.

In the Dardanelles, the flow rates are considerably lower than the observations in Jarosz et al. [2013] between 1 September 2008 - 31 August 2009. The biggest discrepancy occur during winter and early spring. Simulated lower layer volume fluxes are approximately 45% and 65% less than observed estimates for the northern and southern Dardanelles, respectively. Similarly, upper layer volume fluxes are 55% and 60% less in the simulation.

3.3.2 Inter-annual variability of the Marmara Sea circulation

In this section, we present the circulation of the Marmara Sea developed as a result of the atmospheric conditions and volume fluxes through the straits described in the previous section. The focus is mainly on the upper layer circulation.

Figure 3.7 shows the annual mean of the current velocity at the surface and 30 m for 2009, 2011 and 2013 and the mean for the 2009-2013 period. The annual means of the surface circulation

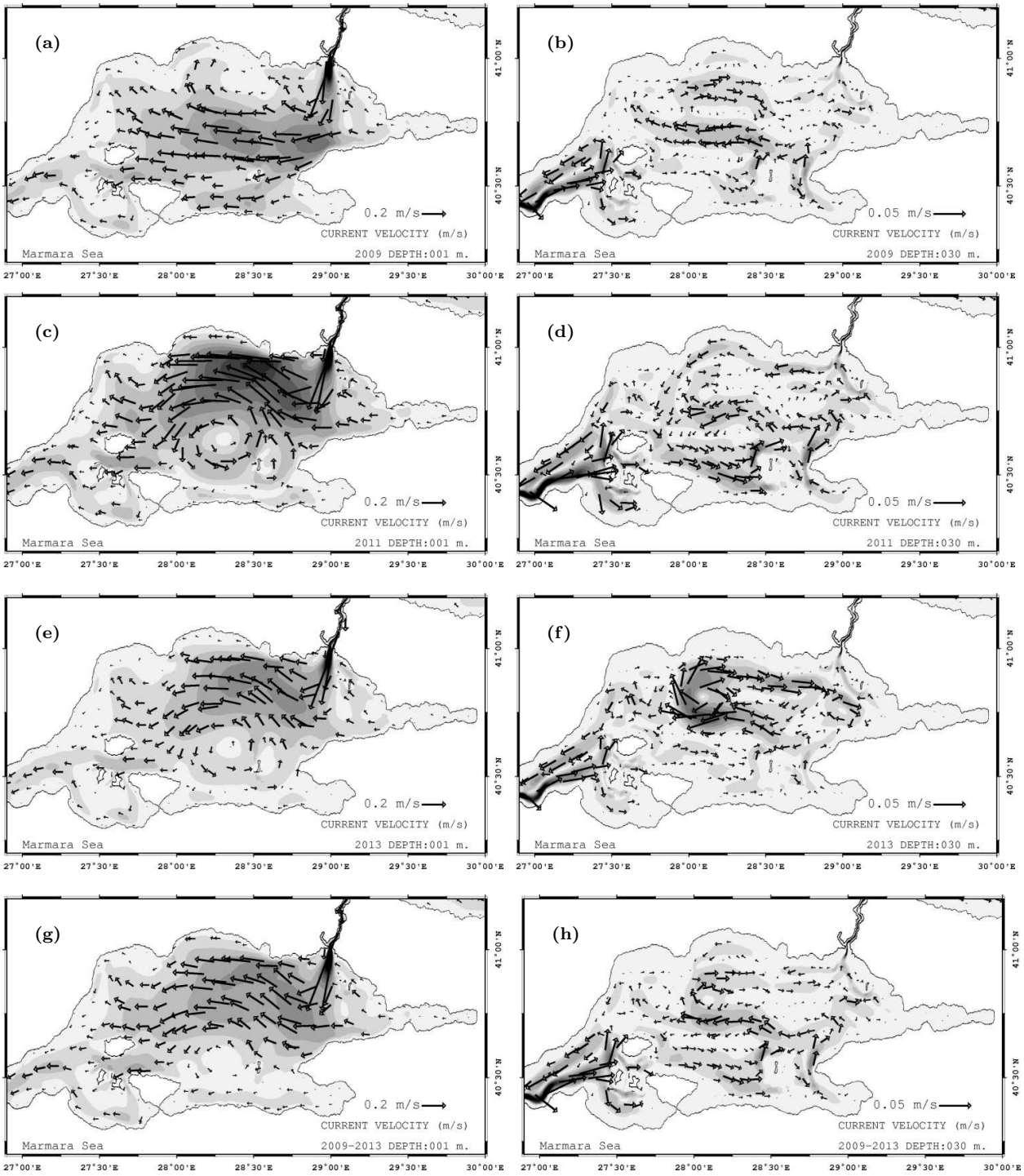

Fig. 3.7. Annual mean of current velocity in the Marmara Sea. a) 2009 at the surface, b) 2009 at 30 m, c) 2011 at the surface, d) 2011 at 30 m, e) 2013 at the surface, f) 2013 at 30 m. The mean for the 2009-2013 period are shown in g) at the surface and h) at 30 m

show two different circulation structures. In 2009 (Fig. 3.7a), the Bosphorus plume reaches the Bozburun peninsula and turns west towards the middle of the basin. One branch of the flow heads to north and forms an anti-cyclone close to the Trachian coast. The southern branch instead splits into two when it reaches to Marmara Island. The southwestward flow traverses the Marmara Sea after turning south merging with the flow circulating around the islands in the

southwestern Marmara Sea and eventually exiting from the Dardanelles. This circulation pattern in the western Marmara Sea is persistent throughout the simulation but with different intensities. This type of circulation structure has also been reported by other studies [Beşiktepe et al., 1994; Chiggiato et al., 2012]. In 2011 (Fig. 3.7c), the circulation in the middle of the Marmara Sea evolves into a single cyclonic structure. The Bosphorus plume deviates to the northwest after exiting the strait, afterwards turning southeast following the lateral boundaries. Most of the flow heads west to the exit and a small cyclone recirculates in the east. The shift in the circulation can be explained by the shift of the wind stress maximum towards the north (Fig. 3.3). Sannino et al. [2015] demonstrates a similar cyclonic pattern in the central Marmara Sea due to the potential vorticity input by the Bosphorus. However, in our case, the main driver of the cyclone is the wind forcing. The cyclonic surface circulation dominates also the mean between 2009-2013. The mean surface circulation in the Marmara Sea can be sketched as in Fig. 3.8.

Below the pycnocline at 30 m, two main structures can be identified. An anti-cyclonic formation appears in the central basin intensifying in 2013. On the Dardanelles side, a flow enters into the Marmara Sea partially heading south east. Another structure recirculates and joins the southwestward flow exiting the Marmara Sea. In 2011, a meander heading west is formed in the northern basin different from other years which may be a result of the deepening of the upper layer due to stronger wind stress.

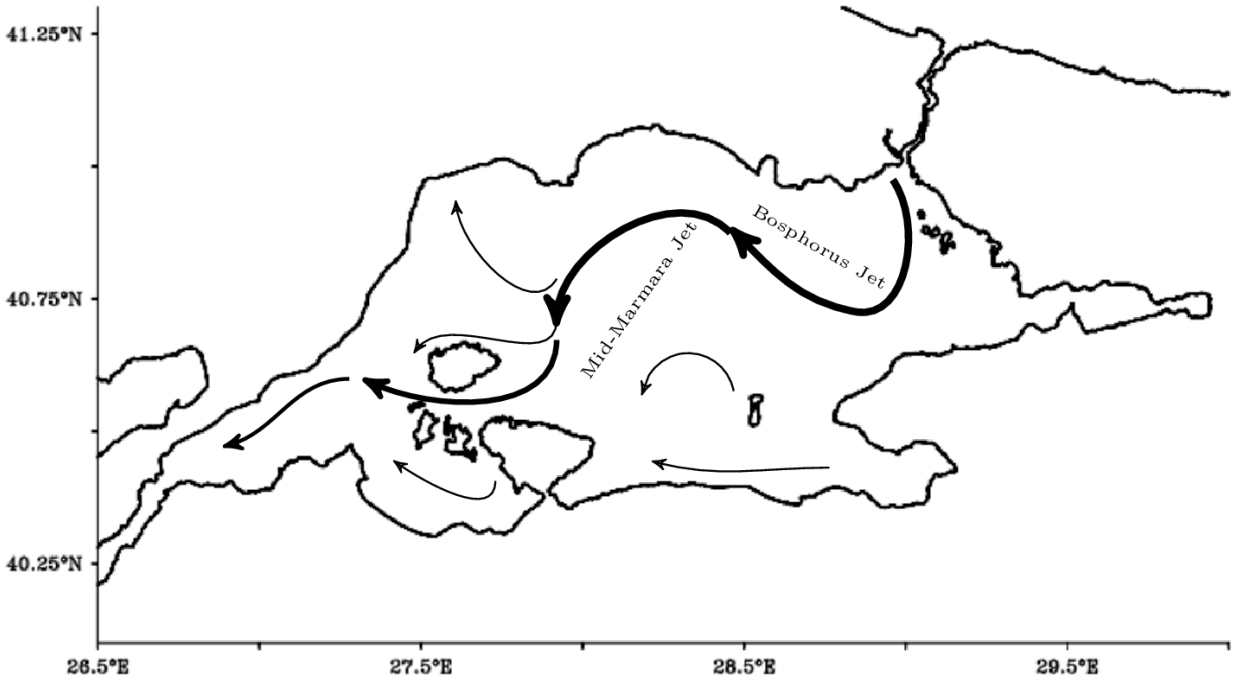

Fig. 3.8. Schematic representation of the surface mean circulation in the Marmara Sea for the 2009-2013 period.

The circulation structures can also be identified in the annual mean vorticity (Fig. 3.9). Coastal shelves in the south and near the peninsulas are shaped by the wind stress curl shown in Fig. 3.3. Northern and western coasts consist of anti-cyclonic vortices. Conversely, positive vorticity dominates the southern coast. The Bosphorus jet generates a dipole vorticity field, which is anti-cyclonic in the west and cyclonic in the east. Positive and negative vorticity in the northern and southern coasts of the islands and peninsulas, respectively, are another common structure for all the years. After 2011, the center of the large scale gyre is located at 28°20'N - 40°35'E.

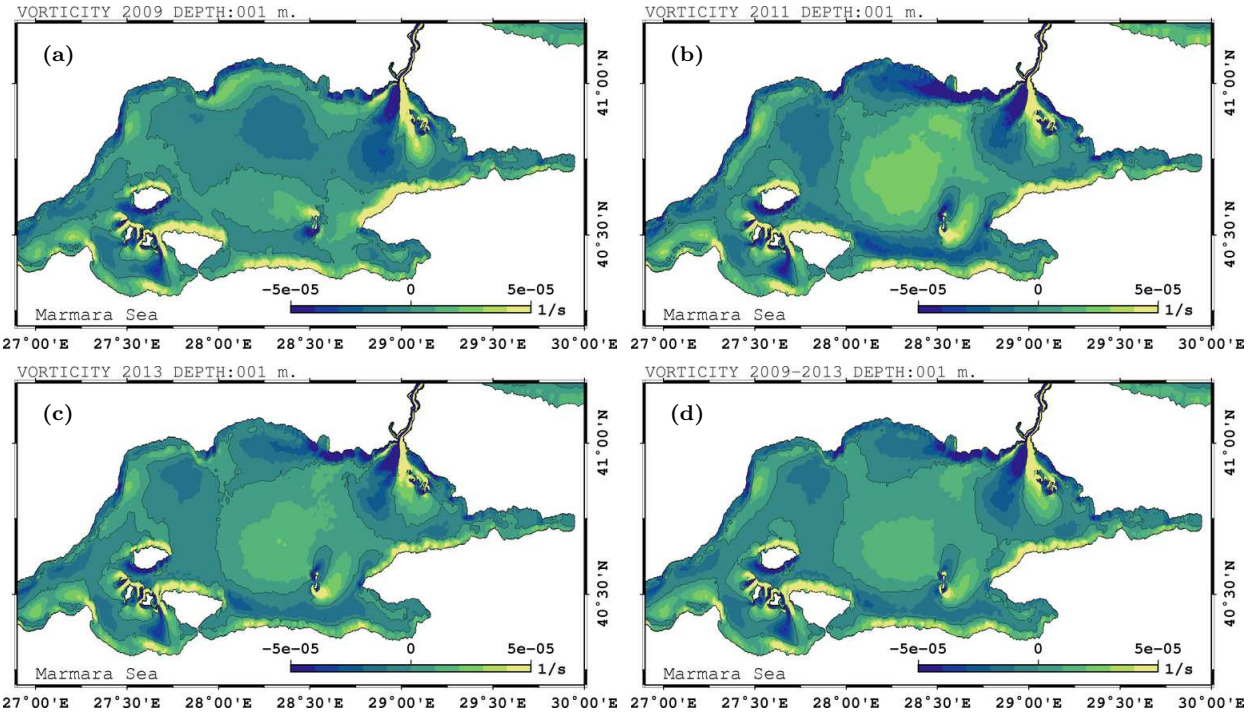

Fig. 3.9. Annual mean of vorticity in the Marmara Sea at the surface. a) 2009 b) 2011 c) 2013, d) the surface vorticity mean for the 2009-2013 period.

3.3.3 Kinetic energy of the Marmara Sea

The Marmara Sea is a very energetic basin exposed to strong atmospheric cyclone passages along with surface jets and density driven subsurface circulation. These forcings and flow structures act together to energize the circulation. Using the six-year integration, it is now possible to estimate the energy input by the wind. Here we compare the wind work in the Marmara Sea with the computations of Cessi et al. [2014] for the Mediterranean, the Red Sea and the Baltic Sea. The wind work in the Black Sea is estimated by Kara et al. [2008].

The time series of monthly mean wind stress shown in Fig. 3.10. It exhibits inter-annual

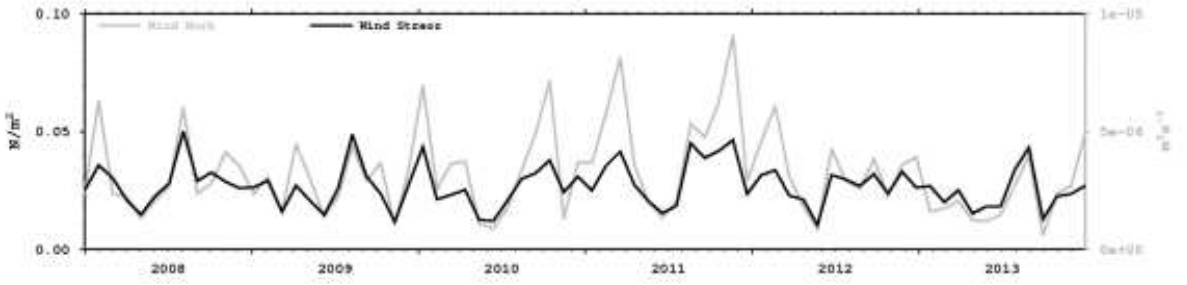

Fig. 3.10. Monthly time series of the wind work (m^3s^{-3}) and wind stress (Nm^{-2}) in the Marmara Sea. The wind work is shown in gray and right vertical axis. The wind stress is the black curve and its values are shown on the left vertical axis.

differences with a mean about 0.03 N/m^{-2} and a maximum around 0.05 Nm^{-2} in August 2008. The monthly mean is highly variable and there is not exactly a well-defined seasonal cycle between 2008-2013. The monthly mean of the wind work $\frac{\partial E}{\partial t}$ per unit area computed following Cessi et al. [2014] is:

$$\frac{\partial E}{\partial t} = \frac{1}{\rho_0 A} \int_A \tau \cdot \mathbf{u}_s dxdy \tag{3.2}$$

where ρ_0 is the surface density, τ is the wind stress, $\mathbf{u}_s$ is the velocity at the sea surface and A is the surface area of the Marmara Sea.

The wind work in the Marmara Sea is positively correlated with the wind stress and is always positive. It is highest in 2011 and the maximum monthly mean wind work is 9.1x10^{-6} in the autumn of 2011.

For a comparison with the other marginal seas accounted by Cessi et al. [2014], we normalize $\frac{\partial E}{\partial t}$ by the volume of the Marmara Sea instead of the surface area. The six-year mean of the wind work is computed as 1.09x10^{-8} m^2/s^{-3} one order of magnitude higher than the Mediterranean Sea. The wind work in the Baltic Sea was computed as 9.15x10^{-9} m^2/s^{-3}, which is comparable to the Marmara Sea but still below it.

The resulting volume-mean kinetic energy in the Marmara Sea is calculated as 0.006 m^2s^{-2} (Fig. 3.11) for six years. The daily mean kinetic energy time series reveals that strong wind events are able to energize the basin up to 0.03 m^2s^{-2}. The monthly volume-mean kinetic energy averages fluctuate between 0.005-0.01 m^2s^{-2}. It is higher in winter and early spring, whereas it is always below the mean in summer. The highest kinetic energy input are in October 2010, April 2011 and November 2011.

The kinetic energy is higher in the upper layer of the water column. The time-mean of surface kinetic energy is about 0.03 m^2s^{-2}. Daily surface averages are capable of reaching 0.2 m^2s^{-2}. The monthly mean increases to approximately 0.05 m^2s^{-2} in November 2011.

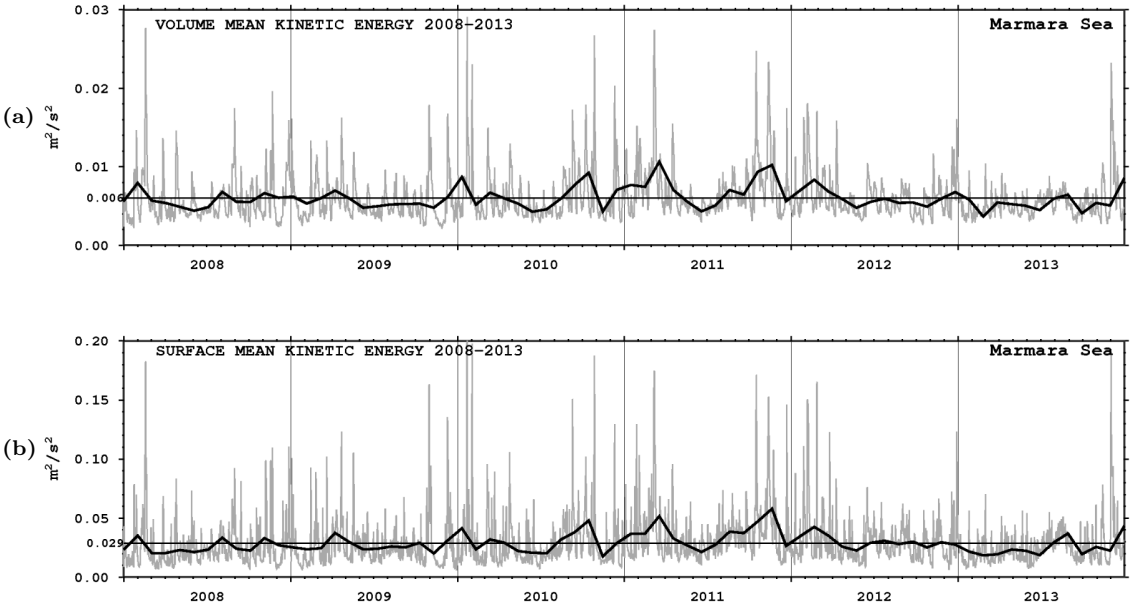

Fig. 3.11. a) Volume and b) surface mean of kinetic energy in the Marmara Sea. The daily and monthly averages are plotted by gray and black, respectively. Units are in m^2s^{-2}

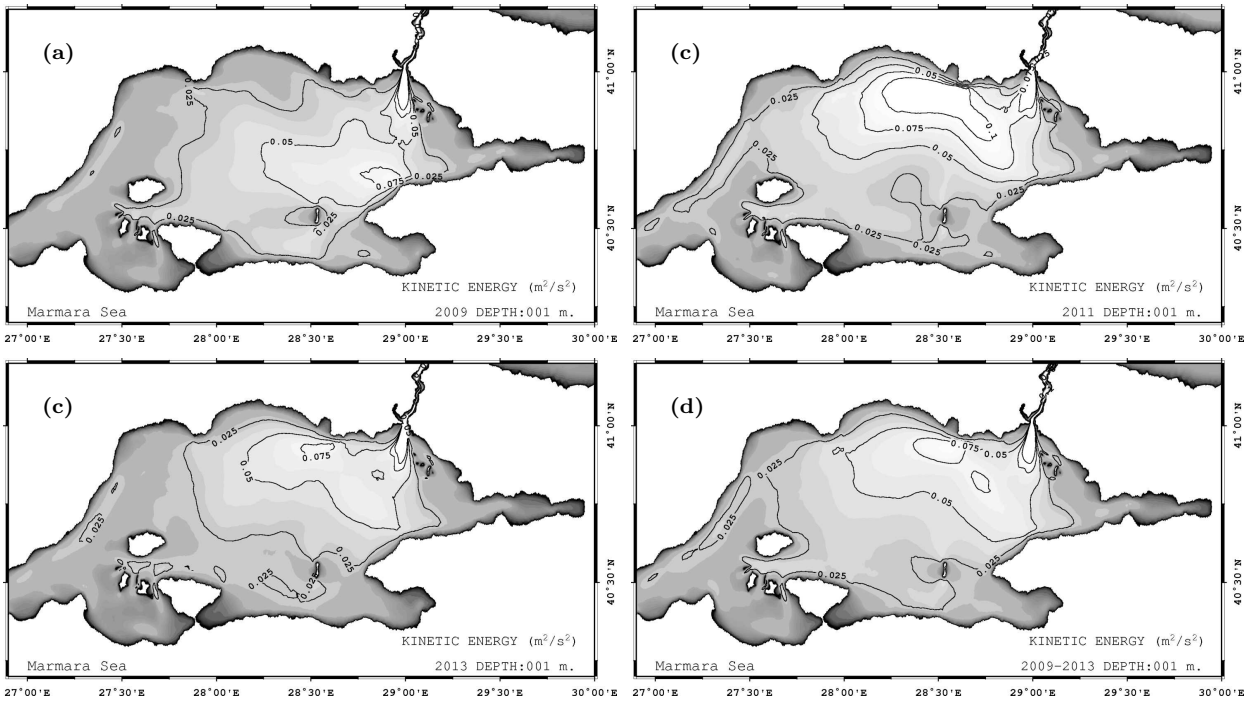

Fig. 3.12. Annual mean of kinetic energy for in the Marmara Sea a) 2009 b) 2011 c) 2013. d) The time-mean for the 2009-2013 period. Units are in m^2s^{-2}.

The buoyancy gain in the Marmara Sea is shown in PART I. Cessi et al. [2014] showed that it is a sink of kinetic energy. The buoyancy gain is mainly due to the Bosphorus inflow, thus the latter competes with the wind work to change the kinetic energy of the basin. On the other hand, the spatial distribution of the surface kinetic energy shows that the surface jet itself out of

Bosphorus and the wind forcing energize the northeastern basin. Figure 3.12 shows the annual mean of surface kinetic energy for 2009, 2011 and 2013 as well as the time-mean for the 2009-2013 period. The kinetic energy of the Bosphorus outflow is always greater than 0.075 m^2s^{-2}. In 2009, a kinetic energy maximum appears in the north of the Bozburun peninsula where the Bosphorus jet arrives before moving west. In the western basin, it is generally less than 0.025 m^2s^{-2}. The kinetic energy maximum due to the wind forcing overtakes the kinetic energy due to the Bosphorus jet only in 2011. The kinetic energy intensifies in the central north and exceeds 0.1 m^2s^{-2}. Almost all of the basin except near the coastal areas has a kinetic energy higher than 0.025 m^2s^{-2}. Energy is mostly confined in the north-east of the central basin in 2013. The time-mean for 2009-2013 reflects the characteristics of 2011 but with less amplitude.

3.4 Summary and discussion

This study focused on the inter-annual variability of the TSS. PART I presented the water mass structure and the comparison with the observations. The model results agree qualitatively with the observations and the performance of the model was good in the near Bosphorus area but less so in the Dardanelles. The position of the interface between the upper layer and the lower layer is stable during the six-year integration.

PART II focuses on the dynamical analysis and the circulation of the Marmara Sea. First, the volume fluxes through the straits have been compared with the observations and analyzed. The range of the along-strait velocities matches with the observations but show generally lower amplitudes. In the Dardanelles, however, the model solution departs from the observations especially in the northern exit. The net volume flux at the southern exit is about 70% of the observed value.

The circulation in the Marmara Sea as a result of volume fluxes and atmospheric forcing mainly shows two patterns. The first is dominated by the buoyant plume of the Bosphorus which first moves to south, turns northwest and exits the Dardanelles in the southwest. This type of circulation has been observed and modeled by several studies. The other formation includes a main cyclone in the central basin as a result of intensifying and expanding wind stress over the Marmara Sea. The Bosphorus jet is directed to the west immediately after it exits the strait and kicks a cyclone formation starting from the northern coast. Small scale vortices are also formed in various parts of the basin with a permanent vortex in the northwest.

The long term simulation with atmospheric forcing made it possible to evaluate the impact of

the wind and compute the kinetic energy in the Marmara Sea. The wind work in the Marmara Sea is shown to be higher even than the Baltic Sea. The high energy input by the wind significantly increases the kinetic energy in the Marmara Sea. During the strong cyclone passages kinetic energy can increase by 10-fold of its time-average. Moreover, the annual mean of kinetic energy input from the wind can exceed the one from the Bosphorus jet depending on the wind stress structure.

Overall the results suggest directions for future modeling on the inter-annual variability of the TSS. The system is highly sensitive to the choice of parameterizations and surface boundary conditions. We have shown that wind forcing determines the surface circulation in the Marmara Sea together with the Bosphorus jet. A higher resolution atmospheric forcing for wind would improve the model estimates in the Marmara Sea. The forcing for precipitation is also very coarse for this small domain. Since the model is sensitive to the water budget of the Black Sea, lateral open boundary conditions would improve the solutions for volume and salt fluxes.

Chapter 4

Observing System Simulation Experiments in the Marmara Sea

Abstract

In this study, an observing system simulation experiment (OSSE) is presented in the Marmara Sea. A high resolution ocean circulation model and an ensemble data assimilation tool are coupled in the Turkish Straits System. The OSSE methodology is used to assess the possible impact of a ferrybox network in the eastern Marmara Sea. A reference experiment without assimilation is performed. Then, synthetic temperature and salinity observations are assimilated along the track of the ferries in the second experiment. The results suggest that a ferrybox network in the Marmara Sea may improve the analysis significantly. The salinity and temperature errors get smaller in the upper layer of the water column. The impact of the assimilation is negligible in the lower layer due to the strong stratification. The circulation in the Marmara Sea, particularly the Bosphorus outflow, helps to propagate the error reduction towards the western basin where no assimilation is performed. Overall, the proposed ferrybox network can be a good start to design an optimal sustained marine observing network in the Marmara Sea for assimilation purposes.

4.1 Introduction

The Marmara Sea is one of the compartments of a water passage known as the Turkish Straits System (hereafter TSS). The TSS connects the Black Sea and the Mediterranean by two narrow straits, namely the Bosphorus and the Dardanelles, along with the Marmara Sea.

Salty and dense Mediterranean waters and brackish Black Sea waters form a two-layer exchange flow through the TSS. In combination with the complex topography, flow structures in different scales generate a challenging environment for oceanographic studies.

Until recently, the need for the high resolution in the straits permitted to model the compartments of the system separately due to the computational cost. However, the integral models of the system emerged with the increasing computational capacity in the recent years [Gürses, 2016; Sannino et al., 2015].

In this study, we present first data assimilation experiments performed in the TSS. The in-situ observations are generally scarce and collected by dedicated projects [Beşiktepe et al., 1994; Chiggiato et al., 2012; Özsoy et al., 2001; Tugrul et al., 2002; Ünlüata et al., 1990] for a limited area and time in the Marmara Sea. Moreover, the resolution and frequency of the satellites are still not sufficient to monitor the system continuously. For these reasons, a sustainable marine monitoring network is required in the Marmara Sea. We propose a ferrybox network which already has the infrastructure as public transportation in the Marmara Sea.

We follow the OSSE methodology to achieve our goal. The OSSE methodology is used widely in the atmospheric community since four decades for different purposes such as design of new observation tools, the error assessment in the large models and parameter estimation [Arnold Jr and Dey, 1986; Masutani et al., 2010]. Atlas [1997] summarizes the criteria established by the atmospheric community to perform credible OSSE. Halliwell Jr et al. [2015, 2014] gave an example of an ocean OSSE in the Gulf of Mexico by following those criteria for the first time. In Aydoğdu et al. [2016], we studied a fishery observing system in the Adriatic Sea considering the same criteria.

In the next section, the main characteristics of the TSS relevant to this study are summarized. In section 4.3, the modeling and data assimilation environment in the TSS is reported. Section 4.4 is devoted to the OSSE design. The nature run and forecast model are introduced. Ferrybox network design is also detailed and the methodology for impact assessment is outlined. The results are presented in section 4.5. The paper is summarized and concluded in the last section.

4.2 Overview of the Turkish Straits System

The Marmara Sea with the Bosphorus and the Dardanelles Straits constitutes the Turkish Straits System (TSS) which connects the Black Sea and the Mediterranean. The exchange of contrasting water masses forms a highly stratified water column structure throughout the system. The brackish surface waters of the Black Sea flow towards the Mediterranean in the upper layer and the salty and dense Mediterranean Sea waters occupy the lower layer of the water column [Ünlüata et al., 1990]. In addition to the strong stratification, the complex topography of the two narrow straits and an internal sea with shallow shelves and deep depressions generate a unique and challenging environment for oceanographic studies.

The Bosphorus is an elongated narrow strait connecting the Black Sea and the Marmara Sea. The upper layer flow is dominated by the Black Sea waters with salinity about 18 psu. The lower layer waters originate from the Mediterranean and reach to the Black Sea with a salinity about 37 psu. The interface depth between the two layers is mainly determined by the salinity. In summer, a three layer temperature structure appears. A warm upper layer due to the atmospheric heat flux overlays a cold intermediate layer propagates from the Black Sea. Warmer Mediterranean waters stay at the bottom layer [Altiok et al., 2012]. The constriction in the mid-section and the sill in the southern section of the strait apply a hydraulic control on the flow and produce a surface jet at the Marmara Sea exit [Sözer, 2013]. The velocity of the Bosphorus jet can exceed 2 m/s [Jarosz et al., 2011b]. Therefore, the jet is one of the key players on the dynamics of the Marmara Sea. It enhances the mixing by entraining lower layer waters [Ünlüata et al., 1990], energizes the Marmara Sea circulation in the eastern basin [Beşiktepe et al., 1994] and produces mesoscale eddies due to the potential vorticity balance [Sannino et al., 2015].

The wind is another important factor on the dynamics of the Marmara Sea. Many strong cyclones pass over the Marmara Sea especially in winter [Book et al., 2014]. The northeasterly winds dominate the system throughout the year. In chapter 3, we have shown that the wind work in the Marmara Sea is higher even from the Baltic Sea.

The third important dynamical constituent is the density-driven baroclinic flow at the lower layer [Hüsrevoğlu, 1998]. The velocity of the flow in the lower layer can reach to 1 m/s [Jarosz et al., 2012].

The high complexity of the system requires integral modeling approaches to understand the links between its different compartments.

4.3 The Turkish Straits System Ensemble Modeling and Data Assimilation Environment

The modeling and data assimilation environment of the TSS includes an ocean general circulation model, the Finite Element Sea-ice Ocean Model (FESOM), and an ensemble-based data assimilation framework, the Data Assimilation Research Testbed (DART).

The FESOM is an unstructured mesh ocean model using finite element methods to solve the hydrostatic primitive equations with Boussinesq approximation [Danilov et al., 2004; Wang et al., 2008]. It is developed by Alfred Wegener Institute as a first global ocean model using an unstructured mesh. Gürses [2016] applied the FESOM to the TSS and a performed realistic simulation of the integral system using atmospheric forcing. We recently performed inter-annual simulations using a similar model setup. Two six years simulations using different surface salinity boundary conditions has been completed and evaluated.

The DART is an open-source community facility developed in NCAR [Anderson et al., 2009]. It provides software packages to work with low-order models for different research activities. Furthermore, it is interfaced with various high-order models for geophysical research from climate predictions [Karspeck et al., 2013; Raeder et al., 2012] to short-term atmosphere and ocean forecasting [Hoteit et al., 2013; Schwartz et al., 2015].

The DART has a couple of different stochastic and deterministic ensemble Kalman filtering algorithms. In our application, we use the Ensemble Adjustment Kalman Filter (EAKF) as described in Anderson [2001]. The EAKF is a deterministic ensemble Kalman filter, that is, the observations are not perturbed randomly before they are assimilated. One of the main advantages of EAKF for our application is that it preserves the prior covariance information. In the TSS, where different dynamics compete and generate circulation structures in various scales, the prior information is crucial for the dynamical balances among different scales. In addition, the covariances are updated in every assimilation cycle which is important to sustain the high frequency variability of the system.

One of the main issues to take into consideration in ensemble data assimilation is the filter divergence. It is the consequence of insufficient ensemble spread which leads to assign more weight to the prior information that may cause the rejection of massive amount of observations. As a result, the analysis will depart from the observations [Anderson, 2001]. There are techniques to prevent the filter divergence such as inflating the covariances [Hamill et al., 2001]. In the DART,

an inflation can be applied by simply multiplying the prior covariances by a constant slightly bigger than 1. For the same purpose, we implemented a random number generator to FESOM to maintain the ensemble spread by perturbing desired physical parameters.

Houtekamer and Mitchell [1998] shows that correlations are estimated better in large ensembles. Since it is expensive to maintain large ensembles in large geophysical models, they propose a technique called localization to overcome the difficulty of estimating the small correlations associated with remote observations. The localization technique allows to update the prior state without using the observations beyond a cutoff radius, which may have small or spurious correlations. In the DART, the cutoff radius can be set as a constant value in radians. It utilizes the fifth order piecewise rational function used by Gaspari and Cohn [1999]. The high spatial variability in the TSS urges to use the localization.

For interfacing FESOM and DART, a forward operator that maps model state vector into observation space, characterized by a type of physical quantity, geo-referenced location and time, is written. This operator provides the background state values corresponding to the observations from the state vector to the filter. We decided to apply a simple, but theoretically justifiable (i.e., optimal) nearest-neighbor mapping. The forward operator searches for the closest horizontal grid point in the state vector. Then, it finds the closest vertical location. The corresponding model grid in the prior state vector is determined to update the state variable.

The working principle of the FESOM/DART coupling can be schematized as in Fig. 4.1. DART interface requires two model specific routines converting the model restart files to DART state vectors and vice versa. After the initial state vectors are provided from each ensemble member, DART determines the observations in the current assimilation window and assimilates them by applying some quality control, if required. The updated state vectors are again converted to the model restart files as an initial ensemble for the next assimilation cycle. In many applications, the model executable to advance the state is called by the DART until the next available observation. However, in our implementation they work as separate sequential processes. After the DART finishes updating the state, FESOM executables are called to iterate the model state for the next assimilation cycle. The model stops even if there is no observation in the next cycle and DART executables are called again. This process continues until the experiment finishes.

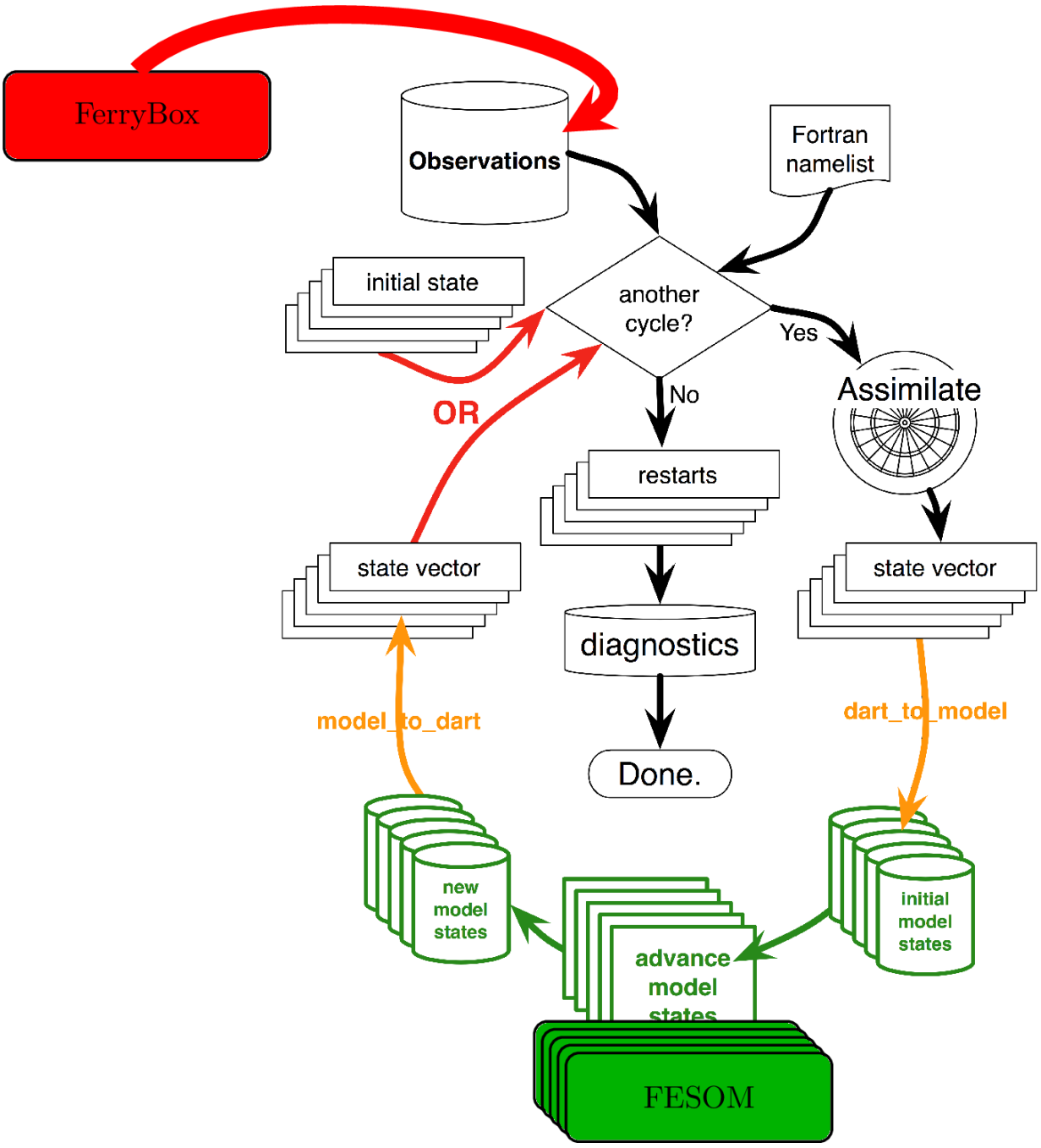

Fig. 4.1. Flow of FESOM/DART interface. Reproduced after Anderson et al. [2009] with modifications for the TSS application

4.4 Design of the OSSE

The OSSE methodology used here can be schematized as in Fig. 4.2. A ferrybox network design is proposed in the eastern Marmara Sea and the impact assessment is performed using the FESOM/DART ensemble data assimilation environment. The methodology and tools are detailed in the subsequent sections.

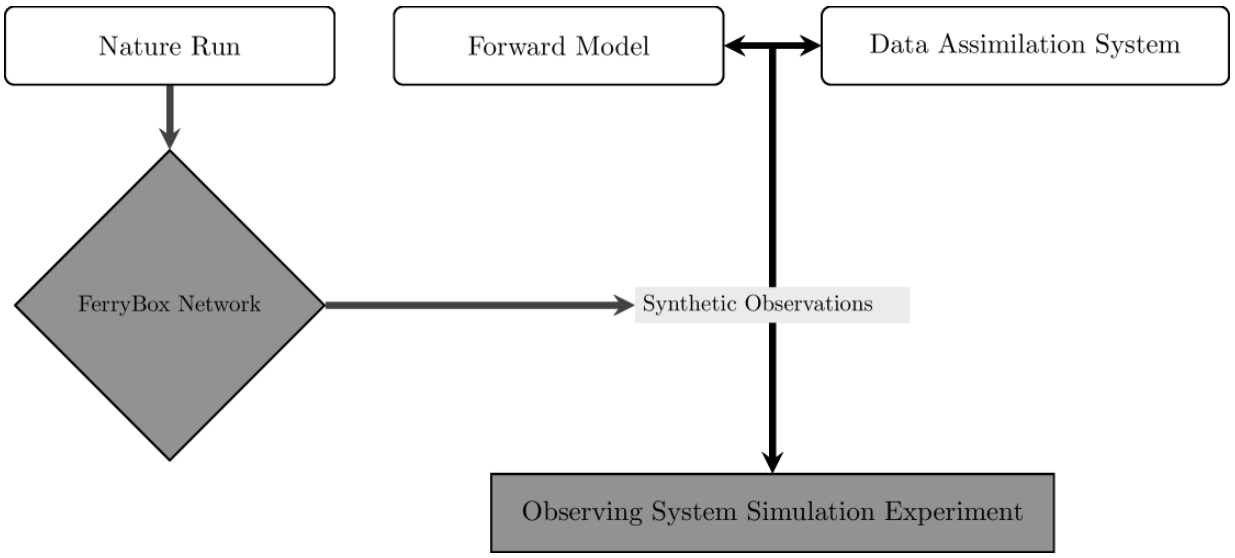

Fig. 4.2. OSSE methodology applied in Turkish Straits System

4.4.1 The Nature Run and The Forecast Model

The OSSE methodology requires a realization of the true atmosphere or ocean which is called the nature run (NR). The NR is the closest possible realization of the system to the truth. Therefore, it should satisfy the main properties of the geophysical system. It is used for generating the synthetic observations to assimilate and assessing the impact of the assimilation. Another requirement is called forecast model (FM) which is employed to assimilate the synthetic observations provided by the NR.

The fraternal twin methodology is used to perform the OSSE. In the fraternal twin methodology, the NR and the FM use the two different configurations of the same model. Here, the difference between the NR and the FM configurations is the surface salinity boundary condition (see Chapter 2). The former has the relaxation boundary condition for the sea surface salinity and the latter uses the mixed salinity boundary condition. Two long-term simulations are performed with both configurations and validated with the in-situ observations. The simulations starts from 1 January 2008 and are integrated for six years until 31 Decemeber 2013. We demonstrated that they do not deviate from each other unrealistically during the OSSE period which is 1-8 January 2009. The output of the NR are saved hourly for the OSSE period to generate synthetic observations.

The ensemble consists of 30 members. Two different perturbations are applied to maintain the ensemble spread during the experiments. First, an initial ensemble is produced for 1 January 2009 using the method schematized in Fig. 4.3. The five years means of the temperature and salinity for January are computed from the inter-annual simulation. Then, the deviations of

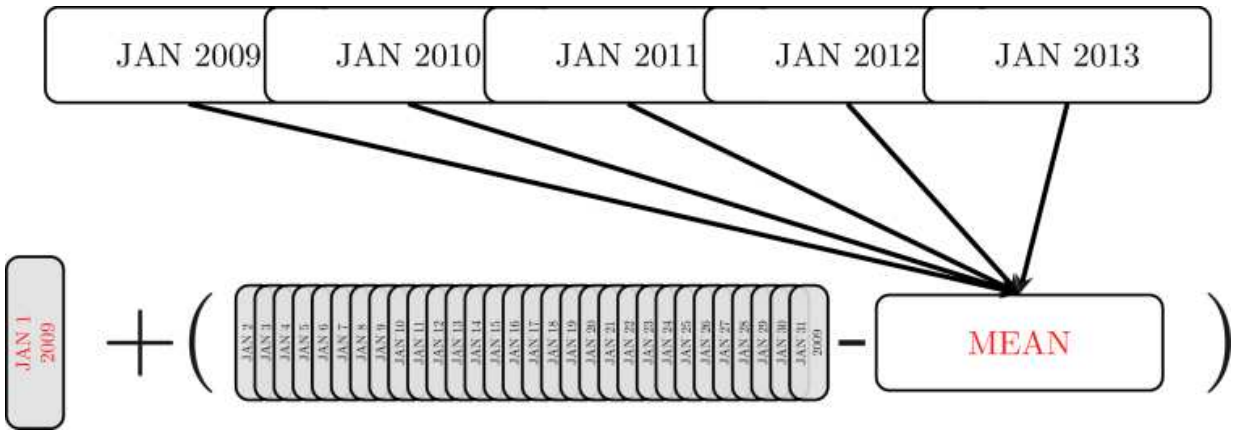

Fig. 4.3. Schematic representation of the methodology used to generate the initial ensemble. MEAN is the average of January over five years between 2009-2013

each day between 2-31 January 2009 from the inter-annual mean are calculated. Finally, these deviations are added to the temperature and salinity fields to provide an initial perturbation for each ensemble member. In Fig. 4.4, the variance of the initial ensemble for salinity and temperature for the depths 5 m, 12 m and 20 m are shown. The horizontal distributions of the variance are similar for both variables. The variance is larger in the exits of the straits. In particular, the spread at the Bosphorus exit for the upper layer down to 15 m is larger due to the variability in the outflow. Correspondingly, the Dardanelles inflow to the Marmara Sea increase the variance in the lower layer. Such a distribution of initial variance in the Marmara Sea is appropriate to initialize the experiments since the assimilation of synthetic observations are performed in the impact area of the Bosphorus outflow where the ensemble spread can be diminished by the assimilation.

Secondly, the background vertical diffusivity κ_{v0} is randomly perturbed every timestep by fitting a gaussian with a mean of 0 and a standard deviation of 5% of the κ_{v0}.

4.4.2 The Eastern Marmara Sea Ferrybox Network Design

The Marmara region has the highest urban population in Turkey. It involves the metropolitan city of Istanbul which is divided into two by the Bosphorus and surrounded by the Black Sea in the north and the Marmara Sea in the south. As a consequence, a network of ferries developed as an essential way for transportation. The main hub for the ferries is Istanbul which is connected to the other cities around the Marmara Sea by several ferries (Fig. 4.5a).

In the Marmara Sea, it is not easy to deploy instruments such as argo or glider since there is an intense ship traffic. However, the infrastructure for a ferrybox network is already available.

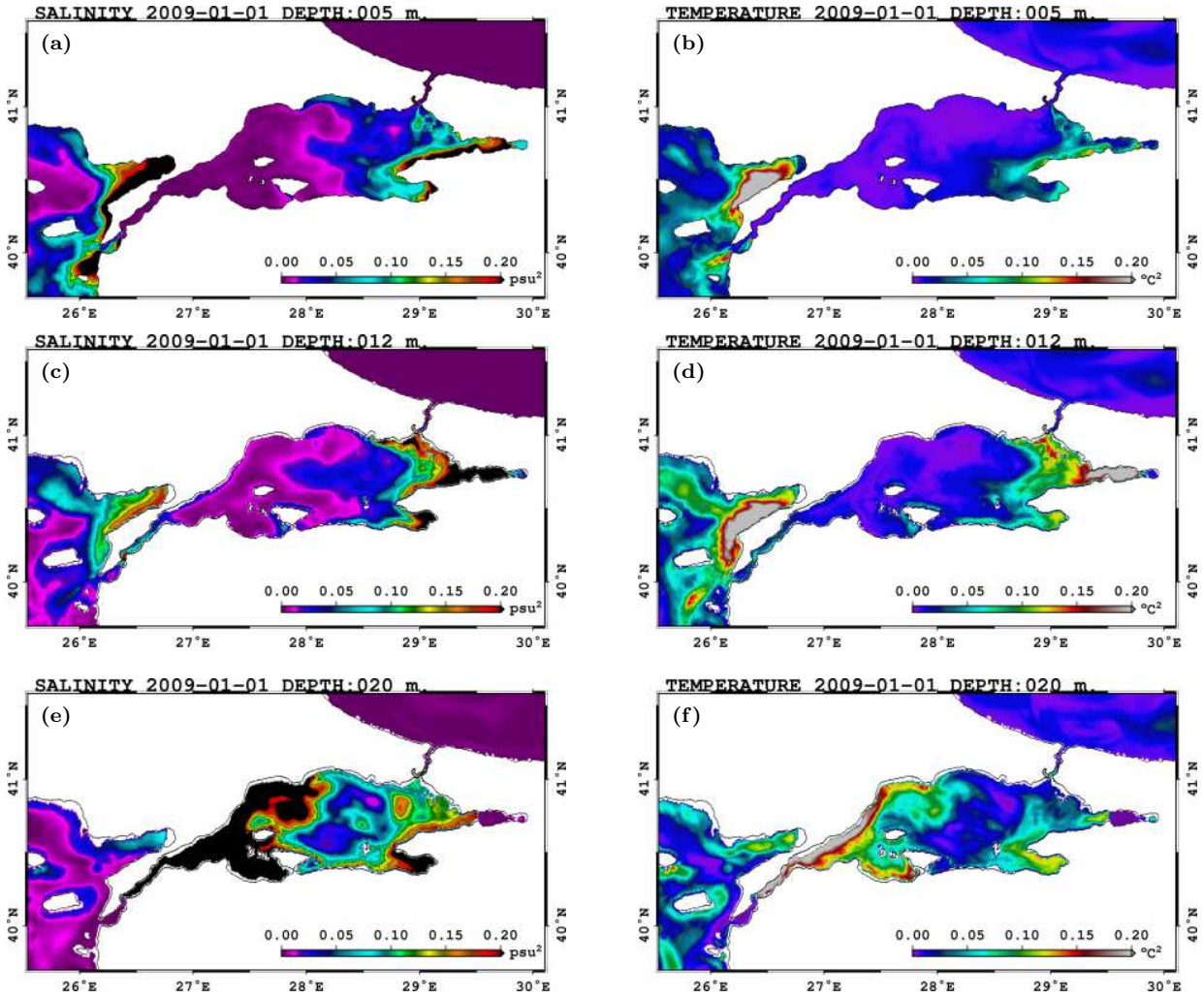

Fig. 4.4. Salinity (left) and temperature (right) variance of the initial ensemble at 5 m., 12 m. and 20 m. depth for 01/01/2009.

The ferry lines in the Marmara Sea cover most of the eastern basin including the Marmara Sea exit of the Bosphorus. Using the ferry network as a monitoring system would be a optimal way for a sustainable ocean observing network in the Marmara Sea.

The current state-of-the-art Ferrybox networks are summarized by Petersen [2014]. They are used more after the European network for Ferrybox measurements project[1], especially in the northern European seas. In the Mediterranean, there is a ferrybox system between Piraeus and Heraklion operated by HCMR [Korres et al., 2014]. A ferrybox is mainly loaded by temperature, salinity, turbidity and chlorophyll-a fluorescence sensors, and a GPS receiver for position control. Oxygen, pH, pCO_2 or algal groups as well as air pressure, air temperature and wind sensors can also be installed [Petersen, 2014]. The ferrybox observations can be used for analyzing the state of the ocean [Seppälä et al., 2007], comparison with other instruments [Sørensen et al., 2007] and

[1] http://www.ferrybox.org

can also be assimilated to improve analysis of the ocean models [Grayek et al., 2011].

The sampling rate of the data can differ in each system. The data used in Grayek et al. [2011] is sampled in 10 s intervals. For our OSSE, we are using the sampling rate of 1 min. following Korres et al. [2014]. The synthetic observations are obtained from hourly NR outputs in varying spatial location along the track of the ferries. The depth of the sampling is set to simply 5 m, an average depth given by Grayek et al. [2011]. A random error is added by fitting a gaussian with standard deviation of 0.1°C for temperature and 0.04 psu for salinity following Aydoğdu et al. [2016] in order to simulate realistic measurement. Observational errors are assumed to be 0.5°C and 0.25 psu for temperature and salinity as proposed by Grayek et al. [2011].

ROUTE	LOCATION	DISTANCE	SPEED	DURATION	TIME TABLE
Yenikapi	28.956E-41.002N	46.2km (28.7mi.)	23 kn	75 min.	09:45,15:45,21:45
|					
Yalova	29.274E-40.661N				07:15,13:45,19:45
Yenikapi	28.956E-41.002N	110.0km (68.5mi.)	27 kn	150 min.	07:30
|					
Bandirma	27.967E-40.354N				18:30
Ambarli	28.676E-40.966N	70.0km (43.2mi.)	12 kn	210 min.	20:00
|					
Topcular	29.434E-40.690N				16:00

Table 4.1: The unidirectional ferrylines used in this study. The locations, distance between the ports, speed of the ferries, the duration of the cruise and time of departure from each port are listed.

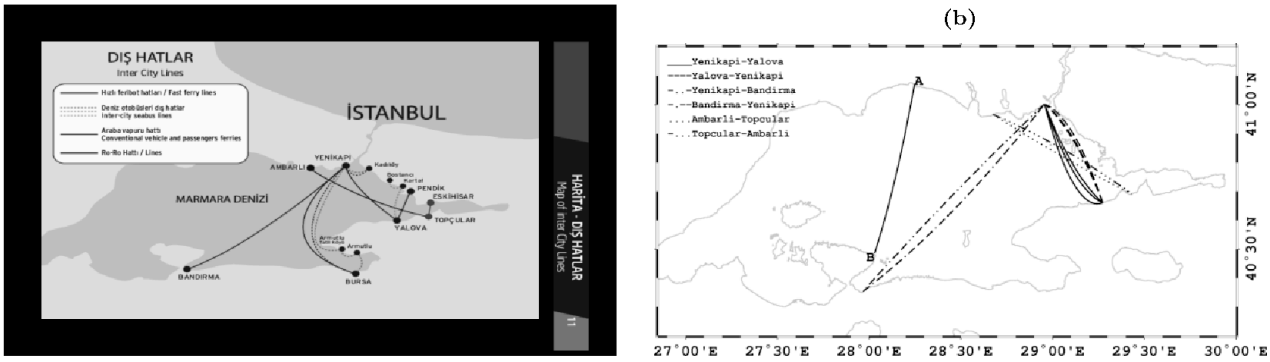

Fig. 4.5. a) The routes of the intercity ferry lines from Istanbul and to Istanbul suggested by the operating company IDO. b) Approximate unidirectional ferry lines. The legend shows the direction of the ferry. The section A-B is used only for evaluation of the assimilation impact.

Three different ferry routes are chosen from the map in Fig. 4.5a, and their tracks are approximated by observing from the real-time Marine Traffic application (Fig. 4.5b). The longest duration for a cruise in the eastern Marmara Sea is about ∼3.5 hours between Ambarlı-Topçular (Table. 4.1). Another transect used here is YeniKapı-Yalova which takes ∼75 min. and has

cruises every two hours from each port. This route directly crosses the Bosphorus outflow and has the highest number of cruise a day. Therefore, we include six ferries in various periods of the day for YeniKapı-Yalova transect. The last transect chosen is Yenikapı-Bandırma crossing the Marmara Sea from north to south. The navigation on this line takes ∼2.5 hours. This transect is the only one that has direct impact in the southern basin. The resulting synthetic temperature and salinigy observations sampled from the NR for the first day are shown in Fig. 4.6.

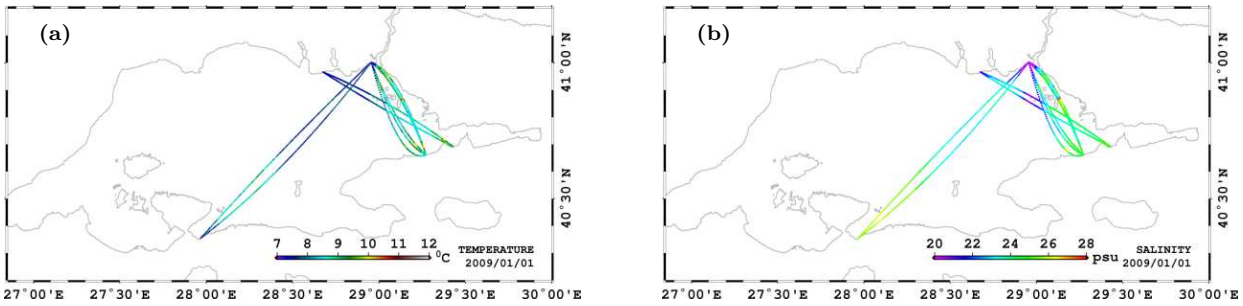

Fig. 4.6. a) Temperature and b) Salinity synthetic observations for the first day.

4.4.3 Experiments

Two experiments are performed as an initial exercise for the data assimilation studies in the Marmara Sea (Table 4.2). The first experiment FB001 is the reference experiment without assimilation. It is used to evaluate the errors when the synthetic observations are not assimilated. In the second experiment, FB002, all the synthetic observations are assimilated in the corresponding assimilation window. A six hours cycle is chosen for each assimilation window, since the area is under the influence of Bosphorus jet which may develop high frequency variability at the surface.

	Start Date	End Date	Assimilation	A.Cycle	Evaluation
FB001	01-JAN-2009 00:00	8-JAN-2009 00:00	NON	N/A	YES
FB002	01-JAN-2009 00:00	8-JAN-2009 00:00	ALL	6 hr	YES

Table 4.2: Summary of the OSSE

The horizontal cutoff radius is set to 3 km. The vertical correlations are considered down to 25 m. depth. The temperature and salinity increments after second and forth assimilation cycle are shown in Fig. 4.7. As it can be seen from temperature corrections after the first cycle, the whole track of Yenikapı-Bandırma route is not assimilated at once since southern section of the data doesn't stay in the current assimilation window. The correction of salinity fields at 20 m is shown in Fig. 4.7b for the third assimilation cycle.

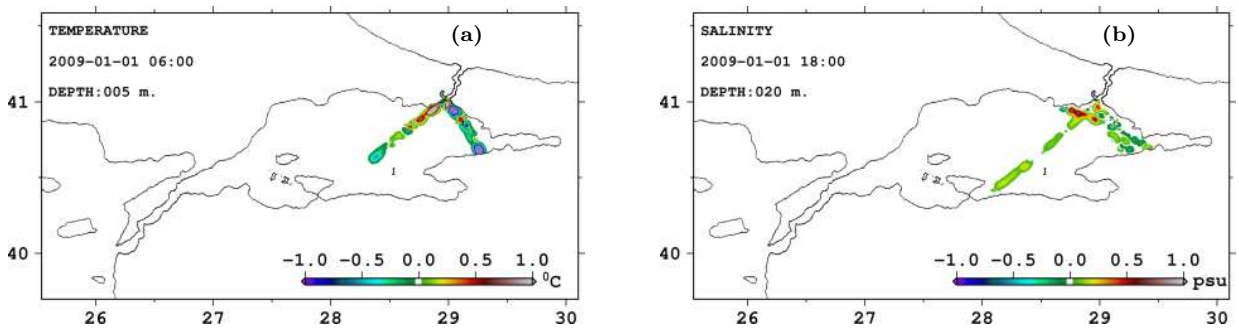

Fig. 4.7. Increments after assimilation for a) temperature at 01-01-2009 06:00 and b) salinity at 01-01-2009 18:00.

4.4.4 Methodology for Impact Assessment

The DART offers tools to have the control on the data without any difficulty. It allows to decide to use a set of data for assimilation or evaluation. It also checks if any operator fails during the mapping of the state vector to the observations. The quality of the data can also be subjected to a statistical control for the outlier values. The data is rejected if $x_b - y >$ T times the expected value of the difference between the prior state and the observation. Here, y is the observation and x_b is the corresponding prior mean of the ensemble. The expected value is computed as:

$$E(x_b - y) = \sqrt{\sigma_{x_b}^2 + \sigma_y^2} \tag{4.1}$$

T is chosen as 3 for both temperature and salinity in these experiments.

The first diagnostic we use for the impact assessment is the RMS of misfits (innovation) which are the root mean square of the difference between the prior and observation. We also use the horizontal maps of the misfits to determine the spatial distribution of error.

Although we don't assimilate any data below 5 m, it is important to assess the vertical distribution of the errors, particularly to follow the behavior of the strongly stratified water column in the Marmara Sea. For this purpose, we generated an extra synthetic dataset from the NR only for evaluation in the north-south section (see A-B in Fig. 4.5) away from the region of assimilation. We compare the difference between prior ensemble mean and synthetic observations along the transect A-B.

The OSSE methodology allows various ways to evaluate the analysis since the NR is assumed to be the true state of the system. We exploit this assumption to compare the experiments with the NR to understand the impact of assimilation better.

One diagnostics we use in this sense is the RMS of difference between the ensemble mean and the NR computed in the first 10 m of the water column for the whole basin. The propagation of

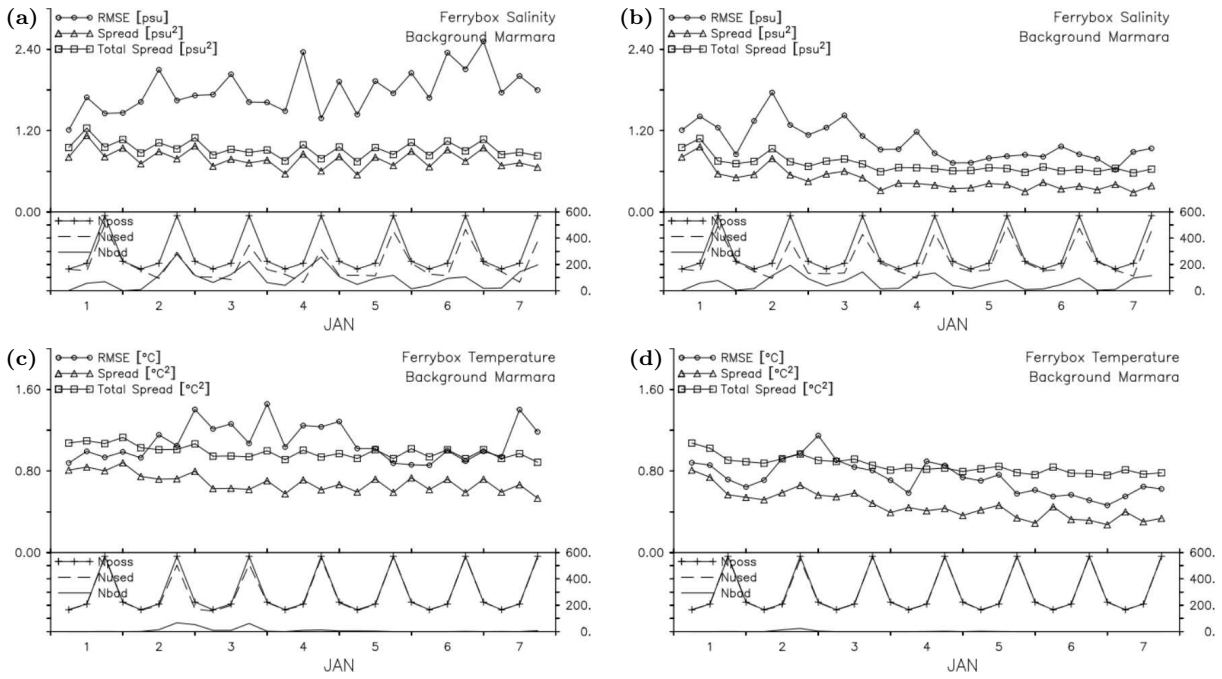

Fig. 4.8. Six hourly timeseries of RMSE, spread and total spread of salinity (top) and temperature (bottom) misfits for FB001 (left) and FB002 (right). Bottom panel of each figure shows the number of available (Nposs), used (Nused) and outlier (Nbad) observations in each assimilation cycle.

the error reduction can be traced from the spatial maps of this diagnostic.

Besides the error statistics, ensemble spread for temperature and salinity is also shown in some figures to see whether the ensemble collapses. Total spread, which is the sum of the ensemble spread and the observational error, are also overlaid.

4.5 Results

Figure 4.8 shows the time evolution of RMS of misfits, ensemble spread and total spread for temperature and salinity. The RMS of salinity misfits continuously grows in FB001. It fluctuates around 2 psu and reaches to 2.4 psu at the end of sixth day. In FB002, assimilation of the observations decrease the RMS of misfits, significantly. The RMS of misfits is generally below 1.2 psu. Although there is an increase of error in the first two days a gradual reduction takes place during the following days. The RMS of temperature misfits is similar to that of salinity after the second day. The error grows in FB001 even though the trend is not as obvious as in salinity errors of the same experiment. The skill of the analysis is improved at the end of the experiment FB002.

Another important aspect worth to mention is that the ensemble still has enough spread at the end of the experiments, although it is larger in FB001 than FB002 as expected. In other

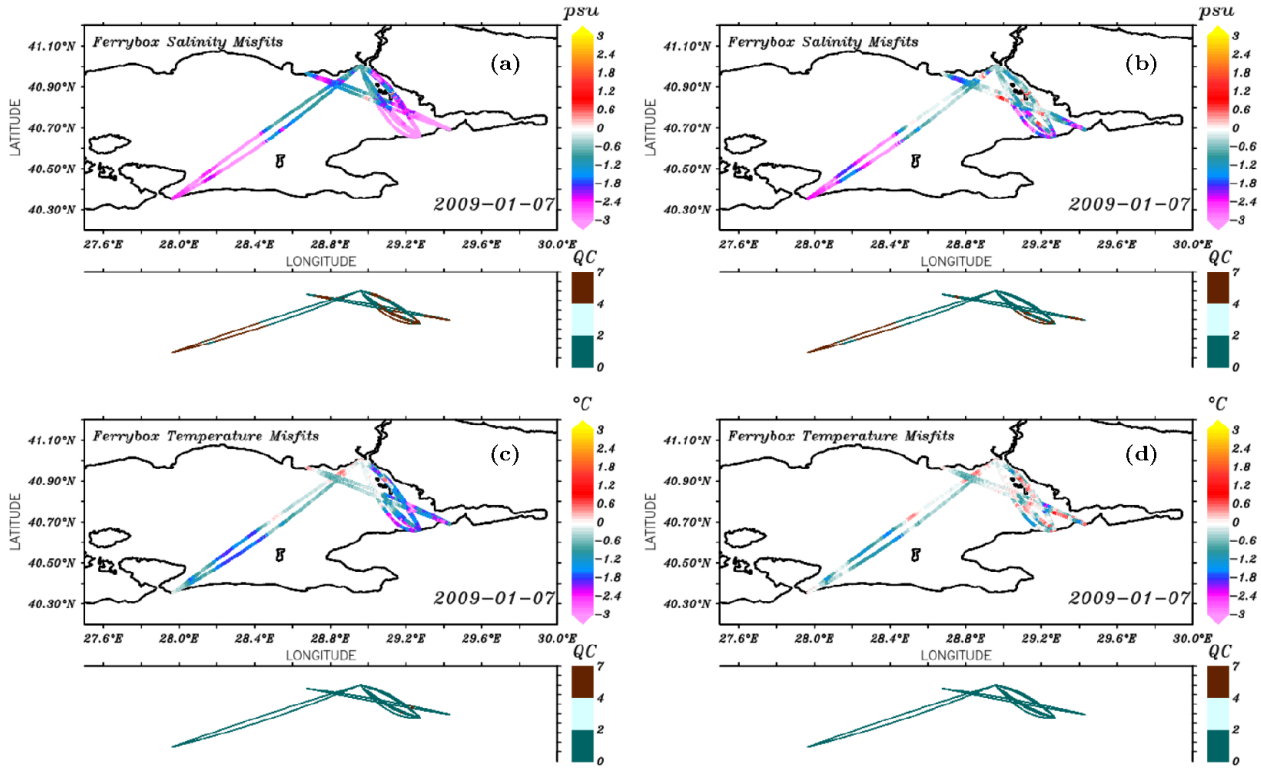

Fig. 4.9. Horizontal distribution of salinity (top) and temperature (bottom) misfits along the ferrylines in 7 January 2009 for FB001 (left) and FB002 (right). The small panels show the outlier observations in quality controls by brown color.

words, ensemble didn't collapse after a week of assimilation. We recall that the ensemble spread is maintained by perturbing the background vertical diffusivity on top of the initial ensemble spread. The method seems promising at least for short-term experiments.

As discussed in section 4.4.4, the data are subjected to a quality control before assimilation. The bottom panels of the Fig. 4.8 shows the number of available observations (Nposs), number of used observations (Nused) and number of outlier observations (Nbad). The increase in the number of used observations in FB002 points out an improvement also in the regions in which the observations were mostly outliers.

In the last day of experiments (Fig. 4.9), the salinity misfits are better almost everywhere in FB002. There is apparently a reduction in errors in the northern basin. Assimilation decreases the number of outlier salinity observations especially on the route between Yenikapı and Yalova. Moreover, misfits are improved partially in the southern basin where less of observations are assimilated. The number of outlier temperature observations is not significant in both experiments. The misfits are reduced everywhere but more dramatically in the southern and eastern basin. Overall, the assimilation of temperature and salinity observations in the selected transects notably helps to correct the subsurface fields.

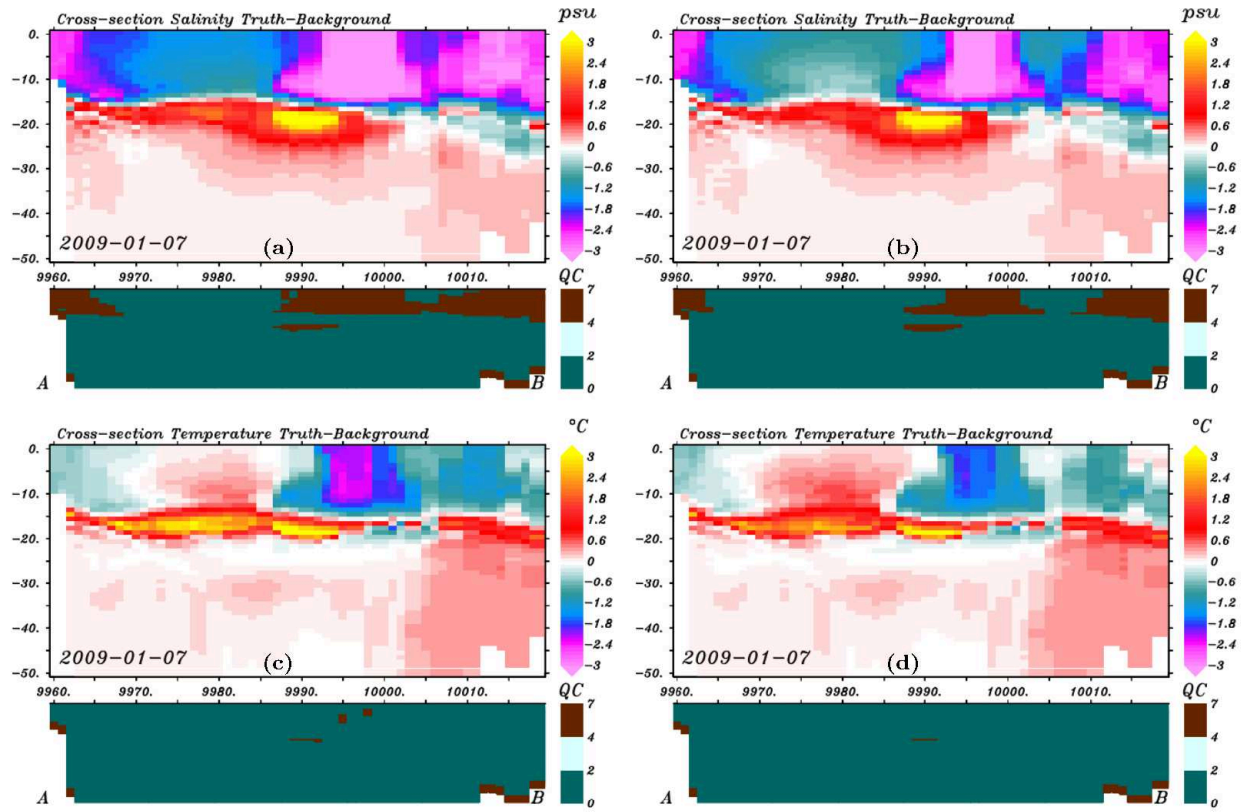

Fig. 4.10. Vertical distribution of salinity (top) and temperature (bottom) misfits along the cross-section A-B in Fig. 4.5 in 7 January 2009 for FB001 (left) and FB002 (right). The small panels show the outlier observations by brown.

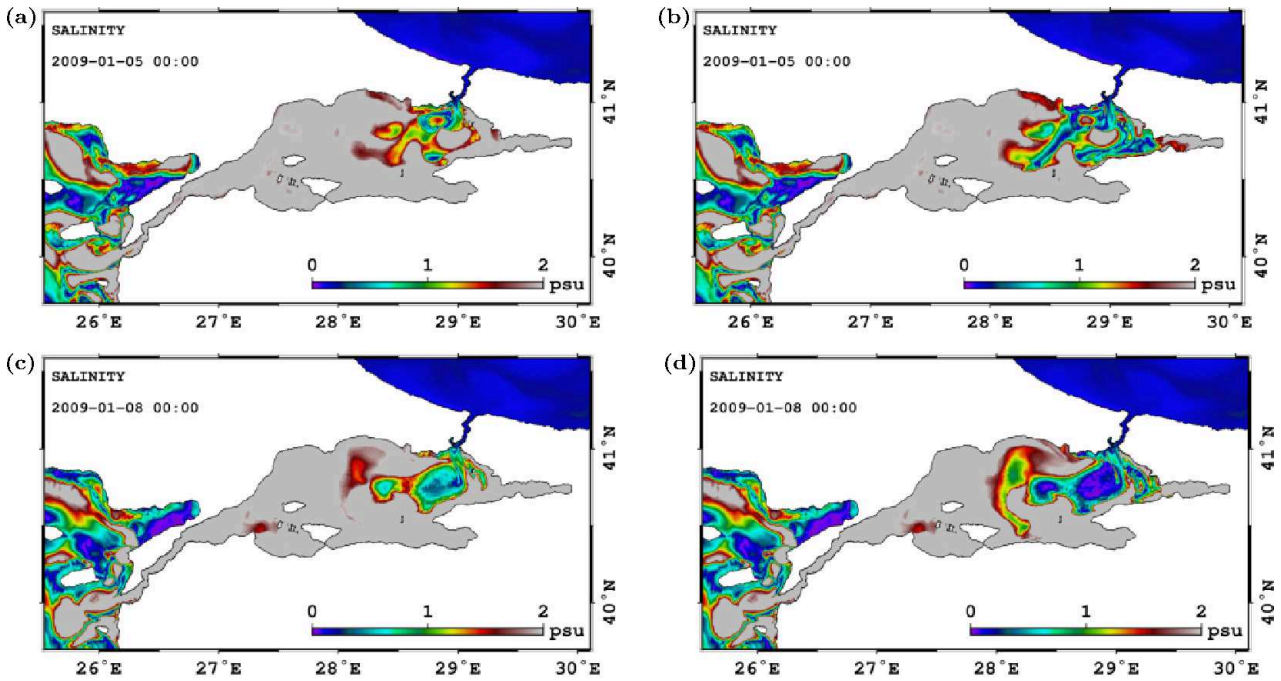

Fig. 4.11. RMS of the difference between NR and prior salinity at the first 10 m. Comparison of FB001 (left) and FB002 (right) are shown for 05-01-2009 (top) and 08-01-2009 (bottom).

The enhancement of the analysis is also noticed in the remote areas such as the A-B transect in the mid-basin (see Fig. 4.5). Figure 4.10 shows the difference between the synthetic observations and prior state down to 50 m depth is shown along the transect after the last assimilation cycle. Comparison of salinity differences in FB001 and FB002 reveals the improvement in the northern section down to 15 m depth. The southern part away from the coast also gets better skill. The midst of the transect still has large discrepancies in both experiments at the end of seven days. The correction in the remote area suggests a mechanism related to the outflow of Bosphorus and the surface circulation of the Marmara Sea. The water masses which are corrected by assimilation in the eastern basin are pushed towards the west and reduce the error.

Figure 4.11 depicts the RMS of the difference between NR and prior salinity at the first 10 m depth. It clearly supports the mechanism suggested above. The distribution of RMS of differences in the non-assimilation case shows that the Bosphorus outflow also has some capability to reduce the difference since the Black Sea water masses governs the upper layer of the Marmara Sea (Fig 4.11a and 4.11c). Therefore, the conclusion that the improvement is due to the assimilation is not straightforward. However, comparison of the FB001 and FB002 reveals the role of the assimilation of ferry tracks on the error reduction, clearly. The two snapshots from the fifth and the last day of the experiments confirms the westward propagation of error reduction. In the fifth day, lower RMS of differences elongate towards the Gulf of Izmit in the east. The westwards propagation is more pronounced in the last day. The mid-basin has lower errors after the experiment almost everywhere in the north-south orientation including A-B transect shown before.

Finally, temperature fields are already closer to the truth in the fifth day even in the western basin. After seven days of assimilation, the temperature error in the Bosphorus plume is significantly reduced. The southern and central basin has improvements as much as 0.5°C locally.

4.6 Summary and Discussion

We presented the data assimilation experiments performed in the Marmara Sea for the first time. The main characteristics of the TSS has been summarized. For the study, a general ocean circulation model, FESOM and an ensemble data assimilation framework, DART has been coupled. The implementation of the data assimilation environment has been reported.

The TSS is an important water passage for the oceanography of the neighboring Black and Aegean Seas. It also has important impact on the their ecosystem by maintaining the exchange

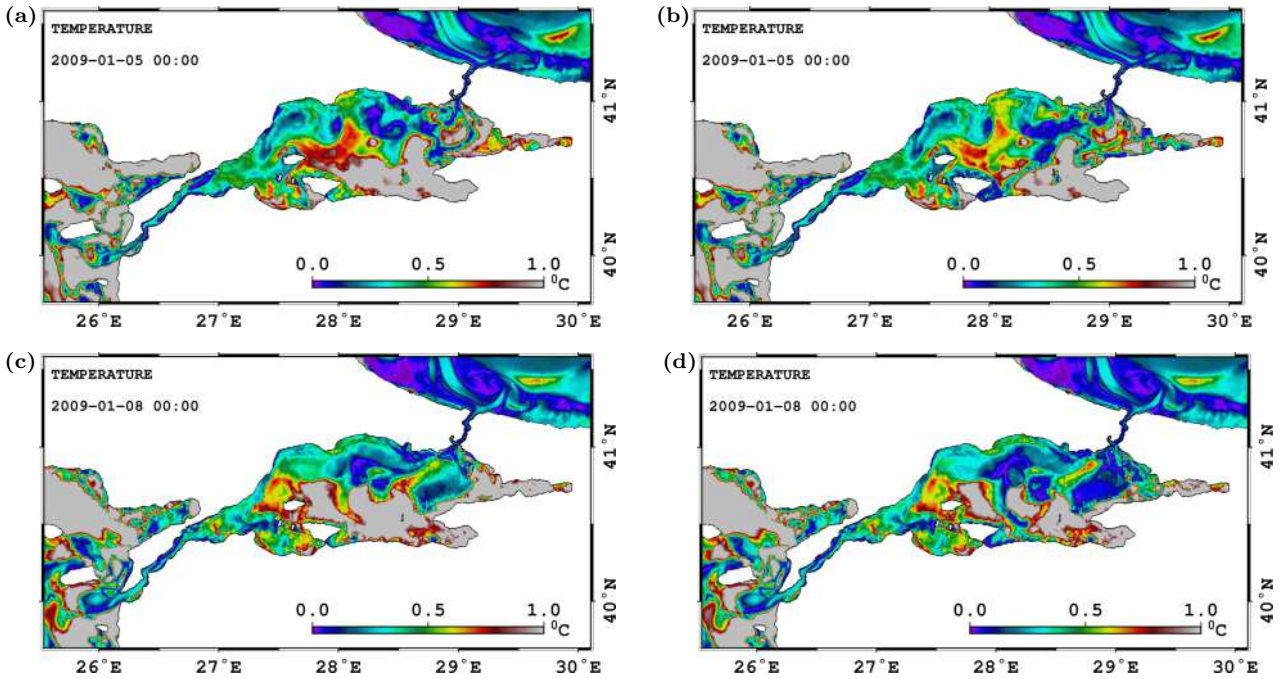

Fig. 4.12. RMS of the difference between NR and prior temperature at the first 10 m. Comparison of FB001 (left) and FB002 (right) are shown for 05-01-2009 (top) and 08-01-2009 (bottom).

of water masses and nutrients. The high population in the cities surrounding the system and intense marine traffic through the passages adds social and economical reasons to monitor the TSS in a sustainable way.

The observations in the TSS has been obtained by dedicated projects for short time periods or limited spatial coverage. Moreover, the satellite measurements are still low-resolution for monitoring and assimilation purposes. In this study, we proposed a sustainable marine monitoring network using the ferry lines in the eastern Marmara Sea. We think that loading the ferries which operate everyday from Istanbul to various cities around the Marmara Sea temperature and salinity sensors can provide immense amount of data both in time and space. Following this motivation, we tested a ferrybox network including some of the ferry transects in the eastern Marmara Sea.

The OSSE methodology has been used to assess the impact of ferrybox measurements. We tried to satisfy the main criteria determined by approximately forty years experience of the atmosphere and ocean communities. However, it was still not possible to perform OSE to compare with OSSE due to the lack of data during the experiment period.

The results of the two experiments presented here are promising. We showed that the assimilation of the salinity and temperature observations significantly improve the analysis in the Marmara Sea. The Bosphorus jet has an important role in the propagation of the error reduction towards the western basin where no data is assimilated. Moreover, the Marmara Sea circulation

helps to improve the southern basin even in short timescales. The lower layer doesn't show any response to assimilation since the stratification between the upper and lower layers is strong and the observations are at 5 m.

In conclusion, the results encourage for further data assimilation studies in the Marmara Sea. The investigations can be extended to different observing systems, different areas of the sea or different dynamical focuses. Moreover, we believe the unique dynamics of the system demonstrated its ability to be a good natural laboratory for the future data assimilation studies.

General Summary and Conclusions

In this thesis, we presented the design of sustained marine monitoring networks in the coastal seas using state of the art modeling and data assimilation methods. The study involves three steps that we have taken to design an observing network in the Turkish Straits System (TSS).

As a first step, we studied the OSE and OSSE methodologies in the Adriatic Sea using a Fishery Observing System (FOS) operating since 2007. The FOS is a ship of opportunity monitoring system developed to collect in-situ environmental data. We evaluated the design of the FOS in 2007 using single value temperature measurements averaged over the fishing net hauling period. We have shown that assimilation of FOS observations improves the quality of the analysis in terms of RMS errors significantly with respect to simulation. The OSE results point out that decreasing the number of vessels by leaving the coverage unaltered, and decreasing the number of measurements does not have a critical impact on the quality of the analysis. In OSSE, we tested the impact of introducing CTD salinity and temperature measurements between January-April 2007 and demonstrated that the salinity assimilation does not change the quality of the analysis significantly during the mixing season.

The next aim is to apply a similar approach in the TSS. We performed the first multi-year simulations using three dimensional ocean circulation models for the integral system driven by the atmospheric forcing. In the first part, the two six years simulations in the TSS has been investigated in terms of the evolution of the water mass structure throughout the system. The simulations are evaluated in the first and last year of the experiments with CTD observations. We have demonstrated that the model is capable of simulating the main climatological characteristics of the system. Moreover, the impact of different surface salinity boundary condition is shown to be significant especially for the density-driven lower layer flows. The annual average of the net volume fluxes through the Bosphorus are compatible with the observed estimates, however, they are always lower in the Dardanelles. Upper layer and lower layer volume fluxes are always below the historical estimates. The annual average of the circulation in the Marmara Sea has two main characteristics. The first pattern is an S-shaped circulation where the buoyant plume of the Bosphorus first moves to south and turns to northwest and exits the Dardanelles in the southwest. This structure appears when the wind forcing is more intense in the central and southern Marmara Sea. When the wind forcing shifts to the north, the Bosphorus plume immediately deviates to the west and forms a cyclonic structure in the central basin following the northern coast. Long term simulation allowed us to compare the wind work in the Marmara Sea with other marginal seas. The wind work is shown to be higher than even the Baltic Sea. As a result, the wind forcing

and the Bosphorus jet give rise to a highly energetic surface circulation.

Finally, we performed the first data assimilation experiments in the Marmara Sea by using OSSE methodology. The idea is to use the ferry lines between different cities around the Marmara Sea as a ferrybox network to monitor the eastern basin continuously. We have chosen ten ferries operating everyday as an observation network. An ensemble-based Kalman filter is coupled with the model to assimilate the synthetic temperature and salinity observations. The results show that the ferrybox network has a potential to improve the analysis in the Marmara Sea significantly. Moreover, the assimilation in the Bosphorus outflow helps to correct the central and western basin by propagating the water masses westward.

Bibliography

Acara, A. (1958). Fluctuation of the surface water temperature and salinity of the bosphorus. rapp. p. V. Reun. CIESMM 1(31), 255–258.

Alpar, B., E. Dogan, H. Yuce, and H. Altiok (2000). Sea level changes along the turkish coasts of the black sea, the aegean sea and the eastern mediterranean. Mediterranean Marine Science 1(1), 141–156.

Altiok, H., H. İ. Sur, and H. Yüce (2012). Variation of the cold intermediate water in the black sea exit of the strait of istanbul (bosphorus) and its transfer through the strait. Oceanologia 54(2), 233–254.

Alvarez, A. and B. Mourre (2014). Cooperation or coordination of underwater glider networks? an assessment from observing system simulation experiments in the ligurian sea. Journal of Atmospheric and Oceanic Technology 31(10), 2268–2277.

Anderson, J., T. Hoar, K. Raeder, H. Liu, N. Collins, R. Torn, and A. Avellano (2009). The data assimilation research testbed: A community facility. Bulletin of the American Meteorological Society 90(9), 1283–1296.

Anderson, J. L. (2001). An ensemble adjustment kalman filter for data assimilation. Monthly weather review 129(12), 2884–2903.

Arnold Jr, C. P. and C. H. Dey (1986). Observing-systems simulation experiments: Past, present, and future. Bulletin of the American Meteorological Society 67(6), 687–695.

Artegiani, A., E. Paschini, A. Russo, D. Bregant, F. Raicich, and N. Pinardi (1997). The adriatic sea general circulation. part i: Air-sea interactions and water mass structure. Journal of physical oceanography 27(8), 1492–1514.

Atlas, R. (1997). Atmospheric observation and experiments to assess their usefulness in data assimilation. J. Meteor. Soc. Jpn 75, 111–130.

Aydoğdu, A., N. Pinardi, J. Pistoia, M. Martinelli, A. Belardinelli, and S. Sparnocchia (2016). Assimilation experiments for the fishery observing system in the adriatic sea. Journal of Marine Systems 162, 126 – 136. Progress in marine science supported by European joint coastal observation systems: The JERICO-RI research infrastructure.

Benetazzo, A., A. Bergamasco, D. Bonaldo, F. Falcieri, M. Sclavo, L. Langone, and S. Carniel (2014). Response of the adriatic sea to an intense cold air outbreak: Dense water dynamics and wave-induced transport. Progress in Oceanography 128, 115 – 138.

Beşiktepe, Ş. T., H. I. Sur, E. Özsoy, M. A. Latif, T. Oğuz, and Ü. Ünlüata (1994). The circulation and hydrography of the marmara sea. Progress in Oceanography 34(4), 285–334.

Bogdanova, C. (1969). Seasonal fluctuations in the inflow and distribution of the mediterranean waters in the black sea. In: Basic Features of the Geological Structure, of the Hydrologic Regime and Biology of the Mediterranean Sea L.M. FOMIN,editor, Academy of Sciences, USSR, Moskow., 131–139. English translation 1969 Institute of Modem Languages, Washington DC.

Book, J. W., E. Jarosz, J. Chiggiato, and Ş. Beşiktepe (2014). The oceanic response of the turkish straits system to an extreme drop in atmospheric pressure. Journal of Geophysical Research: Oceans 119(6), 3629–3644.

Büyükay, M. (1989). The surface and internal oscillations in the bosphorus, related to meteorological forces. M. Sc. ThesisInstitute of Marine Sciences, Middle East Technical University, Erdemli, Içel, Turkey, 169.

Cessi, P., N. Pinardi, and V. Lyubartsev (2014). Energetics of Semienclosed Basins with Two-Layer Flows at the Strait. Journal of Physical Oceanography 44(3), 967–979.

Chiggiato, J., E. Jarosz, J. W. Book, J. Dykes, L. Torrisi, P. M. Poulain, R. Gerin, J. Horstmann, and Ş. Beşiktepe (2012). Dynamics of the circulation in the Sea of Marmara: Numerical modeling experiments and observations from the Turkish straits system experiment. Ocean Dynamics 62(1), 139–159.

Danilov, S., G. Kivman, and J. Schröter (2004). A finite-element ocean model: principles and evaluation. Ocean Modelling 6(2), 125–150.

Demyshev, S., S. Dovgaya, and V. Ivanov (2012). Numerical modeling of the influence of exchange through the bosporus and dardanelles straits on the hydrophysical fields of the marmara sea. Izvestiya, Atmospheric and Oceanic Physics 48(4), 418–426.

Dobricic, S. and N. Pinardi (2008). An oceanographic three-dimensional variational data assimilation scheme. Ocean Modelling 22(3-4), 89–105.

Dobricic, S., N. Pinardi, M. Adani, A. Bonazzi, C. Fratianni, and M. Tonani (2005). Mediterranean forecasting system: An improved assimilation scheme for sea-level anomaly and its validation. Quarterly Journal of the Royal Meteorological Society 131(613), 3627–3642.

Dobricic, S., N. Pinardi, P. Testor, and U. Send (2010, June). Impact of data assimilation of glider observations in the ionian sea (eastern mediterranean). Dynamics of Atmospheres and Oceans 50(1), 78–92.

Dombrowsky, E., L. Bertino, G. Brassington, E. Chassignet, F. Davidson, H. Hurlburt, M. Kamachi, T. Lee, M. Martin, S. Mei, et al. (2008). Godae systems in operation. In GODAE final symposium, Nice 2008.

Falco, P., A. Belardinelli, A. Santojanni, N. Cingolani, A. Russo, and E. Arneri (2007). An observing system for the collection of fishery and oceanographic data. Ocean Science 3(2), 189–203.

Gaspari, G. and S. E. Cohn (1999). Construction of correlation functions in two and three dimensions. Quarterly Journal of the Royal Meteorological Society 125(554), 723–757.

Grayek, S., J. Staneva, J. Schulz-Stellenfleth, W. Petersen, and E. V. Stanev (2011, October). Use of FerryBox surface temperature and salinity measurements to improve model based state estimates for the German Bight. Journal of Marine Systems 88(1), 45–59.

Gregg, M. C. and E. Özsoy (2002). Flow, water mass changes, and hydraulics in the bosphorus. Journal of Geophysical Research: Oceans 107(C3).

Gunduz, M., S. Dobricic, P. Oddo, N. Pinardi, and A. Guarnieri (2013). Impact of levantine intermediate water on the interannual variability of the adriatic sea based on simulations with a fine resolution ocean model. Ocean Modelling 72, 253–263.

Gündüz, M. and E. Özsoy (2015). Blocking of the upper layer flow in the çanakkale (dardanelles) strait and its influence on fish catches. Journal of the Black Sea/Mediterranean Environment 21(3).

Gürses, O. (2016). Dynamics of the Turkish Straits System: A Numerical Study with a finite element ocean model based on an unstructured grid approach. Ph. D. thesis, Institute of Marine Sciences, METU.

Haines, K. (2010). Ocean data assimilation. In Data Assimilation, pp. 517–547. Springer.

Halliwell Jr, G., V. Kourafalou, M. Le Hénaff, L. Shay, and R. Atlas (2015). Osse impact analysis of airborne ocean surveys for improving upper-ocean dynamical and thermodynamical forecasts in the gulf of mexico. Progress in Oceanography 130, 32 – 46.

Halliwell Jr, G., A. Srinivasan, V. Kourafalou, H. Yang, D. Willey, M. Le Hénaff, and R. Atlas (2014). Rigorous evaluation of a fraternal twin ocean osse system for the open gulf of mexico. Journal of Atmospheric and Oceanic Technology 31(1), 105–130.

Hamill, T. M., J. S. Whitaker, and C. Snyder (2001). Distance-dependent filtering of background error covariance estimates in an ensemble kalman filter. Monthly Weather Review 129(11), 2776–2790.

Hoteit, I., T. Hoar, G. Gopalakrishnan, N. Collins, J. Anderson, B. Cornuelle, A. Köhl, and P. Heimbach (2013). A mitgcm/dart ensemble analysis and prediction system with application to the gulf of mexico. Dynamics of Atmospheres and Oceans 63, 1–23.

Houtekamer, P. L. and H. L. Mitchell (1998). Data assimilation using an ensemble kalman filter technique. Monthly Weather Review 126(3), 796–811.

Huang, R. X. (1993). Real Freshwater Flux as a Natural Boundary Condition for the Salinity Balance and Thermohaline Circulation Forced by Evaporation and Precipitation.

Hüsrevoğlu, S. (1998, 7). Modeling Of The Dardanelles Strait Lower-layer Flow Into The Marmara Sea. Ph. D. thesis, Institute of Marine Sciences, METU.

Jarosz, E., W. J. Teague, J. W. Book, and c. Beşiktepe (2011a). Observed volume fluxes in the bosphorus strait. Geophysical Research Letters 38(21), n/a–n/a. L21608.

Jarosz, E., W. J. Teague, J. W. Book, and c. Beşiktepe (2011b). On flow variability in the Bosphorus Strait. Journal of Geophysical Research: Oceans (1978–2012) 116(C8).

Jarosz, E., W. J. Teague, J. W. Book, and c. Beşiktepe (2012). Observations on the characteristics of the exchange flow in the dardanelles strait. Journal of Geophysical Research: Oceans 117(C11), n/a–n/a. C11012.

Jarosz, E., W. J. Teague, J. W. Book, and c. Beşiktepe (2013). Observed volume fluxes and mixing in the dardanelles strait. Journal of Geophysical Research: Oceans 118(10), 5007–5021.

Johns, B. and T. Oguz (1989). The modelling of the flow of water through the bosphorus. Dynamics of Atmospheres and Oceans 14, 229–258.

Kara, A. B., A. J. Wallcraft, H. E. Hurlburt, and E. Stanev (2008). Air–sea fluxes and river discharges in the black sea with a focus on the danube and bosphorus. Journal of Marine Systems 74(1), 74–95.

Karspeck, A. R., S. Yeager, G. Danabasoglu, T. Hoar, N. Collins, K. Raeder, J. Anderson, and J. Tribbia (2013). An ensemble adjustment kalman filter for the ccsm4 ocean component. Journal of Climate 26(19), 7392–7413.

Korres, G., M. Ntoumas, M. Potiris, and G. Petihakis (2014, December). Assimilating Ferry Box data into the Aegean Sea model. Journal of Marine Systems 140, 59–72.

Kourafalou, V., P. De Mey, M. Le Hénaff, G. Charria, C. Edwards, R. He, M. Herzfeld, A. Pascual, E. Stanev, J. Tintoré, et al. (2015). Coastal ocean forecasting: system integration and evaluation. Journal of Operational Oceanography 8(sup1), s127–s146.

Kourafalou, V. H. and K. Barbopoulos (2003). High resolution simulations on the north aegean sea seasonal circulation. In Annales Geophysicae, Volume 21, pp. 251–265.

Latif, M., E. Özsoy, T. Oguz, and Ü. Ünlüata (1991). Observations of the mediterranean inflow into the black sea. Deep Sea Research Part A. Oceanographic Research Papers 38, S711–S723.

Latif, M. A., E. Ozsoy, T. Oguz, and H. Sur (1992). Volume flux measurements in the bosporous using an acoustic doppler current profiler. Rapp. Comm. Int. Mer Medit 33, 221.

Leblond, E., P. Lazure, M. Laurans, C. Rioual, P. Woerther, L. Quemener, and P. Berthou (2010). The recopesca project: a new example of participative approach to collect fisheries and in situ environmental data. Mercator Ocean-Quarterly Newsletter (37), 40–48.

Luo, D., Y. Yao, and S. B. Feldstein (2014). Regime transition of the north atlantic oscillation and the extreme cold event over europe in january-february 2012. Monthly Weather Review 142(12), 4735–4757.

Madec, G. (2008). NEMO ocean engine.

Maderich, V., Y. Ilyin, and E. Lemeshko (2015). Seasonal and interannual variability of the

water exchange in the turkish straits system estimated by modelling. Mediterranean Marine Science 16(2), 444–459.

Marsigli, L. (1681). Osservazioni intorno al bosforo tracio overo canale di constantinopoli, rappresentate in lettera alla sacra real maest cristina regina di svezia da luigi ferdinando marsigli. Nicoló Angelo Tinassi, Roma.

Masuda, S. (2014). An observing system simulation experiment for the western north pacific region. The Scientific World Journal 2014.

Masutani, M., T. W. Schlatter, R. M. Errico, A. Stoffelen, E. Andersson, W. Lahoz, J. S. Woollen, G. D. Emmitt, L.-P. Riishøjgaard, and S. J. Lord (2010). Observing system simulation experiments. In Data Assimilation, pp. 647–679. Springer.

Munk, W. and C. Wunsch (1982). Observing the ocean in the 1990s. Philosophical Transactions of the Royal Society of London. Series A, Mathematical and Physical Sciences 307(1499), 439–464.

Nielsen, J. N. (1912). Hydrography of the Mediterranean and adjacent waters.

Nilsson, J. A. U., S. Dobricic, N. Pinardi, P.-M. Poulain, and D. Pettenuzzo (2011, December). Variational assimilation of lagrangian trajectories in the mediterranean ocean forecasting system. Ocean Science Discussions 8(6), 2503–2525.

Oguz, T., E. Özsoy, M. A. Latif, H. I. Sur, and Ü. Ünlüata (1990). Modeling of hydraulically controlled exchange flow in the bosphorus strait. Journal of Physical Oceanography 20(7), 945–965.

Oguz, T. and H. Sur (1989). A 2-layer model of water exchange through the dardanelles strait. Oceanologica Acta 12(1), 23–31.

Oke, P. R. and T. J. OKane (2011). Observing system design and assessment. In Operational Oceanography in the 21st Century, pp. 123–151. Springer.

Özsoy, E., D. Di Iorio, M. C. Gregg, and J. O. Backhaus (2001). Mixing in the bosphorus strait and the black sea continental shelf: observations and a model of the dense water outflow. Journal of Marine Systems 31(1), 99–135.

Ozsoy, E., M. A. Latif, S. Besiktepe, N. Cetin, M. C. Gregg, V. Belokopytov, Y. Goryachkin,

and V. Diaconu (1998). The bosporus strait: Exchange fluxes, currents and sea-level changes. NATO SCIENCE SERIES 2 ENVIRONMENTAL SECURITY 47(2), 1–28.

Özsoy, E., T. Oğuz, M. Latif, Ü. Ünlüata, H. Sur, and Ş. Beşiktepe (1988). Oceanography of the turkish straitssecond annual report. Submittes to: Istanbul Water and Sewerage Administration. The Middle East Technical University, Institute of Marine Sciences, Erdemli, Turkey.

Peneva, E., E. Stanev, V. Belokopytov, and P.-Y. Le Traon (2001). Water transport in the bosphorus straits estimated from hydro-meteorological and altimeter data: seasonal to decadal variability. Journal of Marine Systems 31(1), 21–33.

Petersen, W. (2014). FerryBox systems: State-of-the-art in Europe and future development. Journal of Marine Systems 140, Part A, 4–12.

Pinardi, N., A. Bonazzi, E. Scoccimarro, S. Dobricic, A. Navarra, A. Ghiselli, and P. Veronesi (2008). Very large ensemble ocean forecasting experiment using the grid computing infrastructure. Bulletin of the American Meteorological Society 89(6), 799–804.

Pinardi, N. and G. Coppini (2010). Preface" operational oceanography in the mediterranean sea: the second stage of development". Ocean Science 6(1), 263–267.

Raeder, K., J. L. Anderson, N. Collins, T. J. Hoar, J. E. Kay, P. H. Lauritzen, and R. Pincus (2012). Dart/cam: An ensemble data assimilation system for cesm atmospheric models. Journal of Climate 25(18), 6304–6317.

Raicich, F. (2006). The assessment of temperature and salinity sampling strategies in the mediterranean sea: idealized and real cases. Ocean Science 2(2), 97–112.

Reynolds, R. W., T. M. Smith, C. Liu, D. B. Chelton, K. S. Casey, and M. G. Schlax (2007). Daily high-resolution-blended analyses for sea surface temperature. Journal of Climate 20(22), 5473–5496.

Sannino, G., A. Sözer, and E. Özsoy (2015). Recent advancements on modelling the exchange flow dynamics through the turkish strait system. In B. Öztürk (Ed.), Proceedings of MedCLIVAR 2014 Conference: Understanding Climate Evolution and Effects on Environment and Societies in the Old World Region., pp. 110–116. TUDAV.

Schwartz, C. S., G. S. Romine, R. A. Sobash, K. R. Fossell, and M. L. Weisman (2015). Ncars experimental real-time convection-allowing ensemble prediction system. Weather and Forecasting 30(6), 1645–1654.

Seppälä, J., P. Ylöstalo, S. Kaitala, S. Hällfors, M. Raateoja, and P. Maunula (2007). Ship-of-opportunity based phycocyanin fluorescence monitoring of the filamentous cyanobacteria bloom dynamics in the baltic sea. Estuarine, Coastal and Shelf Science 73(34), 489 – 500.

Sørensen, K., M. Grung, and R. Röttgers (2007). An intercomparison of in vitro chlorophyll a determinations for meris level 2 data validation. International Journal of Remote Sensing 28(3-4), 537–554.

Sözer, A. (2013). Numerical Modeling Of The Bosphorus Exchange Flow Dynamics. Ph. D. thesis, Institute of Marine Sciences, METU.

Storto, A., S. Ciliberti, E. Peneva, and F. Macchia (2016). Quality information document for black sea physical reanalysis product. Technical report, Copernicus Marine Environment Monitoring Service.

Timmermann, R. and H. H. Hellmer (2013). Southern ocean warming and increased ice shelf basal melting in the twenty-first and twenty-second centuries based on coupled ice-ocean finite-element modelling. Ocean Dynamics 63(9), 1011–1026.

Tugrul, S., T. Besiktepe, and I. Salihoglu (2002). Nutrient exchange fluxes between the aegean and black seas through the marmara sea. Mediterranean Marine Science 3(1), 33–42.

Tutsak, E. (2012, 9). Analyses of atmospheric and marine observations along the turkish coast. Master's thesis, Institute of Marine Sciences, METU.

Ünlüata, Ü., T. Oğuz, M. Latif, and E. Özsoy (1990). On the physical oceanography of the turkish straits. In The physical oceanography of sea straits, pp. 25–60. Springer.

Wallcraft, A. J., A. B. Kara, and H. E. Hurlburt (2005). Convergence of laplacian diffusion versus resolution of an ocean model. Geophysical Research Letters 32(7), n/a–n/a. L07604.

Wang, Q., S. Danilov, and J. Schröter (2008). Finite element ocean circulation model based on triangular prismatic elements, with application in studying the effect of topography representation. Journal of Geophysical Research: Oceans (1978–2012) 113(C5).

Wekerle, C., Q. Wang, S. Danilov, T. Jung, and J. Schrter (2013). The canadian arctic archipelago throughflow in a multiresolution global model: Model assessment and the driving mechanism of interannual variability. Journal of Geophysical Research: Oceans 118(9), 4525–4541.

Xie, P. and P. A. Arkin (1997). Global precipitation: A 17-year monthly analysis based on gauge observations, satellite estimates, and numerical model outputs. Bulletin of the American Meteorological Society 78(11), 2539–2558.

Zavatarelli, M. and N. Pinardi (2003). The adriatic sea modelling system: a nested approach. In Annales Geophysicae, Volume 21, pp. 345–364.

Zervakis, V., D. Georgopoulos, and P. G. Drakopoulos (2000). The role of the north aegean in triggering the recent eastern mediterranean climatic changes. Journal of Geophysical Research: Oceans 105(C11), 26103–26116.

Zodiatis, G. (1994). Advection of the black sea water in the north aegean sea. The Global Atmosphere and Ocean System 2(1), 41–59.